NASA CONTRACTOR REPORT

NASA CR-7

c. 1

NASA CR-733

STEADY-STATE AND DYNAMIC PROPERTIES OF JOURNAL BEARINGS IN LAMINAR AND SUPERLAMINAR FLOW REGIMES

II. FULL-FLOATING-RING BEARINGS

by F. K. Orcutt and C. W. Ng

Prepared by
MECHANICAL TECHNOLOGY INCORPORATED
Latham, N. Y.
for Lewis Research Center

NATIONAL AERONAUTICS AND SPACE ADMINISTRATION • WASHINGTON, D. C. • JUNE 1967

NASA CR-733

STEADY-STATE AND DYNAMIC PROPERTIES OF JOURNAL BEARINGS IN LAMINAR AND SUPERLAMINAR FLOW REGIMES

II. FULL-FLOATING-RING BEARINGS

By F. K. Orcutt and C. W. Ng

Prepared under Contract No. NASw-1021 by
MECHANICAL TECHNOLOGY INCORPORATED
Latham, N.Y.

for Lewis Research Center

NATIONAL AERONAUTICS AND SPACE ADMINISTRATION

For sale by the Clearinghouse for Federal Scientific and Technical Information
Springfield, Virginia 22151 – CFSTI price $3.00

FOREWORD

The work described in this report was performed by Mechanical Technology Incorporated under NASA Contract NASw-1021. One purpose of the work was to obtain and experimentally verify steady-state and dynamic design data for two journal bearings: the tilting-pad and full floating ring bearings. The design data cover operation in both laminar and turbulent flow regimes with incompressible lubricants. A second purpose was to investigate the fundamentals of Taylor vortex flow and turbulence in concentric and eccentric annuli.

The work was done under the technical management of Joseph P. Joyce, Space Power Systems Division, NASA-Lewis Research Center, with William J. Anderson, Fluid System Components Division, NASA-Lewis Research Center, as research consultant. This report was originally prepared as MTI Report 65TR33.

ABSTRACT

This topical report presents a theoretical analysis of the plain cylindrical, full floating ring bearing with pressurized lubricant supply. Calculated design data are given for the bearing with ratios of inner-to-outer film clearance of 0.7 and 1.3, and for three values of dimensionless supply pressure. These data include laminar and turbulent flow conditions for Reynolds Numbers, based on inner film clearance, up to 9000. Experimental measurements of bearing performance were obtained for correlation with the calculated data. The correlation is good leading to the conclusion that the calculated data are effective for design analysis purposes. The plain cylindrical floating ring bearing was subject to large-amplitude fractional-frequency whirl instability when very low viscosity lubricant (0.65 cs) was used. When a more viscous lubricant (5.0 cs) was used, the whirl amplitudes were small and whirl was suppressed completely by increasing speed beyond the whirl onset speed.

NOMENCLATURE

B	damping coefficient, pound second/inch
C	radial clearance, inch
D	diameter, inch
e	eccentricity, inch
f	$= \frac{F}{W}$
F	frictional force, pound
F_o	steady-state force, pound
F_t	tangential force, pound
F_x, F_y	components of dynamic force, pound
K	stiffness coefficient, pound/inch
L	bearing length, inch
m	mass of the ring, pound second^2/inch
N	revolution per second
P_D	$= \frac{P_s}{\mu N(R/C)^2}$
P_s	circumferential supply pressure, psig
Q	flow, inch^3/second
R	Radius, inch
R_1	radius of shaft and inside radius of the floating sleeve, inch
R_2	outside radius of the sleeve and inside radius of the bearing, inch
Re_s	$= \frac{2\pi R_1 C_1 N_1}{\nu}$
Re_1	$= \frac{2\pi R_1 C_1 (N_1 - N_2)}{\nu}$
Re_2	$= \frac{2\pi R_2 C_2 N_2}{\nu}$
S	Sommerfeld Number $= \frac{\pi NLD(R/C)^2}{W}$
S_s	bearing Sommerfeld number $\frac{\pi\mu NLD_1(R_1/C_1)}{W}$
W	torque = RF, inch-pound
W	unidirectional load, pound

α	$= N_2/N_1$
ε	eccentricity ratio
μ	absolute viscosity, pound-second/inch^2
ν	kinematic viscosity, inch^2/second
ρ	density, pound second^2/inch^4
Φ	attitude angle , degrees
ω	angular speed, radians/second
ω_o	whirl angular speed, radians/second

Subscripts

1	refer to the shaft
2	refer to the floating sleeve
m	refer to the mean values
s	refer to the shaft operating condition
i	refer to the inner surface of the film
o	refer to the outer surface of the film

TABLE OF CONTENTS

STEADY-STATE AND DYNAMIC PROPERTIES OF JOURNAL BEARINGS IN LAMINAR AND SUPERLAMINAR FLOW REGIMES

II. Full-Floating-Ring Bearings

By F. K. Orcutt and C. W. Ng
Mechanical Technology Incorporated

SUMMARY

The floating-ring bearing is a promising candidate for application to high-speed rotary machinery lubricated by liquid metals primarily because it can have significantly lower power loss than any other suitable journal bearing type. Bearings in these applications operate far within the turbulent flow regime and bearing power loss can be a significant portion of net system power. High speeds and low lubricant viscosity also means that the rotor-bearing system dynamics including critical speeds, stability, and response to dynamic load will be of critical importance. The double film of the floating-ring bearing should produce high damping which is desirable, but this presumption,and the frequent though not universal success of the bearing in high speed applications, represents nearly all of the available information on the dynamic characteristics of this bearing.

This report presents theoretical design data and experimental observations of the plain floating ring bearing performance which were not heretofore available. The design data enable the designer to calculate the steady-state eccentricity ratio, minimum film thickness, torque, and lubricant flow rate for a wide range of floating-ring bearing design parameters and for laminar or turbulent flow operation. Dynamic stiffness and damping coefficients are given also for a more limited range of design parameters. These may be used in connection with a rotor-bearing dynamics analysis to investigate the stability, critical speeds, and dynamic response of the system.

The experimental measurements agree very well with the theoretical design data with respect to both steady-state and dynamic properties. It is clear that the theoretical results can be used effectively in design analysis. When a very low viscosity lubricant, e.g. 0.65 cs,was used in the experiments, large amplitude, fractional-frequency whirl instability was observed. With a more viscous lubricant, e.g. 5.0 cs, which provides greater damping, the whirl amplitudes were small and whirl was usually suppressed completely as speed was increased well beyond the whirl-onset speed. The plain floating-ring bearing does not appear to be suitable for use in high-speed liquid-metal lubricated machines because of instability. However, modifications similar to those made to improve the performance of single-film journal bearings should improve the bearing stability characteristics.

Comparison of the tilting-pad and floating-ring journal bearings of the same size and similar total clearance operating at the same conditions shows that the tilting-pad bearing operates with about five times greater minimum film thickness and about 1.6 times greater power loss than the floating-ring bearing. Within the range of stable operation for the floating-ring bearing,

the shaft vibration amplitude in response to rotating unbalance load is nearly the same for the floating-ring and unpreloaded tilting-pad bearings.

INTRODUCTION

This report presents design data for the floating-ring journal bearing in laminar and turbulent flow regimes and describes experimental studies which verify and supplement the design data. The incentive for this work has been the need to develop reliable rotor-bearing systems for high rotational speed turbo-machinery for space power applications using liquid metals as the working fluid and as the bearing lubricant.

Liquid metals have very low kinematic viscosity compared with oils and other conventional bearing lubricants. Because of this, liquid-metal lubricated bearings for high-speed rotors generally operate in the turbulent regime. Low lubricant viscosity also means low bearing damping and stiffness which increases the difficulty of obtaining good rotor-bearing system dynamical behavior. Even with conventional lubricants, the most important and difficult aspects of the design of high-speed rotor-bearing systems are the dynamic characteristics; critical speeds, stability, and response to dynamic load.

Bearing power loss rises rapidly with Reynolds' number in turbulent film bearings (Ref. 4). In prototype space power systems involving rotary machines with liquid-metal lubricated bearings, the bearing power loss has been an appreciable percentage of the net system output. In addition to the effect on system efficiency, high bearing power losses mean that large quantities of lubricant must be circulated through the bearings for cooling, and there may be substantial thermal gradients in the region of the bearings. Structural distortion and misalignments caused by thermal gradients may adversely affect bearing performance.

The floating ring bearing was chosen for analysis and evaluation in this program primarily because of its very low power loss. In the floating-ring bearing, the drag on the shaft comes only from shear of the inner film, between the shaft and the ring. Rotation of the ring reduces power loss both because the inner film shear rate is reduced and because the film Reynolds' number, or level of turbulence, is reduced. The double films of the floating-ring bearing also result in a large damping effect which should contribute to good dynamic characteristics. Large damping capacity has been given as the reason for the success of the floating-ring bearing in many high-speed applications, such as turbo-superchargers, in spite of the fact that the bearing lacks the inherent stability of some other journal bearing types, such as the tilting-pad bearing.

DESCRIPTION OF THE FLOATING RING BEARING

The floating-ring bearing consists simply of a free floating-ring around the shaft with a fixed outer bearing outside the ring. Figure 1 shows the experimental floating-ring bearing mounted in the test bearing housing. Lubricant is supplied under pressure to a circumferential groove cut into the outer bearing and into the ring outer surface at the midplane. Eight radial holes connect the outer groove to a second circumferential groove on the inner surface of the ring. Lubricant under pressure flows axially outward from the center grooves in both films to atmospheric pressure at the ends of the bearing films. For analysis, each film can be divided into two similar plain cylindrical bearings with supply pressure at one end and atmospheric pressure at the other end, and with slenderness ratio of L/2D.

In practice, multiple axial grooves are sometimes cut into the ring surfaces to provide for easier flow of lubricant through the bearing and to improve the bearing stability. The plain, ungrooved bearing was chosen for this investigation because it is the more standard design on which some information is available in the literature (Refs. 1 and 2), and because theoretical analysis of this configuration, while lengthly and cumbersome, is feasible. Analysis of the axial-grooved bearing is greatly complicated by the fact that the performance will vary depending on the position of the grooves with respect to the static load direction. In the floating-ring bearing with grooves in the inner film, the grooves constantly change position with respect to the static load direction and the performance characteristics will vary cyclically depending on the instantaneous relationship between the grooves and the direction of static load.

In the test bearing, the ring is steel with a phosphorus bronze coating on the bearing surfaces and on the axial positioning surfaces at the ends of the ring. There are radial grooves cut into the axial locating surfaces effectively forming flat pad thrust bearings which run against a step in the outer bearing housing at one end and a steel snap ring at the other. The outer bearing is hardened steel.

The ends of the ring are extended beyond the actual bearing surfaces to provide reference surfaces for displacement sensors which measure ring motion.

The test bearing design parameters are:

Shaft diameter (D_1) = 4 inches

Slenderness ratio (L/D_1) = 1.0

Ratio of bushing diameters (D_2/D_1) = 1.2

Inner film clearance ratio (C_1/R_1) = 1.5×10^{-3} in./in.

Ratio of film clearances (C_2/C_1) = 0.7 and 1.3

Shaw and Nussdorfer (ref. 1) reported irregular rotation of the bushing when the ratio of film clearances in their experiments was greater than 1.0, while bushing speed was stable and reproducible for values of C_2/C_1 of less than 1.0. One reason for choosing two values of C_2/C_1, one on either side of 1.0, was to check this observation and inquire further into the reasons for it.

SUPERLAMINAR FLOW IN BEARING FILMS

There are two distinct modes of superlaminar flow that can occur in journal bearing films. The first of these is vortex flow and the second is fully developed turbulence.

The transition to vortex flow in the annular space between two concentric cylinders, with the inner cylinder rotating and the outer one stationary or rotating at a lower speed, occurs at a critical value of the Reynolds' number given by:

$$Re_{crit} = \left(\frac{2\pi RNC}{\nu}\right)_{crit} = 41.1 \sqrt{\frac{R}{C}} \qquad (1)$$

where:

Re = Reynolds' number

R = Bearing radius

N = Speed of rotation of the inner cylinder, or difference in speeds of the inner and outer cylinders, R.P.S.

C = Radial clearance, inches

ν = Kinematic viscosity, in^2/sec

This criterion for onset of vortex flow was determined both analytically and experimentally by G. I. Taylor (ref. 3). It has been found experimentally to apply, approximately, for lightly loaded (and, hence, nearly concentric) journal bearings (refs. 4 and 5). It also applies qualitatively to eccentric journal bearings, except that the transition speed is then greater than the value predicted by Eq. (1) (ref. 6).

At the critical Reynolds' number, vortices are generated in the annular space between the concentric cylinders, due to the radial centrifugal pressure gradient. This flow is hydrodynamically stable, however it is accompanied by a measurable increase in the drag loss, analogous to that encountered in turbulent flow. Fully developed turbulence has been found experimentally to set in when the Reynolds' number ($Re = \frac{2\pi RNC}{\nu}$) reaches a value of about 1000 to 1500, for the case of rotating inner cylinder and a stationary or slower speed outer cylinder.

Equation (1) shows that the onset of Taylor vortices will occur in journal bearings at values of Reynolds' number that range from about 750 for a clearance ratio (C/R) of 0.003 inches per inch, to about 1300 for a clearance ratio of 0.001 inches per inch. Thus, except in cases where bearings with excessively large clearance ratios are used, the region where Taylor vortices occur without developed turbulence in the fluid film is quite small. All the turbulent lubrication analysis, which is the basis of the calculated bearing data which will be presented, presumes fully developed turbulence in the fluid film.

In classical analysis of fluid film bearings, it is assumed that the lubricant flow in the clearance spaces is laminar. This is generally true of conventional bearings which have small clearance (of the order of 10^{-3} in./in.) and which are lubricated with hydrocarbon oils whose kinematic viscosity is high (of the order of 10^{-2} to 10^{-1} in^2/sec). The situation is quite different in the case of high-speed rotating machinery lubricated with liquid metals or other low kinematic viscosity lubricants. The combination of low kinematic viscosity and high operating speed results in superlaminar flow in the bearing film. This is illustrated in Table I, which shows the speed at which transition to turbulence should occur for a lightly loaded 4 inch diameter plain journal bearing. The onset of turbulence is taken to occur when the fluid film Reynolds' number reaches 1500.

When operating with low viscosity lubricants, the low friction advantage of the floating-ring bearing is enhanced by the fact that rotation of the ring results in lower inner film Reynolds' numbers than would be the case for a plain cylindrical bearing with the same clearance as the floating-ring bearing inner film clearance.

TABLE I

COMPARISON OF ESTIMATED SPEEDS FOR ONSET OF TURBULENCE USING VARIOUS LUBRICANTS[a,b]

Lubricant	Kinematic Viscosity (in^2/sec)	Speed for Onset of Developed Turbulence, RPM
Water (80 F)	1.33×10^{-3}	2,700
SAE 10 Oil (150 F)	2.16×10^{-2}	60,200
Potassium (1200 F)	3.31×10^{-4}	920
Sodium (1200 F).	3.86×10^{-4}	1,072
Silicone Oil (0.65 cs) . . .	1.01×10^{-3}	2,820
Air (80 F and 15 psia) . . .	2.52×10^{-2}	70,400
Mercury (400 F).	1.2×10^{-4}	336

[a] Bearing diameter = 4.0 inches, C_1/R_1 = 0.0015.

[b] These values are computed for concentric, plain journal bearings.

PART I

ANALYSIS AND PRESENTATION OF DESIGN DATA

The theoretical analyses for calculation of the steady-state properties (load capacity, friction torque, flow and shaft/ring speed ratio) and the dynamic properties (stiffness and damping coefficients) are described. Calculated design data are given in graphical form for the bearing with L/D = 1 for laminar and turbulent flow (Reynolds' numbers up to 9000) and for values of outer-to-inner film clearance of 0.7 and 1.3.

ANALYSIS FOR CALCULATION OF STEADY-STATE PROPERTIES

The floating-ring bearing is a journal bearing in which there is a loose ring between the shaft and the bearing housing. In this way the fluid film is separated into an inner film and an outer film:

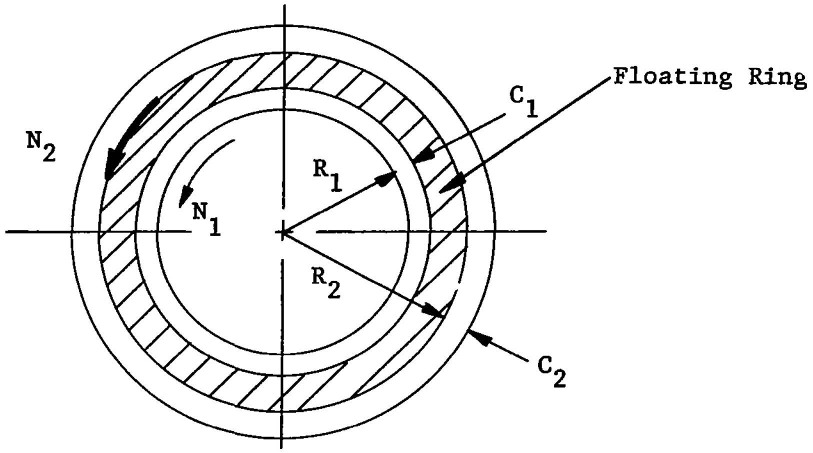

The quantities connected with the inner film are identified by subscript 1 whereas subscript 2 refers to the outer film. The symbols are defined in the Nomenclature.

In order to calculate the load carrying capacity and the friction torque on the shaft, it is necessary to find those positions of the journal center and the ring center, with respect to the bearing center, at which the ring is in steady-state equilibrium. The equilibrium positions are established once the following quantities are known:

1. The eccentricity ratio ϵ_1 and the attitude angle ϕ_1 of the journal center with respect to the center of the ring.

2. The eccentricity ratio ϵ_2 and the attitude angle ϕ_2 of the ring center with respect to the center of the bearing.

3. The ratio between the ring speed, N_2, rps, and the shaft speed, N_1, rps. Denote this ratio as:

$$\alpha = \frac{N_2}{N_1} \tag{2}$$

The equilibrium values of these quantities are determined by making a force balance and a torque balance for the ring. The load on the inner film has to equal the load on the outer film in both magnitude and direction, and the friction torque due to the inner film must equal the friction torque due to the outer film.

The load carrying capacity and the friction torque are calculated from the lubrication equation (Reynolds' equation) by means of a computer, see ref. 7. Each film is calculated separately. The results are obtained in dimensionless form, and the input and output parameters are:

Input Parameters. —

Length-to-diameter ratio: $\frac{L}{D}$ Eccentricity ratio: ϵ

$$\text{Reynolds number:}\quad Re = \frac{2\pi\rho R(N_i - N_o)C}{\mu} \tag{3}$$

$$\text{Dimensionless supply pressure:}\quad P_D = \frac{P_s}{\mu(N_i+N_o)(\frac{R}{C})^2} \tag{4}$$

Output Parameters.—

$$\text{Sommerfeld number:}\quad S = \frac{\mu(N_i+N_o)DL}{W}(\frac{R}{C})^2 \tag{5}$$

$$\text{Average friction factor:}\quad (\frac{R}{C} f)_m \tag{6}$$

$$\text{Dimensionless tangential force:}\quad \bar{F}_t = \frac{F_t}{\mu(N_i+N_o)DL(\frac{R}{C})^2} = \frac{1}{S}\frac{F_t}{W} \tag{7}$$

$$\text{Dimensionless flow:}\quad \frac{Q}{RCL(N_i+N_o)} \tag{8}$$

Attitude angle: ϕ

where:

f = (friction force)/(load)

T = friction torque, lbs in.

N_i = speed at inner surface of film, rps

N_o = speed at outer surface of film, rps

P_s = supply pressure, psig

Q = flow, in^3/sec

Other symbols are given in the Nomenclature.

The dimensionless supply pressure from Eq. (4) can be written:

$$P_D = \frac{P_s}{\mu(N_i+N_o)(\frac{R}{C})^2} = \frac{1}{S}\cdot\frac{P_sDL}{W} \tag{9}$$

The dimensionless supply pressure P_D must be given as input to the computer calculation but once the results of the calculation are available, P_D can be replaced by P_sDL/W from Eq. (9).

For a given length-to-diameter ratio, L/D, the computer program is used to generate results for a wide range of ϵ, Re and P_D. Making use of Eq. (9), the results (i.e., S, $\frac{R}{C}f$, $\overline{F}_t$ and $\frac{Q}{RCL(N_i+N_o)}$) are plotted as a function of P_sDL/W for each value of ϵ and Re. Then, for a chosen value of P_sDL/W, a table can be constructed which gives S, $\frac{R}{C}f$, $\overline{F}_t$ and $\frac{Q}{RCL(N_i+N_o)}$ as functions of ϵ and Re. Similar tables can be obtained for other values of P_sDL/W. In this way the results in each table are functions of only two variables, namely ϵ and Re, thus facilitating the interpolation required in calculating the floating-ring bearing.

The parameters defining the operating conditions for the complete floating-ring bearing are chosen as:

$$\left.\begin{array}{ll}
\text{Sommerfeld number:} & S_s = \frac{\pi\mu N_1 D_1 L}{W}\left(\frac{R_1}{C_1}\right)^2 \quad (10)\\[2ex]
\text{Reynolds' number:} & Re_s = \frac{2\pi\rho R_1 N_1 C_1}{\mu} \quad (11)\\[2ex]
\text{Supply pressure parameter:} & \frac{P_s D_1 L}{W} \\[2ex]
\text{Friction factor:} & \left(\frac{R_1}{C_1}f\right)_s = \frac{T_s}{WC_1} \quad (13)\\[2ex]
\text{Dimensionless flow:} & \frac{Q}{R_1C_1LN_1} \quad (14)
\end{array}\right\}\text{Floating-Ring Bearing} \quad (12)$$

It is seen that the parameters are all based on the dimensions of the inner film and the shaft speed.

Referring to the schematic at the beginning of this section, and Eqs. (2) through (8), the dimensionless parameters for the two films become:

Inner film.—

Sommerfeld number:

$$S_1 = \frac{\mu(N_1+N_2)D_1L}{W}\left(\frac{R_1}{C_1}\right)^2 = (1+\alpha) \cdot S_s/\pi \tag{15}$$

Reynolds' number:

$$Re_1 = \frac{2\pi\rho R_1(N_1-N_2)C_1}{\mu} = (1-\alpha)\ Re_s \tag{16}$$

Supply pressure parameter:

$$\frac{P_sD_1L}{W} \tag{17}$$

Average friction factor:

$$\left(\frac{R_1}{C_1}f\right)_{m1} \tag{18}$$

Dimensionless tangential force:

$$\bar{F}_{t1} = \frac{1}{S_1}\frac{\bar{F}_{t1}}{W} \tag{19}$$

Dimensionless flow:

$$\frac{Q_1}{R_1C_1LN_1(1+\alpha)} \tag{20}$$

Outer film.—

Sommerfeld number:

$$S_2 = \frac{\mu N_2D_2L}{W}\left(\frac{R_2}{C_2}\right)^2 = \alpha \cdot \left(\frac{R_2}{R_1}\right)^3\left(\frac{C_1}{C_2}\right)^2 S_s/\pi \tag{21}$$

Reynolds number:

$$Re_2 = \frac{2\pi\rho R_2 N_2 C_2}{\mu} = \alpha \left(\frac{R_2}{R_1}\right) \cdot \left(\frac{C_2}{C_1}\right) Re_s \tag{22}$$

Supply pressure parameter:

$$\frac{P_s D_2 L}{W} = \left(\frac{R_2}{R_1}\right) \cdot \frac{P_s D_1 L}{W} \tag{23}$$

Average friction factor:

$$\left(\frac{R_2}{C_2} f\right)_{m2} \tag{24}$$

Dimensionless tangential force:

$$\bar{F}_{t2} = \frac{1}{S_2} \frac{F_{t2}}{W} \tag{25}$$

Dimensionless flow:

$$\frac{Q_2}{R_2 C_2 L N_2} = \frac{1}{\alpha} \left(\frac{R_1}{R_2}\right) \left(\frac{C_1}{C_2}\right) \cdot \frac{Q_2}{R_1 C_1 L N_1} \tag{26}$$

The two films are combined into the composite floating-ring bearing by means of a force balance and a torque balance for the ring. The force balance expresses that the load on either side of the ring is the same and equal to W. The corresponding equation is obtained by eliminating S_s between Eqs. (15) and (21) to get:

Force balance:

$$S_2 = \frac{\alpha}{1+\alpha} \left(\frac{R_2}{R_1}\right)^3 \left(\frac{C_1}{C_2}\right)^2 S_1 \tag{27}$$

It should be noted that it is only necessary to take a force balance in the direction of the applied load ("the vertical direction"). The force balance in the perpendicular direction ("the horizontal direction") is automatically satisfied through the method employed in computing the previously mentioned computer results where the horizontal force is set equal to zero. This requirement is actually used to determine the attitude angle.

Let the friction torque be denoted as T. Then, the torques on the shaft and on the ring, determined from the lubrication equation, can be expressed in dimensionless form by:

Torque on shaft:

$$\left(\frac{R_1}{C_1}f\right)_s = \frac{T_s}{WC_1} = \frac{1-\alpha}{1+\alpha}\left(\frac{R_1}{C_1}f\right)_{m1} + \frac{1}{2}\, S_1\, \epsilon_1\, \bar{F}_{t1} \tag{28}$$

Torque on inside of ring:

$$\frac{T_1}{WC_1} = \frac{1-\alpha}{1+\alpha}\left(\frac{R_1}{C_1}f\right)_{m1} - \frac{1}{2}\, S_1\, \epsilon_1\, \bar{F}_{t1} \tag{29}$$

Torque on outside of ring:

$$\frac{T_2}{WC_2} = \left(\frac{R_2}{C_2}f\right)_{m2} + \frac{1}{2}\, S_2\, \epsilon_2\, \bar{F}_{t2} \tag{30}$$

A torque balance requires: $T_1 = T_2$ or, by using Eqs. (29) and (30):

Torque balance:

$$\frac{1-\alpha}{1+\alpha}\left(\frac{R_1}{C_1}f\right)_{m1} - \frac{1}{2}\, S_1\, \epsilon_1\, \bar{F}_{t1} - \frac{C_2}{C_1}\left[\left(\frac{R_2}{C_2}f\right)_{m2} + \frac{1}{2}\, S_2\, \epsilon_2\, \bar{F}_{t2}\right] = 0 \tag{31}$$

The simultaneous solution of the force balance, Eq. (27) and the torque balance, Eq. (31), yields the complete solution for the floating-ring bearing. However, a direct solution is not possible since the various parameters involved are quite complex functions and are only available in numerical form, given by tables as previously mentioned. Instead, the solution is obtained by an iteration procedure employing interpolation as outlined below:

Computational procedure. –

1. The length-to-diameter ratios: L/D_1 and L/D_2 are known. This allows calculating the Sommerfeld number, the friction factor, the dimensionless tangential force and the dimensionless flow for both films over a range of eccentricity ratios, Reynolds' numbers and dimensionless supply pressures. The calculations are performed with a computer program which solves the lubrication equations, see ref. 7.

2. The dimensions of the bearing are given, i.e., the following values are known: (a) the radius ratio: R_2/R_1 and (b) the clearance ratio: C_2/C_1.

3. The supply pressure is given. Calculate the supply pressure parameters for the inner and outer film from Eqs. (17) and (23). Use the values in combination with the previously obtained computer results to generate tables for the Sommerfeld number, the friction factor, etc. for both films as functions of the eccentricity ratio and the Reynolds' number (i.e., the dimensionless supply pressure has been eliminated as a variable). Thus, to use the tables requires two entries. The tables are set up such that the entries are ϵ and Re for the inner film, and S and Re for the outer film. Interpolation is employed for intermediate values.

4. Select a value of the Reynolds' number Re_S for the complete bearing (Eq. (11)).

5. Select a value of the eccentricity ratio ϵ_1 for the inner film.

6. Estimate a value of the speed ratio $\alpha = N_2/N_1$.

7. Calculate the Reynolds' number Re_1 for the inner film from Eq. (16) with the known values of Re_s and α. Enter the table with ϵ_1 and Re_1 and interpolate to find S_1, $(\frac{R_1}{C_1} f)_{m1}$ and $\bar{F}_{t1}$.

8. Calculate the Reynolds' number Re_2 from Eq. (22) and the Sommerfeld number S_2 from Eq. (27), both pertaining to the outer film.

9. Enter the table for the outer film with the known values of S_2 and Re_2 to determine ϵ_2, $(\frac{R_2}{C_2} f)_{m2}$ and $\bar{F}_{t2}$.

10. Calculate the left-hand side of Eq. (31) and call the thus obtained value Δ. If Δ is not zero as required, choose a new value of the speed ratio α and repeat steps 7 through 10. In this way Δ can be obtained as a function of α and that value of α for which Δ becomes zero, can be determined accurately.

11. Once the correct value of α has been established, the governing parameters for both the inner and the outer film are known corresponding to the assigned values of the Reynolds' number Re_S for the complete bearing and the original value of the eccentricity ratio ϵ_1 for the inner film. Hence, the remaining dimensionless parameters for the complete bearing can be calculated:

Sommerfeld number:

$$S_s = \frac{\pi}{1+\alpha} \cdot S_1 \quad \text{(from Eq. (15))}$$

Friction factor for shaft:

$$\left(\frac{R_1}{C_1}f\right)_s \qquad \text{(from Eq. (28))}$$

Dimensionless flow for complete bearing:

$$\frac{Q}{R_1C_1LN_1} = (1+\alpha)\left[\frac{Q_1}{R_1C_1L(N_1+N_2)}\right]_{\substack{\text{inner}\\ \text{film}}} + \left(\frac{R_2}{R_1}\right)\left(\frac{C_2}{C_1}\right)\left[\frac{Q_2}{R_2C_2LN_2}\right]_{\substack{\text{outer}\\ \text{film}}} \qquad (32)$$

Repeat the calculations for several values of ϵ_1, Re_s and $\frac{P_sD_1L}{W}$

The computed results can be presented in form of design charts. The bearing Sommerfeld S_s is used as abcissa and charts can be made for the speed ratio α, the shaft friction factor, the dimensionless bearing flow and the eccentricity ratios for the two films. The charts contain curves for several values of the Reynolds' number Re_s and each chart is valued for specified values of the supply pressure parameter, the radius ratio R_2/R_1, the clearance ratio C_2/C_1 and the length-to-diameter ratio of the bearing.

ANALYSIS FOR CALCULATION OF DYNAMIC PROPERTIES

The stiffness and damping characteristics of the fluid film in a bearing are used to express the relationship between an imposed dynamic force and the resulting amplitudes and velocities of the journal motion. Let the static load direction be the x-axis and the perpendicular direction be the y-axis. The origin of the coordinate system is located at the steady-state position of the journal center. For a particular bearing, this position is a function of the Sommerfeld number and the Reynolds' number (i.e., it changes with load and speed) and for each position there is a set of fluid film spring and damping coefficients. Hence, for a given bearing configuration and oil supply pressure, the coefficients are functions of the Sommerfeld number and the Reynolds' number. In total there are eight coefficients, namely four spring coefficients, K_{xx}, K_{xy}, K_{yx}, K_{yy} and four damping coefficients B_{xx}, B_{xy}, B_{yx}, B_{yy}. The first index specifies the force direction and the second index gives the direction of the motion. Thus, if the dynamic force has the components F_x and F_y, the relationship between force and motion may be written:

$$F_x = -K_{xx}x - B_{xx}\dot{x} - K_{xy}y - B_{xy}\dot{y} \qquad (33)$$

$$F_y = -K_{yx}x - B_{yx}\dot{x} - K_{yy}y - B_{yy}\dot{y} \qquad (34)$$

The eight dynamic coefficients are calculated from the lubrication equations by means of a computer, see Ref. 9. They are obtained in dimensionless form as:

$$\frac{CK_{xx}}{W}, \frac{CK_{xy}}{W}, \frac{CK_{yx}}{W}, \frac{CK_{yy}}{W}, \frac{C\omega B_{xx}}{W}, \frac{C\omega B_{xy}}{W}, \frac{C\omega B_{yx}}{W} \text{ and } \frac{C\omega B_{yy}}{W}$$

where C is the radial clearance for the film, W is the load and ω is the angular speed in radians/sec.

In the floating-ring bearing there are two fluid films: the inner film between the shaft and the ring, and the outer film between the ring and the bearing housing. The inner film clearance is denoted as C_1 and the clearance for the outer film is C_2. The shaft speed is N_1 rps and the ring speed is N_2 rps. From lubrication theory it is found that the angular speed used in calculating the inner film is $(\omega_1 + \omega_2) = 2\pi(N_1 + N_2)$; whereas for the outer film the angular speed is $\omega_2 = 2\pi N_2$.

It is desirable to combine the dynamic characteristics of the two films in order to determine the eight dynamic coefficients for the complete floating-ring bearing. Thus, if the shaft moves in synchronous whirl with the frequency ω_1 radians /sec and with amplitude components $\bar{x}_1 e^{i\omega_1 t}$, it is desired to express the dynamic forces in the same form as Eqs. (33) and (34);

$$\frac{F_x}{W} = -\left(\frac{C_1K_{xx}}{W} + i\,\frac{C_1\omega_1B_{xx}}{W}\right)\frac{\bar{x}_1}{C_1}\,e^{i\omega_1 t} - \left(\frac{C_1K_{xy}}{W} + i\,\frac{C_1\omega_1B_{xy}}{W}\right)\frac{\bar{y}_1}{C_1}\,e^{i\omega_1 t} \quad (35)$$

$$\frac{F_y}{W} = -\left(\frac{C_1K_{yx}}{W} + i\,\frac{C_1\omega_1B_{yx}}{W}\right)\frac{\bar{x}_1}{C_1}\,e^{i\omega_1 t} - \left(\frac{C_1K_{yy}}{W} + i\,\frac{C_1\omega_1B_{yy}}{W}\right)\frac{\bar{y}_1}{C_1}\,e^{i\omega_1 t} \quad (36)$$

or in short:

$$\begin{Bmatrix} \frac{F_x}{W} \\ \frac{F_y}{W} \end{Bmatrix} = -\begin{Bmatrix} Z_{xx} & Z_{xy} \\ Z_{yx} & Z_{yy} \end{Bmatrix}\begin{Bmatrix} x_1 \\ y_1 \end{Bmatrix} \quad (37)$$

where:

$$Z_{xx} = \frac{C_1K_{xx}}{W} + i\,\frac{C_1\omega_1B_{xx}}{W} \qquad \text{(analogous for } Z_{xy}, Z_{yx}, Z_{yy}\text{)} \quad (38)$$

$$x_1 = \frac{\bar{x}_1}{C_1} e^{i\omega_1 t} \tag{39}$$

$$y_1 = \frac{\bar{y}_1}{C_1} e^{i\omega_1 t} \tag{40}$$

Let the center of the ring have whirl amplitudes $\bar{x}_2 e^{i\omega_1 t}$ and $\bar{y}_2 e^{i\omega_1 t}$ and let:

$$x_2 = \frac{\bar{x}_2}{C_1} e^{i\omega_1 t} \tag{41}$$

$$y_2 = \frac{\bar{y}_2}{C_1} e^{i\omega_1 t} \tag{42}$$

The dimensionless dynamic coefficients for the inner and outer film are obtained in the form:

Inner film:

$$\frac{C_1 K_{xx1}}{W}, \quad \frac{C_1(\omega_1 + \omega_2) B_{xx1}}{W}, \text{ etc} \tag{43}$$

Outer film:

$$\frac{C_2 K_{xx2}}{W}, \quad \frac{C_2 \omega_2 B_{xx2}}{W}, \quad \text{etc} \tag{44}$$

Define:

Inner film:

$$Z_{xx1} = \frac{C_1 K_{xx1}}{W} + i \frac{1}{1+\alpha} \frac{C_1(\omega_1 + \omega_2) B_{xx1}}{W} \tag{45}$$

(similarly for Z_{xy1}, Z_{yx1}, Z_{yy1})

Outer film:

$$Z_{xx2} = \frac{C_1}{C_2} \frac{C_2 K_{xx2}}{W} + i \frac{C_1}{C_2} \frac{1}{\alpha} \frac{C_2 \omega_2 B_{xx2}}{W} \tag{46}$$

(similarly for Z_{xy2}, Z_{yx2}, Z_{yy2})

where:

$$\alpha = \frac{N_2}{N_1}$$

Hence, the dynamic forces acting on the shaft become:

$$\begin{Bmatrix} \frac{F_x}{W} \\ \\ \frac{F_y}{W} \end{Bmatrix} = - \begin{Bmatrix} Z_{xx1} & Z_{xy1} \\ \\ Z_{yx1} & Z_{yy1} \end{Bmatrix} \begin{Bmatrix} x_1 - x_2 \\ \\ y_1 - y_2 \end{Bmatrix} \tag{47}$$

In order to bring Eq. (47) into the same form as Eq. (37) and thereby determine the overall dynamic coefficients it is necessary to eliminate x_2 and y_2 from the equations. This is done by setting up the equations of motion for the ring with mass m:

$$-\frac{C_1 m\omega_1^2}{W} \begin{Bmatrix} x_2 \\ \\ y_2 \end{Bmatrix} = \begin{Bmatrix} Z_{xx1} & Z_{xy1} \\ \\ Z_{yx1} & Z_{yy1} \end{Bmatrix} \begin{Bmatrix} x_1 - x_2 \\ \\ y_1 - y_2 \end{Bmatrix} - \begin{Bmatrix} Z_{xx2} & Z_{xy2} \\ \\ Z_{yx2} & Z_{yy2} \end{Bmatrix} \begin{Bmatrix} x_2 \\ \\ y_2 \end{Bmatrix} \tag{48}$$

or:

$$\begin{Bmatrix} (Z_{xx1} + Z_{xx2} - \frac{C_1 m\omega_1^2}{W}) & (Z_{xy1} + Z_{xy2}) \\ \\ (Z_{yx1} + Z_{yx2}) & (Z_{yy1} + Z_{yy2} - \frac{C_1 m\omega_1^2}{W}) \end{Bmatrix} \begin{Bmatrix} x_1 - x_2 \\ \\ y_1 - y_2 \end{Bmatrix} =$$

$$\begin{Bmatrix} (Z_{xx2} - \frac{C_1 m\omega_1^2}{W}) & Z_{xy2} \\ \\ Z_{yx2} & (Z_{yy2} - \frac{C_1 m\omega_1^2}{W}) \end{Bmatrix} \begin{Bmatrix} x_1 \\ \\ y_1 \end{Bmatrix} \tag{49}$$

Substitute Eq. (49) into Eq. (47) and compare with Eq. (37) to get:

$$\begin{Bmatrix} Z_{xx} & Z_{xy} \\ Z_{yx} & Z_{yy} \end{Bmatrix} = \begin{Bmatrix} Z_{xx1} & Z_{xy1} \\ Z_{yx1} & Z_{yy1} \end{Bmatrix} \begin{Bmatrix} (Z_{xx1} + Z_{xx2} - \frac{C_1 m\omega_1^2}{W}) & (Z_{xy1} + Z_{xy2}) \\ (Z_{yx1} + Z_{yx2}) & (Z_{yy1} + Z_{yy2} - \frac{C_1 m\omega_1^2}{W}) \end{Bmatrix}^{-1}$$

$$\begin{Bmatrix} (Z_{xx2} - \frac{C_1 m\omega_1^2}{W}) & Z_{xy2} \\ Z_{yx2} & (Z_{yy2} - \frac{C_1 m\omega_1^2}{W}) \end{Bmatrix} \qquad (50)$$

Solving for Z_{xx}, Z_{xy}, etc. and using Eq. (38) yields the overall dynamic coefficients for the floating-ring bearing.

In order to perform the calculations it is necessary to have the values of the dynamic coefficients for the inner and outer film (see Eqs. (43) and (44)). They are obtained from a computer program which solves the dynamic lubrication equation but, before using the program it is necessary to know the steady-state operating conditions of the floating-ring bearing, i.e. the eccentricity ratio, the attitude angle, the Reynolds' number and the supply pressure parameter for both the inner and the outer film and also the speed ratio α defining the speed of the ring. This is done by means of the analysis set forth in the preceeding section.

In general the mass of the ring is relatively small such that:

$$\frac{C_1 m\omega_1^2}{W} << \frac{C_2 K_{xx}}{W}$$

in which case it can be ignored in the calculations. This condition applies to all the numerical results given in the present report.

BEARING DESIGN DATA

Calculated design data curves for the steady-state properties of the floating-ring bearing are given in Figs. 2 through 29.

The inner film eccentricity ratio is plotted as a function of bearing Sommerfeld number for each combination of two values of C_2/C_1 (0.7 and 1.3) and three values of supply pressure parameter ($\frac{P_s L D_1}{W}$ = 0.2, 1.5 and 10) in Figs. 2 through 7. Separate curves are given on each graph for laminar flow and shaft Reynolds' numbers of 1000, 5000 and 9000. Once the inner film eccentricity ratio is known, the outer film eccentricity ratio can be determined from the curves of Figs. 8 through 10 for $C_2/C_1 = 0.7$ and Fig. 11 for $C_2/C_1 = 1.3$. There is virtually no effect of Reynolds' number on the eccentricity ratio relationship for $C_2/C_1 = 1.3$ so the curves of Fig. 11 apply to all values of Reynolds' number.

The dimensionless bearing friction is plotted against bearing Sommerfeld number in Figs. 12 through 15. The same curves are given for $\frac{P_s L D_1}{W}$ = 1.5 and 10, since the results are virtually identical for both values.

The ring/shaft speed ratio (N_2/N_1) is given in Figs. 16 through 21.

Dimensionless flow, from which the lubricant supply requirements can be calculated, is plotted against bearing Sommerfeld number in Figs. 22 through 27.

The dimensionless stiffness and damping coefficients for the case of $C_2/C_1 = 0.7$, $\frac{P_s L D_1}{W} = 1.5$ are plotted against eccentricity ratio in Figs. 28 and 29. For a given shaft eccentricity ratio, the effect of Reynolds' number on the dynamic coefficients is small, typically less than 15 percent difference for laminar flow and Re = 5000 for $C_2/C_1 = 0.7$ and $\frac{P_s L D_1}{W} = 1.5$. Therefore, Reynolds' number can be effectively eliminated as a parameter and the presentation and application of the data are made much easier by plotting the coefficients against eccentricity ratio. To use the data it is necessary to determine the inner film steady-state eccentricity ratio for the desired operating conditions from Fig. 4 and then read the coefficients from Figs. 28 and 29. The numerical calculations of dynamic coefficients for the floating-ring bearing are very lengthy so they have so far been obtained only for the one combination of clearance ratio and supply pressure parameter.

PART II

EXPERIMENTAL VERIFICATION OF DESIGN DATA

The dynamic load bearing apparatus and the instrumentation for measurements of floating-ring bearing performance are described. The observed stability characteristics of the test bearing, including a description of the several modes of instability which were encountered and a summary of the effects of bearing design parameters and operating conditions on stability, are given. The calculated and measured steady-state and dynamic performance of the test bearing are compared within the region of stable operation.

DYNAMIC LOAD BEARING APPARATUS

Mechanical Features

This apparatus was designed for the purpose of experimental determination of the static and dynamic properties of journal bearings operating in the laminar or turbulent regimes. The apparatus capabilities include the following:

Bearing Diameter	4.0 inches
Bearing L/D	Up to 1-1/2
Speed	2000 to 11 500 rpm
Static Load	0 to 1000 lb
Dynamic Load	Magnitude depends on speed; load rotational frequency from 2000 to 24 000 rpm in either direction independent of shaft rotation.

The arrangement of the principal mechanical components of the apparatus is shown schematically in Fig. 30. A duplex pair of angular-contact support bearings are at one end of the shaft with the test bearing at the other end. The span between bearings is 40 inches. Static and rotating loads are applied at the test bearing end of the shaft, outboard from the test bearing. Static load is applied through a self-aligning, double-row ball bearing by a cable to which tension is applied by a large, low spring rate (125 lb/in.) coil spring. An upward load, to counterbalance all or part of the shaft weight, can be applied to the same bearing by a spring-type load cell mounted above the shaft. The shaft is shown with a fixed unbalance weight as the rotating load and all of the dynamic load data given here are for synchronous unbalance.

The shaft is of steel tubing (three inches I.D.) with shrink-fitted end sections and is coated with a tungsten carbide cermet in the test bearing area. Test bearing, support bearing, and loader bearing diameters are all concentric within 0.0002 inch TIR. The shaft was balanced, first in a balancing machine and then in place at operating speeds, to approximately 0.08 inch-ounce unbalance. This represents a displacement of the mass center from the geometric center of about 50 microinches. There is very little restraint to shaft motion within a ten mil clearance radius at the test bearing from the support bearings or the drive coupling. The change in upward force required to lift the shaft from bottom to top of such a clearance circle is 1.5 lbs.

Considerable care was taken in the design and fabrication of the apparatus to assure close alignment between test and support bearings. Alignment is checked on each assembly by measuring the squareness of the test-bearing housing face with the shaft axis. The housing face is known to be square with the housing bore within 0.0005 inch on a four-inch radius. There has been no difficulty in maintaining alignment within 0.0003 over the bearing length. Alignment is checked also by comparing the bearing clearance circle dimensions, as measured by the displacement sensors used in the experiments, against the clearance dimensions obtained from separate measurements of bearing, ring, and shaft diameters. These results have been consistent with those obtained from the measurements of squareness of shaft axis and housing face.

The seven and one-half hp variable-speed electric drive is coupled to the support bearing end of the shaft by a dynamically balanced, flexible-disk coupling.

Two lubricants were used in these experiments: a 5.0 cs (77 F) silicone oil with viscosity-temperature coefficient $(1 - \frac{\text{viscosity at 210 F}}{\text{viscosity at 100 F}})$ of 0.55 for laminar flow data, and a 0.65 cs (77 F) silicone oil with viscosity-temperature coefficient of 0.31. Oil is supplied to the test bearing at controlled temperature by a variable-delivery pump. Lubricant returns to the sump by an overflow line which taps into the top of the test bearing housing or by scavenge pumps which drain the cavities outside the clearance seals at either end of the test bearing housing. During operation the housing cavities at either end of the bearing are maintained at atmospheric pressure.

Instrumentation

The following variables must be measured for experimental data or control purposes:

(a) Dynamic motion of the shaft axis at the test bearing and support bearing locations.

(b) Steady-state locus of the shaft axis with respect to the test bearing center.

(c) Static position and dynamic motions of the ring with respect to the bearing.

(d) Shaft speed.

(e) Ring speed.

(f) Static load on test bearing.

(g) Test bearing torque.

(h) Test bearing temperature.

(i) Lubricant flow rate.

The steady-state locus and dynamic motion of the shaft axis are measured by eddy current proximity sensors. (Bentley Nevada Corp. Model D152). At each plane of measurement there are two sensors; one to measure position and motion along the vertical axis and one for the horizontal axis. There are two planes of measurement at the test bearing location (Fig. 1); one at either end of the housing just outside the seal and scavenging rings. The outputs of the two vertical probes, and of the two horizontal probes, at this location are averaged by adding them together using summing amplifiers. This was done to minimize the effects of any shaft bending. Shaft motion was measured at the support bearing location by one pair of probes.

Readout of the shaft locus measurements was by oscilloscope using x-y axis presentation. With this arrangement, the locus of the shaft center is represented as a point whose motion and position within the bearing clearance circle is easily seen. Variable electronic filters set for band-pass operation were used when measuring the response of the shaft to dynamic load. A low-pass operation was needed to eliminate high-frequency fluctuations from the signal caused by magnetic inhomogeneity of the shaft material or stray magnetic fields in the shaft. The high-pass operation eliminates fluctuations due to small amplitude fractional-frequency whirl and is also needed to offset the phase shift in the signal caused by the low-pass operation.

The eddy current proximity sensors are not influenced by the presence, or absence, of silicone oil lubricant in the gap between probe tip and shaft surface. This would not be true of a lubricant which is not a good dielectric. They do experience zero drift with temperature changes. The drift was of the order of .05 percent of the full scale output per degree F. This was not a problem with the shaft position sensors because the probes were in an ambient environment, outside the test bearing housing. During the experiments, frequent checks for zero drift were made by running with zero load so the shaft center should coincide with the bearing center, or, by stopping the shaft quickly after the data at a given speed were complete to see whether the signals return to the levels previously obtained with the shaft bottomed in the bearing clearance.

In connection with the measurements of shaft response to dynamic load, it is necessary to mark or identify the instant when the rotating load is directed along the x-axis and again when it is directed along the y-axis. This is done by magnetic pickups placed on each of these axes to sense the passage of the unbalance weight.

Eddy current proximity sensors were used also to measure the static position and dynamic motions of the ring. Probes were located in the vertical and horizontal planes at each end of the ring (Fig. 1). The outputs of the two probes in either plane can be added together to average out any misalignment or rocking motion,or,either one can be displayed individually on the CRO.

Torque was measured by a strain gage rotary torquemeter coupled into the drive train between the drive motor and the shaft end. Rated capacity of the torquemeter is 200 in-lb. Initially, a commercial null-balance indicator was used for readout and excitation. However, it was found that dynamic fluctuations in torque were not being averaged out properly with this arrangement, so an alternate arrangement was used. Mercury cells were used for excitation, and the output was fed into an electronic filter (SKL Model 308A) set for low-pass operation with a cut-off frequency of several cycles-per-second. In low pass operation, the filter pass band extends to DC. This arrangement gave high sensitivity and extremely good stability and reproducibility of results. The range of variation in the indicated torque for fixed operating conditions for periods of operation of as much as 30 minutes was typically 0.3 in-lb with mean torque values of 10 to 40 in-lbs.

The total torque measured by the torquemeter includes losses in the support and loader bearings, in the clearance seals, and from "windage" for the portion of the shaft which is inside the test bearing housing but which is not enveloped by the test bearing. These superfluous drag losses were determined empirically by making the following modifications to the apparatus:

(1) An externally-pressurized gas-lubricated bearing was substituted for the test bearing to establish support and loader bearing losses for a range of speeds. The gas bearing drag was calculated using Petroff's equation for concentric cylinders and this was subtracted from the total to obtain the correction torques shown in Fig. 31. The effect of load is small and not entirely consistent, so a mean value was used independent of load.

(2) Housing windage and seal ring losses were determined by experiments in which the test bearing end of the shaft was supported by the ball bearing which is normally the static load bearing. A special housing was made which was the same as the test bearing housing except it was thinner by the four-inch section normally occupied by the test bearing. The shaft was run with this housing and the seal rings in place and with lubricant circulating to obtain the seal ring and housing windage drag. The results are shown in Fig. 32. An attempt was made to calculate these losses using the following two approaches: (a) extrapolation of the data on drag between concentric cylinders (ref. 5) to the much higher C/R and Re of the bearing housing, and (b) using data on windage of a rotating cylinder in an infinite body of fluid (ref. 8). The calculated losses using these approaches for 0.65 cs fluid are shown along with the experimental data in Fig. 32. Neither approach was accurate which is not surprising, considering the gross simplifications and extrapolations which were involved. As might be expected, the experimental losses are greater than the calculated results for concentric cylinders and lower than those calculated from windage data.

The shaft speed is measured by a magnetic pickup which senses the passage of a set screw protruding slightly from the shaft surface. The output of the pickup is amplified and supplied to a frequency meter.

Ring speed is measured by means of a shallow spot-face in the ring extension surface which passes under the ring position sensors at one end of the ring. Each time the spot-face passes under the probe, a sharp peak in the probe output voltage results. The frequency of occurrence of the peaks is measured by a frequency meter with a capacitive coupling. The peaks are very brief and sharp so they do not disturb measurements of ring steady-state location and the filters remove them from measurements of ring dynamic motion.

Bearing temperature is measured by a thermocouple mounted flush with the outer bearing surface on the top side about midway between the centerline feed groove and the bearing end. The thermocouple is cemented in place with conductive epoxy. The measured bearing temperature is used to establish lubricant viscosity for determination of Sommerfeld and Reynolds' numbers.

Lubricant flow is measured by a float-type flowmeter in the delivery line to the bearing.

STABILITY CHARACTERISTICS OF THE FLOATING-RING BEARING

The range of conditions over which experimental data were obtained with the floating-ring bearing was restricted by fractional-frequency whirl instability. Under certain conditions, there was fractional frequency whirl with a small, well controlled amplitude and for these conditions data were obtained. Under other conditions, the whirl amplitudes immediately became quite large, taking up 0.8 or more of the bearing clearance, and no other data on bearing performance were obtained. Before proceeding with a comparison of experimental data and theoretical performance, it is desirable to describe generally the phenomenon of whirl instability in the floating-ring bearing and review the behavior of the test bearing in this respect, beginning with a general description of the types of instability which were observed, followed by a discussion of the effects of design and operating variables on test bearing behavior.

General Description of Whirl in the Test Bearing

Because there are two separate bearing films, whirl instability in the floating-ring bearing may take several different forms. The most common type of whirl encountered in the experiments is a circular orbit of the shaft within the ring while the ring remains stable. The frequency of the shaft whirl is from 0.6 to 0.7 times shaft synchronous frequency or about half the sum of the shaft and ring speeds. Figure 33 shows an oscilloscope photograph of the motion of the shaft when the inner film is unstable and the outer film is stable. The once-per-revolution shaft markers appear about every 220 degrees on the orbits showing an orbit frequency of about 0.6 times synchronous. The reason for this whirl frequency can be seen from a somewhat simplified representation of the whirl instability phenomenon. Referring to the sketch below, the shaft and ring are both rotating with frequencies N_1 and N_2 respectively. If the shaft center is stationary, lubricant is forced into the converging section leading to the point of minimum film thickness with a mean velocity closely proportional to $(N_1 + N_2)/2$ and this action is responsible for the load carrying capacity of the bearing.

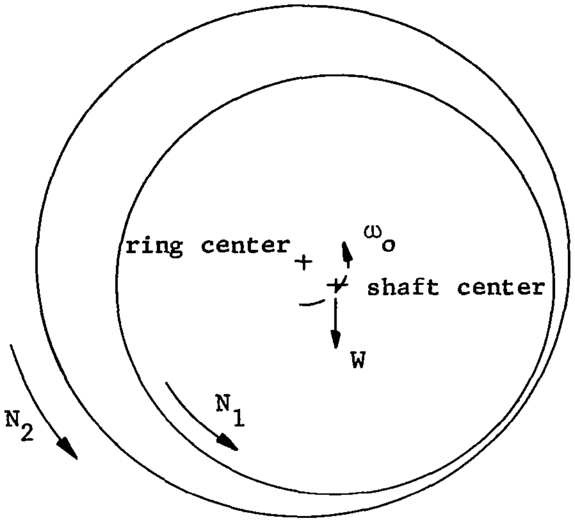

There will be no net flow in the film, and no load capacity, if the shaft center moves in such a way that the point of minimum film thickness moves around the bearing at the same speed as the mean lubricant film velocity. Thus, when the shaft center begins to move in the ring so the whirl frequency (ω_o) is about $\frac{N_1 + N_2}{2}$, there is no restoring force and, if damping is ignored, the orbit radius should rapidly increase until the surfaces contact.

Actually, there were no observed instances where the shaft and ring surfaces actually contacted although the speed was frequently increased to as much as twice the speed at which whirl began. Restoring or restraining forces can be generated by squeeze film or damping action. This explanation applies if the orbit center is not coincident with the bearing center, since the minimum film thickness then varies with angular position about the orbit center. This, or other restraining effects, were sometimes very effective with the floating-ring bearing so that under some conditions the orbit diameter would not become larger than 0.2 or 0.3 times the inner film clearance; and as speed was increased, the orbit would grow smaller until it was no longer distinguishable. This situation is illustrated by the sequence of photos of shaft motion in Fig. 34. These were obtained by multiple exposures with the orbit center shifted along the horizontal axis for each succeeding exposure by using the oscilloscope horizontal position adjustment. At 4700 rpm (orbit at extreme left) the shaft was stable and the shaft locus is a point. Whirl onset speed is 5000 rpm and maximum amplitude occurred at about 5050 rpm. At 6000, 7800, and 9000 rpm the orbit had become progressively smaller until there was no distinguishable motion. Under other conditions which would be expected to result in lower damping, such as increasing C_2/R

and using lower viscosity lubricant, the whirl orbit would grow to about 0.8 times the inner film clearance almost immediately and would remain about the same size in spite of subsequent increases in speed up to as much as 2.5 times the whirl onset speed.

Sometimes the outer film would become unstable and the ring would orbit in the bearing clearance at about half the ring rotational speed. Generally, this occurred when the inner film was also unstable resulting in complex shaft center motion patterns such as those shown in Fig. 35. The oscilloscope photographs which are shown were taken in a sequence with increasing shutter exposure times to show the development of the pattern. There are nearly circular orbits of a frequency of about 0.6 times synchronous (the once-per-revolution markers on the trace appear about every 220 degrees on the orbits). The locus of the centers of these orbits is also a circle, the ring orbit in the bearing, with a much lower frequency (there are about seven inner film orbits and 12 once-per-revolution markers during one low frequency orbit). Increasing speed beyond the onset speed for combined inner-outer film whirl had no noticeable effect on the amplitudes of motion.

There were several occasions when the outer film was unstable while the inner film was stable. When this happened, the ring whirl amplitudes were always small and well controlled. Figure 36a shows the ring motion under these conditions with no rotating load (the orbit frequency is half the ring speed) and Fig. 36b shows the shaft motion. Figs. 36c and 36d show the ring and shaft motions respectively when there was a rotating load. There is a large half-frequency orbit with a small synchronous loop for the ring motion and small loops, presumably due to the ring whirl, superimposed on the larger synchronous motion of the shaft center.

Stability Performance of the Test Bearing

As would be expected, the whirl instability characteristics of the floating-ring bearing varied for the two values of C_2/C_1 and with the lubricant viscosity. The following briefly describes the experimental observations:

C_2/C_1 = 0.7, 5.0 cs lubricant (laminar flow): —

(1) Inner film whirl amplitudes were always small (about 0.2 times the clearance) and increasing speed would suppress whirl.

(2) Whirl began at about the same value of S_s for different combinations of load and speed as follows:

$$\frac{P_s L D_1}{W} = 10; \text{ whirl onset at about } S_s = 2.0$$

$$\frac{P_s L D_1}{W} = 1.5; \text{ whirl onset at about } S_s = 3.5$$

An appreciation for the speed-load combinations which these values of S_s represent can be had from the following:

$$S_s = \frac{0.203\ N\ (\mathrm{rpm})}{W(\mathrm{lb})} \quad \text{for 5.0 cs lubricant}$$

and

$$S_s = \frac{0.0264\ N\ (\mathrm{rpm})}{W(\mathrm{lb})} \quad \text{for 0.65 cs lubricant.}$$

$C_2/C_1 = 0.7$, 0.65 cs lubricant (turbulent flow):-

(1) Inner film whirl amplitudes grew rapidly to 0.7 to 0.8 times the inner clearance and remained about constant with increased speed.

(2) Limiting S_s for whirl onset not as clearly defined as with high viscosity lubricant, but in general onset occurred at about $S_s = 0.7$ except at low speeds, below about 3000 rpm, where the S_s at onset was more nearly 1.5.

$C_2/C_1 = 1.3$, 5.0 cs lubricant (laminar flow):-

Whirl behavior varied considerably depending on value of $\frac{P_s L D_1}{W}$ as follows:

(1) $\frac{P_s L D_1}{W} = 10$: Inner film whirl of large amplitude beginning at S_s very close to the lowest S_s for maintenance of a hydrodynamic outer film, e.g. $S_s \approx 1.0$. Very narrow range of bearing operation within the limits of outer film load capacity and without inner film whirl.

(2) $\frac{P_s L D_1}{W} = 1.5$: Inner film whirl of moderate amplitude (about 0.5 times clearance) beginning at S_s of about 3.0. Simultaneous inner and outer film whirl at high speeds, usually beginning about $S_s = 4.5$.

(3) $\frac{P_s L D_1}{W} = 0.75$: Limited operation under these conditions gave outer film whirl of small amplitude with stable inner film beginning about $S_s = 4.0$.

$C_2/C_1 = 1.3$, 0.65 cs lubricant (turbulent flow): - Inner film whirl of large amplitude beginning at values of S_s just above the minimum S_s for maintenance of outer film. Virtually no whirl-free operating range within the load capacity of the outer film.

From the preceding description of the stability characteristics of the test bearing, it is clear that instability of the floating-ring bearing is a complex, many-faceted phenomena. In the absence of a general analysis which describes the interrelationships among the many design and operating variables, the observations cannot be extrapolated to general design with any confidence. Recognizing this, the following are offered as suggestive, but not conclusive, statements on the stability characteristics of the plain-cylindrical, pressure-fed, floating-ring bearing:

(1) The usual design analysis criterion for stability; the operating condition boundaries for onset of fractional-frequency whirl, is not very meaningful for the floating-ring bearing. The bearing is nearly always subject to whirl at comparatively low speeds, but the whirl amplitudes can be small and well-controlled. When the whirl is well controlled, speed can be raised far beyond the whirl onset speed and the whirl will either be suppressed or the amplitude will not increase.

(2) Extremely low viscosity lubricants have an adverse effect on stability. Obviously, this is not encouraging for application of the plain-cylindrical ring bearing to liquid-metal lubricated applications.

(3) Increasing C_2/C_1 from 0.7 to 1.3, at least when this is done by increasing C_2, has an adverse effect on stability. This, together with the observation on the effect of lubricant viscosity, suggest that it may be desirable to design for high outer film damping.

If the dynamic stiffness and damping coefficients of a bearing are known, it is possible to establish a stability criterion in the form of operating boundaries at which whirl instability should begin (ref. 9). For a particular set of dynamic stiffness $(\frac{C}{W}K)$ and damping $(\frac{C\omega}{W}B)$ coefficients, there will be a particular value of a critical mass parameter, $\frac{C\omega M}{\mu DL(\frac{R}{C})^2}$, below which the system should be stable and above which it should be unstable. The stiffness and damping coefficients vary with Sommerfeld number, Reynolds' number and the design parameters of the bearing such as C_2/C_1, R_1/R_2, and L/D_1. Thus for specified values of $\frac{C_1}{W}K$ and $\frac{C_1\omega_1}{W}B$, all the variables in the critical mass parameter will be fixed except the mass of the rotor supported by the bearing, M. In other words, for a given bearing operating at a specified speed and load, there will be a critical value of rotor mass which must not be exceeded if the system is to remain stable. This is a criterion for onset of instability and experience with liquid-lubricated bearings and especially the floating-ring bearing has shown that frequently they can operate safely at speeds well above the whirl onset speed because the whirl amplitude is well controlled. Therefore, the critical mass criterion is a conservative criterion for design purposes in the case of liquid-lubricated bearings.

As of this time, the critical mass criterion for stability of the floating-ring bearing has not been computed. This is partly because the dynamic coefficients of the floating bearing are available for only one combination of design variables, ($C_2/C_1 = 0.7$, $\frac{P_s L D_1}{W} = 1.5$). Also, as discussed above, the practical significance of a stability criterion based on whirl onset conditions is doubtful for the floating-ring bearing.

STATIC LOAD PROPERTIES OF THE TEST BEARING

The observed stability characteristics of the floating-ring bearing as just described were not encouraging for application of the present, plain cylindrical ring bearing to high-speed,low viscosity, liquid-metal lubricated machines. Nevertheless, experimental measurements of performance were made where permitted by conditions of stable operation or very small whirl amplitudes in order to verify the basic floating-ring bearing theory and because there are many applications with more viscous lubricants in which the bearing should perform very well.

Static Load Capacity

The experimental data which are given, and the theoretical results with which they are compared, are the measured eccentricity of the shaft divided by the sum of the inner and outer film clearance ($\varepsilon_s = \frac{e_s}{C_1 + C_2}$.

The eccentricity of the ring in the bearing was measured also but these results are not given because it became apparent that zero drift of the ring displacement sensors was introducing measurement error which, at times, was nearly half as large as the change in signal equivalent to the outer film clearance. The zero drift was caused by temperature change resulting from the fact that the probes are directly in the path of the lubricant flowing out from the ends of the bearing outer film. The effect on measured dynamic motions of the ring should be too small to seriously affect results since the slope of the voltage-displacement curve changes very little for a substantial zero shift (about ten percent change in slope for a zero shift which is equal to the change in output represented by the outer film clearance).

Measured and calculated load capacities for laminar flow (5.0 cs lubricant) are compared for $\frac{P_s L D_1}{W} = 10$ and 1.5 for the bearing with $C_2/C_1 = 0.7$ in Figs. 37 and 38 and for the bearing with $C_2/C_1 = 1.3$ and $\frac{P_s L D_1}{W} = 1.5$ in Fig. 39.

Agreement between theory and experiment is surprisingly good considering the complexity of the bearing and of its analysis. Certainly it is good enough to conclude that, in this respect at least, the theoretical design data for this bearing can be used effectively. It is assumed that the ratio of inner and outer film eccentricities which make up the total shaft eccentricity are as indicated by the theory. Limited data on ring eccentricity obtained at low speeds where there was no appreciable temperature drift indicated that this was the case. Large amplitude whirl instability limited the data for $C_2/C_1 = 1.3$, $\frac{P_s L D_1}{W} = 1.5$ to eccentricity ratios of about 0.25 and higher and prevented any data from being obtained for $C_2/C_1 = 1.3$, $\frac{P_s L D_1}{W} = 10$. The limiting lubricant supply pressure which could be obtained restricted the data for $C_2/C_1 = 0.7$, $\frac{P_s L D_1}{W} = 10$ to eccentricity ratios of less than about 0.25.

No data are given for $\frac{P_s L D_1}{W} = 0.2$ because, within the limits of load capacity of the test bearings, the bearing operated in a starved lubricant supply condition with this value of supply pressure parameter. Starvation occurs when the flow into the bearing becomes less than the side leakage flow from the region of positive film pressures. When this happens, the angular extent of the full film is shortened until the flows balance. Since the full film does not extend over the full theoretical arc of positive pressure generation for the bearing operating conditions, the measured attitude angle will be lower, the eccentricity will be higher, and the flow will be less than the corresponding theoretical values. The situation was obvious in the experiments because increasing speed resulted in lower attitude angle and nearly constant eccentricity. Starvation can be desirable since it is very effective in stablizing the bearing, because of the reduced attitude angle. However, it is a risky way of accomplishing this because any variation in supply pressure could cause sudden, catastrophic whirl and because bearing film temperatures rise very rapidly at high speeds due to the low flow.

Experimental results with comparable theoretical curves for static load capacity in the turbulent regime (0.65 cs lubricant) are given in Fig. 40. The results are given in dimensional form in order to indicate the changes in conditions for whirl onset with variation in load and supply pressure parameter. Again, agreement between measured and calculated load capacities is very good. There are no results for $C_2/C_1 = 1.3$ because of large amplitude whirl over nearly the entire range of conditions within the outer film load capacity.

Measured and calculated attitude-angle/eccentricity relationships for the case of $C_2/C_1 = 0.7$, $\frac{P_s L D_1}{W} = 1.5$ are compared in Fig. 41. The Reynolds' numbers for the data points in the turbulent flow regime are given by numerals adjacent to each data point. Both theory and experiment indicate a small effect of Reynolds' number on attitude angle for a given eccentricity. Agreement between theory and experiment is good, but not as good as the agreement in static load capacities. This is the usual situation and it is probably caused partly by lower accuracy in attitude angle measurements than in eccentricity measurements. Results for $C_2/C_1 = 0.7$, $\frac{P_s L D_1}{W} = 10$ are given in Fig. 42. The higher supply pressure results in a considerably higher attitude angle which accounts for the lower stability limits for $\frac{P_s L D_1}{W} = 10$ than were obtained for $\frac{P_s L D_1}{W} = 1.5$. Attitude-angle/eccentricity results for $C_2/C_1 = 1.3$, $\frac{P_s L D_1}{W} = 1.5$ are given in Fig. 43. The increase in ratio of clearance results in a higher attitude angle for a given eccentricity ratio and, again, this is consistent with the lower stability limits.

Bearing Friction and Ring Speed

To arrive at a measurement of bearing torque, corrections for support and loader bearing drag, and for drag in the seals and from the areas inside the test bearing housing but outside the bearing were made. The determination of these losses has been described in the section on apparatus. Measured and calculated test bearing friction torques are presented in dimensionless form in Fig. 44 for the case of $C_2/C_1 = 0.7$, laminar flow, and Fig. 45 for $C_2/C_1 = 0.7$, turbulent flow. The Reynolds' numbers are indicated by numerals for the turbulent flow data points. Agreement between theory and experiment is good, especially for laminar flow. There is virtually no effect of the supply pressure parameter on the theoretical results for bearing torque, and experimental data also show no discernible effect. Friction data and theory for the $C_2/C_1 = 1.3$ bearing for laminar flow is given in Fig. 46 and, again, the agreement is good.

Friction torques for the floating-ring and tilting-pad bearings are compared in a later section of this report. The level of turbulence has a strong effect on torque. This is illustrated by the design data curves which, for constant Sommerfeld number, show values of torque at Re = 9000 which are about 4 times the values for laminar flow.

Friction torque of the floating-ring bearing is related to the equilibrium ring speed, since this is determined by a balance between inner and outer film drags on the ring. The measured ring speeds were consistently lower than the calculated values with the differences ranging from 10 to about 20 percent. This is illustrated by the results given in Figs. 47 to 49. The apparent reason for the discrepancy is the fact that the theory considers only the shear forces transmitted to the ring by the inner and outer bearing films while, in fact, there are also drag losses from the ends of the ring. These end losses are probably larger in the test bearing, which has elongated end sections for measurement purposes, than they would be in the usual design with ends at the outer edges of the films. The decreased ring speed should be reflected by a proportionate increase in bearing torque. A change in torque of this magnitude is of the same order as the experimental scatter so it is not obvious in the results. The measurements indicated stable, constant velocity ring rotation for all operating conditions and with both values of C_2/C_1. There was a small (about 10 percent) reduction in ring speed when a condition of onset of outer film whirl instability was reached. Aside from this, there was no evidence of the irregularity in ring speed mentioned by Shaw and Nussdorfer for values of C_2/C_1 greater than 1.0.

Flow Rate

Measured and calculated lubricant flow rates are compared in Figs. 50 through 52. Again, the agreement is good. The flow is quite sensitive to Reynolds' number; increasing Reynolds' number from laminar to 5000 halves the flow rate for constant S_s. This effect can be important for it increases greatly the pumping power which must be expended in maintaining adequate flow for cooling through the bearing at high levels of turbulence.

DYNAMIC PROPERTIES OF THE TEST BEARING

The theoretical response motion of the shaft to a rotating unbalance load when supported by the floating-ring test bearing will be an elliptical orbit since the bearing dynamic properties vary with the instantaneous angular position of the shaft center. The forces acting on the shaft are shown together with a typical shaft center locus path in Fig. 53. The forces involved are the rotating unbalance or exciting force, the oil film elastic and damping forces, and the rotor inertia force which is directed at the local center of curvature of the locus path. For a given exciting force magnitude and frequency and effective shaft mass, the shaft center locus path will depend on the oil film forces, as determined by the bearing spring and damping coefficients. If there are sufficient independent data points, the bearing coefficients can be determined from simultaneous measurements of instantaneous shaft center locus, and the instantaneous force applied to the bearing through summation of forces as follows:

$$K_{xx}y + K_{xy}y + B_{xx}\dot{x} + B_{xy}\dot{y} = -F_x + F_o$$

$$K_{yy}y + K_{yx}x + B_{yy}\dot{y} + B_{yx}\dot{x} = -F_y$$

where K and B are the fluid film stiffness and damping coefficients respectively; F_o is the static load and F_x and F_y are the dynamic force components (the x coordinate is the static load direction and the y coordinate is the direction normal to the static load). Eight independent data points are required for such a determination and just four independent data points can be obtained from a single response orbit (a change in rotating load magnitude or in the direction of shaft rotation does not yield an independent response orbit). Since direct experimental determination of the bearing dynamic coefficients is not feasible for this reason, the most straightforward and practical way of comparing experimental and theoretical dynamic properties of the test bearing is to compare measured and calculated response orbits. The theoretical stiffness and damping coefficients of the test bearing are used as input to a rotor dynamics analysis of the test apparatus which calculates the theoretical response orbit for a given unbalance, speed and static load.

The analysis is described in detail in Appendix A, which is taken from Ref. 13. It makes use of an equivalent bearing-rotor system in which the shaft is assumed to be rigid and the eight bearing coefficients are reduced to four effective coefficients by lumping the direct and cross coupling terms. A rotor dynamics computer program which includes the effects of shaft and pedestal flexibility and which can be used with bearings having cross coupling coefficients is available (ref. 10), but it is cumbersome to use and the assumption of a rigid shaft was not regarded as a serious deficiency in an analysis of the test apparatus which has a very stiff shaft (free-free natural frequency is above 40 000 cpm). The rotor dynamics program also computes the experimental response orbit from measurements of the x and y coordinates of two points on the orbit at which the rotating load is in a known direction (the points on the orbit indicated by the signals from the magnetic pickups which mark the passage of the unbalance weight). The comparison of theoretical and experimental response orbits amounts to a verification of the theoretical bearing coefficients by a procedure in which the theoretical data are used to perform a design analysis of the test apparatus, which is then compared with experimental performance.

Response to Dynamic Load

The effects of rotating unbalance on the shaft locus within the floating-ring test bearing are illustrated in Fig. 54 in which shaft and ring locus measurements are shown for the same operating conditions with and without unbalance load. This is a light static load, low-eccentricity, condition and the shaft orbit is nearly circular. Ordinarily, the ellipticity of the orbits become more noticeable at higher eccentricities. The unbalance load is quite high for this speed and the response orbit is larger than the normal limit for data collection (orbit diameter about 0.3 times the radial clearance instead of below the usual limit of 0.2). The limitation on response orbit amplitudes was normally applied to maintain linearity between exciting force and response orbit amplitudes and to avoid transmitting large dynamic forces through the pedestals and support structure. The once-per-revolution marker superimposed on the shaft orbit shows clearly that the orbit frequency is synchronous. The raw experimental data for dynamic load response measurements includes the x and y coordinates of each of two points marked by the breaks in the orbits caused by passage of the unbalance weight past the horizontal or vertical plane. In addition, approximate measurements of the major semi-axis dimension and its inclination from the horizontal axis were obtained to serve as a check on the orbits calculated from the two sets of coordinates.

The synchronous ring orbit shown in Fig. 54 is comparatively unusual. Ordinarily, there was very little, if any, distinguishable, reproducible synchronous response of the ring to unbalance load when lighter unbalances were used. There were ring motions apparently caused by the rotating load, but they were not reproducible, synchronous orbits. In all cases, the ring response motions were much smaller than the shaft motions so the instantaneous variation in eccentricity was mostly within the inner film. The motion of the ring was of similar amplitude and phase angle at both ends indicating a prodominantly translational motion of the ring.

The computer response program calculates the theoretical response orbit and also computes the experimental orbit from the measured x and y coordinates of the two points on the orbit at which the rotating load direction is known. The measured and calculated orbits can be compared by superimposing the experimental and theoretical major and minor axes of the response orbits in the manner illustrated in Fig. 55. The agreement is very good, especially with respect to amplitude of motion. The information of particular interest to the designer of a rotor-bearing system is the maximum shaft vibration amplitude as a function of speed and load. Figures 56 and 57 show experimental response orbit major semi-axis amplitudes with partial comparative theoretical results for the bearing with $C_2/C_1 = 0.7$ and laminar flow (5.0 cs lubricant) and turbulent flow (0.65 cs lubricant) respectively. The comparison between measured and calculated response orbits is incomplete because the bearing dynamic coefficients have not been calculated for the entire range of operating conditions and design variables. Where comparisons are made, the agreement is good which is encouraging evidence that the theoretical dynamic coefficients for the floating-ring bearing are satisfactory for design analysis purposes. Experimental data only, for the bearing with $C_2/C_1 = 1.3$ in the laminar flow regime, is given in Fig. 58.

The experimental data indicate comparatively little effect of static load on the dynamic characteristics of the system. Most of the data points are for conditions which result in steady-state eccentricity ratios of 0.2 or greater and the theoretical stiffness and damping coefficients for $\frac{P_s L D_1}{W} = 1.5$ (Figs. 28 and 29) do not vary strongly with eccentricity ratio above about $\varepsilon = 0.25$.

Critical Speeds

Figure 59 shows the critical speed map of the dynamic load bearing apparatus for a constant support bearing stiffness of 1.35×10^6 lb/in (ref. 11) and allowing the test bearing stiffness to vary as indicated. The first critical speed lies within the operating speed range for the anticipated range of test bearing stiffnesses. Actually, with test bearings, such as the floating-ring bearing, which have four direct and cross-coupling stiffness coefficients, there are no well defined critical speeds. Instead, there are critical speed ranges which encompass the variation in stiffness with direction and the effects of damping in a manner which is not entirely clear. For design analysis purposes, there are several approaches to an investigation of the critical speed characteristics of a rotor-bearing system when the bearings have four stiffness coefficients. The dynamic load response calculations can be performed for the operating speed range to establish speed ranges of large response amplitude thus indicating the critical speed ranges which should be avoided. Another simplier, but less precise, approach is to consider just the direct stiffness coefficients (K_{xx} and K_{yy}) since these seem to define the limits of the critical speed range rather well. This has been done in Fig. 59. The broken lines show the bearing stiffness characteristics as speed is varied for constant load. The intersections of these curves and the first critical speed plot indicate a critical speed range of about 3600 rpm to 5800 rpm. The response data for a nearly comparable condition, Fig. 56, show a response peak in the vicinity of 5000 rpm.

PART III

APPLICATION OF THE FLOATING-RING BEARING TO HIGH-SPEED, LIQUID-METAL LUBRICATED MACHINERY

The merits and drawbacks of the floating-ring bearing for high-speed, liquid-metal lubricated machinery applications are discussed. The performance of the floating-ring and tilting-pad journal bearings for equivalent operating conditions is compared in graphical form.

DISCUSSION OF THE APPLICATION OF FLOATING-RING BEARINGS TO LIQUID-METAL LUBRICATED, HIGH-SPEED MACHINERY

The floating-ring bearing has the advantage of very low power loss. This can be a very significant advantage, especially in smaller space power units where bearing friction is a sizable fraction of net power output. Other advantages favoring the floating-ring bearing include:

(1) Relative simplicity in construction and installation as compared to the tilting-pad or an externally-pressurized bearing.

(2) Low pumping power to maintain an adequate flow of lubricant for cooling because of the double film and low power loss.

(3) High damping results in good capacity for absorbing dynamic load and reducing transmitted vibrations.

The theoretical design data for the plain cylindrical floating-ring bearing have proven to be surprisingly accurate in predicting the static and dynamic performance. Calculated static load capacity, torque, flow and shaft response to dynamic load compare very closely with experimental results. The agreement is definitely encouraging for the application of the theoretical data to design analysis. Addition of a third independent parameter, the supply pressure parameter, to the Sommerfeld and Reynolds' numbers which are usually used in analysis of bearings in the turbulent flow regime, makes the calculation and application of theoretical design data cumbersome. Because the calculations are so lengthy, theoretical dynamic properties have been obtained for only a part of the range of design variables for which static load data are available. Also, the stability analysis which makes use of the dynamic stiffness and damping coefficients to calculate the conditions for onset of fractional-frequency whirl has not been performed. There would be limited purpose for doing so because it has been shown experimentally that information on the degree of control of the whirl orbit amplitude is of considerably greater practical importance with the plain cylindrical floating-ring bearing than knowledge of the whirl onset speed.

The unmodified, plain cylindrical floating-ring bearing cannot be recommended for high-speed, liquid-metal lubricated applications because of probable stability problems. With more viscous lubricants, represented by 5.0 cs silicone fluid,fractional-frequency whirl may occur but the whirl orbit amplitudes are likely to be small and well controlled. However, with very low viscosity lubricants, such as 0.65 cs silicone which was used to simulate liquid metals in these experiments, whirl orbit amplitudes were nearly as large as the bearing clearance. The whirl onset speed can be delayed, and the orbit amplitudes will then be better controlled, if the bearing is run with a relatively heavy static load or if the lubricant supply pressure is reduced to the point of starving the bearing. Neither step is regarded as practically feasible in a high-speed space power machine.

The uniquely low power loss of the floating-ring bearing and its simplicity in construction and application are powerful incentives for further efforts aimed at overcoming the disadvantages of the plain ring bearing. There are a number of modifications of the single-film journal bearing aimed at improved stability which should be effective with the floating-ring bearing also. Examples of such modifications include axial grooving and herringbone grooving (Ref. 14).

In addition to whirl instability, other problems have been identified with the floating-ring bearing. On start-up under static load, there is a tendency for the ring to remain stationary so the outer film does not form. Bearing operation under these conditions was satisfactory, although power loss was high. Ring rotation will begin when the inner film shear drag exceeds the static friction at the ring-bearing contact, so increasing the shaft speed should eventually cause the ring to turn. This was generally, but not always, observed in the experiments within the operating speed range. Sometimes it was necessary to reduce the static load to start the ring. The floating-ring bearing generally operates with lower minimum film thickness than other bearings because the clearance is divided between two films. The implication of low minimum film thickness is low tolerance to dirt and surface irregularities or distortions. However, there are special circumstances with the floating-ring bearing which tend to mitigate this. During operation, the ring is coupled to the shaft and to the bearing only by shear of the inner and outer films respectively. For this reason, either film can be interrupted or break down completely without large, damaging tangential forces resulting at the point of film failure. During the experiments, the load capacity of the outer film was frequently exceeded, so film breakdown occurred and the ring stopped with the bearing under load at high shaft speeds. There was no significant damage to the ring or bearing surfaces and reducing the load would cause the ring to restart with no evident impairment in performance.

There are many possible approaches to achieve greater assurance of ring start-up. One of the simplest is to drill small holes through the ring so lubricant will flow from the loaded area of the inner film across the ring to the outer film to provide some hydrostatic support of the ring load. Once the ring starts, the holes should have very little effect on performance because the pressure distribution in inner and outer films are similar and nearly coincident.

The misalignment which the floating-ring bearing can tolerate is limited by the total clearance dimensions. Much greater misalignment could be accepted if the outer bearing were a segment of a sphere. To do this, the outer housing and bearing would have to be split for assembly but there should be no other serious problems if a large radius of curvature is used. This would also eliminate the need for separate ring axial positioning bearing surfaces.

COMPARISON OF THE PERFORMANCE OF THE FLOATING-RING AND TILTING-PAD BEARINGS

Theoretical analysis and experimental measurements have been made also for the four-pad (80 degree pad arc) tilting-pad bearing (L/D = 1.0, C/R = 3 x 10^{-3} in./in., pivot position = 44 degrees from pad inlet) for the same range of operating conditions with the same apparatus (Ref. 12). Two values of preload coefficient (m = 1 - clearance at the pad pivots/machined clearance of the pads) were used; m = 0 and m = 0.5. The tilting-pad bearing has excellent dynamic characteristics, especially stability, but its friction should be considerably higher than that of the floating-ring bearing, especially at high Reynolds' numbers. The total machined radial clearance (C_p) of the tilting-pad bearing was 6.0 mils compared with 5.1 mils total radial clearance for the floating-ring bearing with C_2/C_1 = 0.7 and 6.9 mils with C_2/C_1 = 1.3. Comparison in performance will be made with the C_2/C_1 = 0.7 bearing because of the poor stability characteristics of the bearing with C_2/C_1 = 1.3. The difference in clearances tends to give some advantage to the tilting-pad bearing with respect to friction and some disadvantage with respect to load capacity and dynamic properties in a dimensional comparison such as will be made here. The comparative data which are given are experimental data in all cases. Agreement between experimental and theoretical performance was good for both bearings.

There are two approaches to a comparison of static load capacity of the two bearings. Figure 60 shows a comparison of steady-state eccentricity ratios (based on shaft eccentricity and total clearance for the floating-ring bearing and pivot clearance for the tilting-pad bearing) for comparable loads as speed was varied. The floating ring bearing appears to be superior from this viewpoint with the preloaded tilting-pad bearing out-performing the same bearing without preload. This comparison can be misleading since the vital factor should probably be the minimum film thickness instead of eccentricity ratio. Minimum film thickness is the more important factor with respect to the effects of foreign debris in the film, geometrical irregularity of the surfaces or effects of misalignment. A comparison based on minimum film thickness (measured at the pivots only of the tilting-pad bearing* and for the outer film of the floating-ring bearing) is given in Fig. 61. The relative merit of the bearings is reversed when film thickness is the criterion since the minimum film thickness of the floating-ring bearing is only about one-fifth the pivot film thickness of the tilting-pad bearing. It should be recognized, though, that the floating-ring bearing can probably withstand considerable ring-bearing surface contact due to overload without serious damage because the ring is coupled to the shaft only by inner film shear forces and operation without ring rotation has been shown to be acceptable.

The friction torque of the two bearings is compared in Fig. 62 for laminar (5.0 cs lubricant) and turbulent (0.65 cs lubricant) conditions. The floating-ring

---

* The minimum film thickness in the tilting-pad bearing normally occurs at the trailing edge of the pad; however, pivot film thickness was chosen for comparison because at very high eccentricities the pivot film thickness is the minimum film thickness and at lower eccentricities foreign debris can pass through the trailing edge minimum film region by tipping the pad. Tilting-pad bearings which have failed almost always have the severe damage concentrated around the pivot location.

bearing torque is generally about 60 percent of the tilting-pad bearing torque except at high Reynolds' numbers where the difference grows larger. The difference would be greater for comparisons with the preloaded tilting-pad bearing or the C_2/C_1 = 1.3 floating-ring bearing.

The dynamic properties of the two bearings can be compared in several ways. A comparison on the basis of stability characteristics results in a clear superiority for the tilting-pad bearing over the plain cylindrical floating-ring bearing. Fractional-frequency whirl was observed with the tilting-pad bearing only with no preload and very light loads and high speeds. Even then the whirl amplitude was extremely small; never more than about 0.2 times the radial clearance. A comparison based on amplitude of vibration in response to unbalance load is shown in Fig. 63. Up to the whirl onset speed, the vibration amplitude of the floating-ring bearing was very close to that of the unpreloaded tilting-pad bearing. Both bearings are very effective in controlling dynamic loads.

APPENDIX A

ANALYTICAL DEVELOPMENT OF EQUIVALENT STIFFNESS AND DAMPING FORCES

By H. S. Cheng
Mechanical Technology Incorporated

The bearing forces, inertia forces and the external exciting force acting on the experimental rotor are shown in Fig. 64. The meaning of the symbols are shown in the Nomenclature following Appendix A.

Taking moment of all forces about 0', we have

$$M\ell_c \ddot{y}_c - F_y \ell_a + T_x = \ell_b m_b R\omega^2 \sin\omega t \tag{A1}$$

$$M\ell_c \ddot{x}_c - F_x \ell_a - T_y = \ell_b m_b R\omega^2 \cos\omega t \tag{A2}$$

where the bearing forces, F_x and F_y, and the inertia torques, T_x and T_y are represented by the following expressions,

$$F_x = -(K_{xx} x_a + C_{xx} \dot{x}_a + K_{xy} y_a + C_{xy} \dot{y}_a) \tag{A3}$$

$$F_y = -(K_{yx} x_a + C_{yx} \dot{x}_a + K_{yy} y_a + C_{yy} \dot{y}_a) \tag{A4}$$

$$T_x = Mk_x^2 \left(\frac{\ddot{y}_a - \ddot{y}'_o}{\ell}\right) + M(k_y^2 - k_z^2)\Omega\left(\frac{\dot{x}_a - \dot{x}'_o}{\ell_a}\right) \tag{A5}$$

$$T_y = -Mk_y^2 \left(\frac{\ddot{x}_a - \ddot{x}'_o}{\ell_a}\right) - M(k_z^2 - k_x^2)\Omega\left(\frac{\dot{y}_a - \dot{y}'_o}{\ell_a}\right) \tag{A6}$$

Assuming the shaft is a rigid body, the following geometrical relations prevails,

$$x_c = x'_o + \left(\frac{\ell_c}{\ell_a}\right)(x_a - x'_o) \tag{A7}$$

$$y_c = y'_o + \left(\frac{\ell_c}{\ell_a}\right)(y_a - y'_o) \tag{A8}$$

Substituting (A3) through (A8) into (A1) and (A2) and dividing then by ℓ_a, we have,

$$M_e \ddot{\bar{x}}_a + \rho \ddot{\bar{x}}'_o + (\bar{K}_{xx}\bar{x}_a + \bar{C}_{xx}\dot{\bar{x}}_a + \bar{K}_{xy}\bar{y}_a + C_{\frac{xy}{\omega}}\dot{\bar{y}}_a) + \beta(\dot{\bar{y}}_a - \dot{\bar{y}}'_o) = \cos\omega t \quad \text{(A9)}$$

$$M_e \ddot{\bar{y}}_a + \rho \ddot{\bar{y}}'_o + (\bar{K}_{yx}\bar{x}_a + \bar{C}_{yx}\dot{\bar{x}}_a + \bar{K}_{yy}\bar{y}_a + \bar{C}_{yy}\dot{\bar{y}}_a) - \beta(\dot{\bar{x}}_a - \dot{\bar{x}}'_o) = \sin\omega t \quad \text{(A10)}$$

where

$$M_e = \frac{M_c}{m_b R L_b}\left[L_c^2 + \left(\frac{k_x}{\ell_a}\right)^2\right]$$

$$k_x = k_y$$

$$\rho = \frac{M_c}{m_b R L_b}\left[L_c(1-L_c) - \left(\frac{k_x}{\ell_a}\right)^2\right]$$

$$\beta = \frac{M_c}{m_b R\omega L_b}\,\frac{(k_z^2 - k_y^2)}{\ell_a^2}\,\Omega$$

(A11)

$$\bar{K}_{xx} = \frac{K_{xx}C}{m_b R\omega^2 L_b}$$

$$\bar{C}_{xx} = \frac{C_{xx}C}{m_b R\omega L_b} \quad \text{etc}$$

$$\bar{x}_a = x_a/C \quad \text{etc}$$

$$\bar{y}_a = y_a/C \quad \text{etc}$$

C = radial clearance of the bearing

and x now stands for $\frac{dx}{d(\omega t)}$.

For small oscillations of the rotor, the following substitutions can be made,

$$\begin{aligned} \bar{x}_a &= A\, e^{i\omega t} \\ \bar{y}_a &= B\, e^{i\omega t} \\ \bar{x}'_o &= E\, e^{i\omega t} \\ \bar{y}'_o &= F\, e^{i\omega t} \end{aligned} \qquad \text{(A12)}$$

where A, B, E and F are complex amplitudes of oscillation at A and O'. Substituting (A12) into (A9) and (A10), we have

$$(\bar{K}_{xx} - M_e + i\,\bar{C}_{xx})\,A + \left[\bar{K}_{xy} + i\,(\bar{C}_{xy} + \beta)\right]\,B = 1 + \rho\,E + i\,\beta\,F \qquad \text{(A13)}$$

$$\left[\bar{K}_{yx} + i\,(\bar{C}_{yx} - \beta)\right]\,A + (\bar{K}_{yy} - M_e + i\,\bar{C}_{yy})\,B = \rho\,F - i\,(1 + \beta\,E) \qquad \text{(A14)}$$

If the motion at O' is given, then E and F become known and Eqs. (A13) and (A14) can be solved for A and B to give

$$A = \frac{us - vq}{ps - rq} \qquad \text{(A15)}$$

$$B = \frac{pv - ur}{ps - rq} \qquad \text{(A16)}$$

where

$$\begin{aligned} p &= \bar{K}_{xx} - M_e + i\,\bar{C}_{xx} \\ q &= \bar{K}_{xy} + i\,(\bar{C}_{xy} + \beta) \\ r &= \bar{K}_{yx} + i\,(\bar{C}_{yx} - \beta) \\ s &= \bar{K}_{yy} - M_e + i\,\bar{C}_{yy} \\ u &= 1 + \rho E + i\beta F \\ v &= \rho F - i\,(1 + \beta E) \end{aligned} \qquad \text{(A17)}$$

The dynamic system represented by Eq. (A13) and (A14) can now be reduced to a much simpler equivalent system containing only effective direct stiffness K_x', K_y' and effective direct damping factors C_x', C_y' without the cross coupling stiffness and damping factors.

The equations governing the motion of the equivalent system are

$$M_e \ddot{x}_a + K_x' \, x_a + C_x' \, \dot{x}_a = \cos\omega t \tag{A18}$$

$$M_e \ddot{y}_a + K_y' \, y_a + C_y' \, \dot{y}_a = \sin\omega t \tag{A19}$$

Comparing (A18) and (A19) with (A15) (A16) we obtain the expression for the effective stiffness and damping factors as follows:

$$K_x' = M_e + \mathcal{R} \left\{ \frac{ps - rq}{us - vq} \right\} \tag{A20}$$

$$K_y' = M_e + \mathcal{R} \left\{ \frac{-i\,(ps - rq)}{vp - ur} \right\} \tag{A21}$$

$$C_x' = \mathcal{I} \left\{ \frac{ps - rq}{us - vq} \right\} \tag{A22}$$

$$C_y' = \mathcal{I} \left\{ \frac{-i\,(ps - rq)}{vp - ur} \right\} \tag{A23}$$

The correlation between the experimental and theoretical characteristics of the test bearing can be achieved by comparing the theoretical and experimental effective stiffness and damping factors. The experimental effective stiffness and damping factors are calculated from motions measured at A and O' using Eqs. (A18) and (A19) while the theoretical K_x', K_y', C_x' and C_y' are determined by Eqs. (A20) through (A23).

NOMENCLATURE FOR APPENDIX A

A	center of the test bearing
B	point of application of the exciting force
C	center of mass of the rotor
F_y, F_x	bearing forces at A
k_x	radius of gyration about an axis passing through C and parallel to O'x
k_y	radius of gyration about an axis passing through C and parallel to O'y
k_z	radius of gyration about O'z
ℓ_a	distance O'A inch
ℓ_b	distance O'B inch
ℓ_c	distance O'C inch
M	mass of rotor pound second^2/inch
m_b	mass of the exciting mass (cap screw)
O'	center of the guide bearing
R	distance of m_b from B
T_x	x component of the inertia torque
T_y	y component of the inertia torque
$\dot{x}$	$\frac{dx}{dt}$
x'_o, x_a, x_c	x coordinates of O', A, C respectively, inch
y'_o, y_a, y_c	y coordinates of O', A, C respectively, inch
Ω	angular speed of the shaft
ω	exciting frequency

REFERENCES

1. Shaw, M. C.; and Nussdorfer, T. J.: An Analysis of the Full-Floating Journal Bearing. NACA Research Memorandum E 7A28a.

2. Kettleborough, C. F.: Frictional Experiments on Lightly-Loaded Fully Floating Journal Bearing. Australian J. of Appl. Sci., 1952-1955.

3. Taylor, G. I.: Stability of a Viscous Liquid Contained Between Two Rotating Cylinders. Phil. Trans. Roy. Sec.(London), series A, vol. 223, 1923.

4. Smith, M. I.; and Fuller, D. D.: Journal Bearing Operation at Superlaminar Speeds. ASME, vol. 78, 1956.

5. Vohr, J. H.: Analysis of Turbulent Lubrication — Volume II — An Experimental Study of Vortex Flow and Turbulence in Concentric and Eccentric Annuli. Mechanical Technology Incorporated report no. MTI-64TR20, final report to NASA on Contract NASw-771, May 1964.

6. DiPrima, R. C.: A Note on the Stability of Flow in Non-concentric Annuli. Mechanical Technology Incorporated report no. MTI-62TR15, August 1962.

7. Ng, C. W.; and Pan, C. H. T.: A Linearized Turbulent Lubrication Theory. ASME paper 64LUB29 presented at International Lubrication Conference (Washington, D.C.) October 1964.

8. Theodorsen, T.; and Reiger, A.: Experiments on Drag of Revolving Disks, Cylinders and Streamline Rods at High Speeds. NACA report no. 793, Thirtieth Annual Report, 744-803, 1944.

9. Lund, J. W.: Attenuation of Bearing Transmitted Noise. vol. 3. Contract NOBs-86914, USN Bureau of Ships, October 1964.

10. Lund, J. W.: The Stability of an Elastic Rotor in Journal Bearings With Flexible, Damped Supports. ASME paper no. 65-APMW-8, to be presented at the Western Conference of the Appl. Mech. Div. (Los Angeles) August 30 - Sept. 2, 1965.

11. Malanoski, S. B.; and Lewis, P.: Rotor-Bearing Dynamics Technology. Part IV — Ball Bearing Design Data. AFAPL-TR65-45. (Also available as Mechanical Technology Incorporated report no. MTI-65TR35, July 1965.)

12. Orcutt, F. K.: Static and Dynamic Properties of the Tilting-Pad Journal Bearing in Laminar and Superlaminar Flow Regimes. Topical report on contract NASw-1021, June, 1965.

13. Orcutt, F. K.; and Arwas, E. B.: Analysis of Turbulent Lubrication. Vol. 1. The Static and Dynamic Properties of Journal Bearings in Laminar and Turbulent Regimes. Mechanical Technology Incorporated report no. MTI-64TR19. Final report to NASA on contract NASw-771, May 1964.

14. Vohr, J. H.; and Chow, C. Y.: Characteristics of Herringbone-Grooved, Gas-Lubricated Journal Bearings. ASME paper no. 64LUB15 presented at the International Lubrication Conference (Washington, D.C.) October 1964.

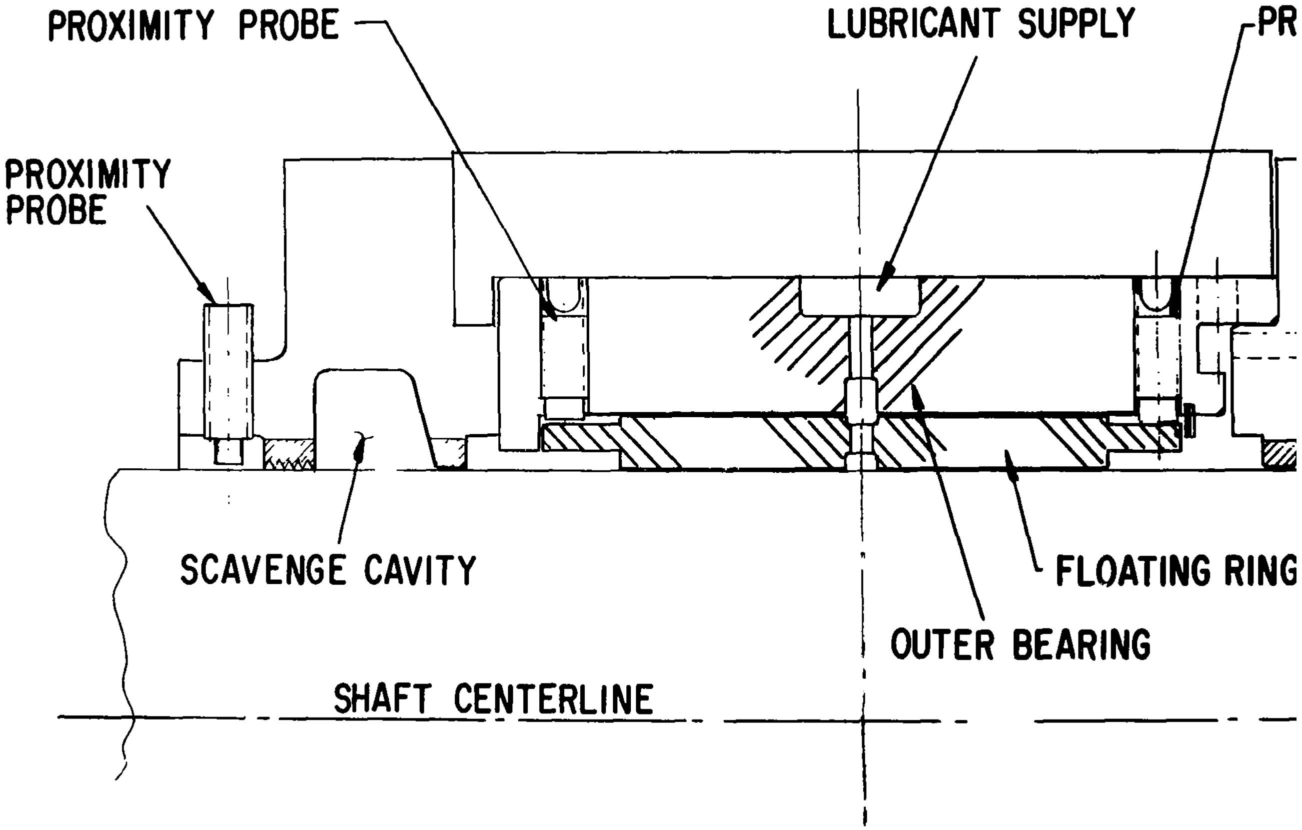

Figure 1. - Floating ring bearing in test bearing housing.

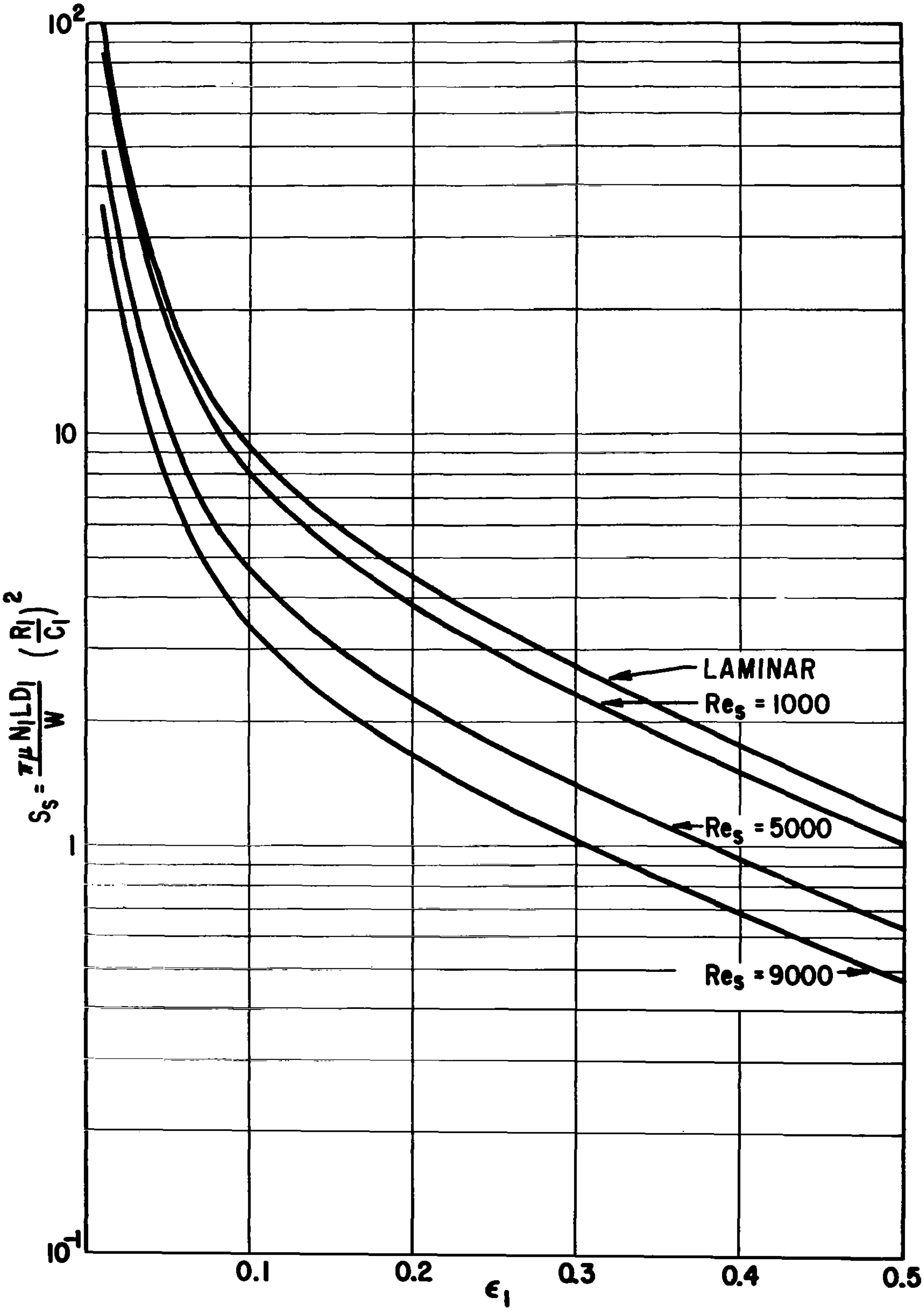

Figure 2. - Inner film static load capacity $C_2/C_1 = 0.7$, $P_s L D_1/W = 0.2$.

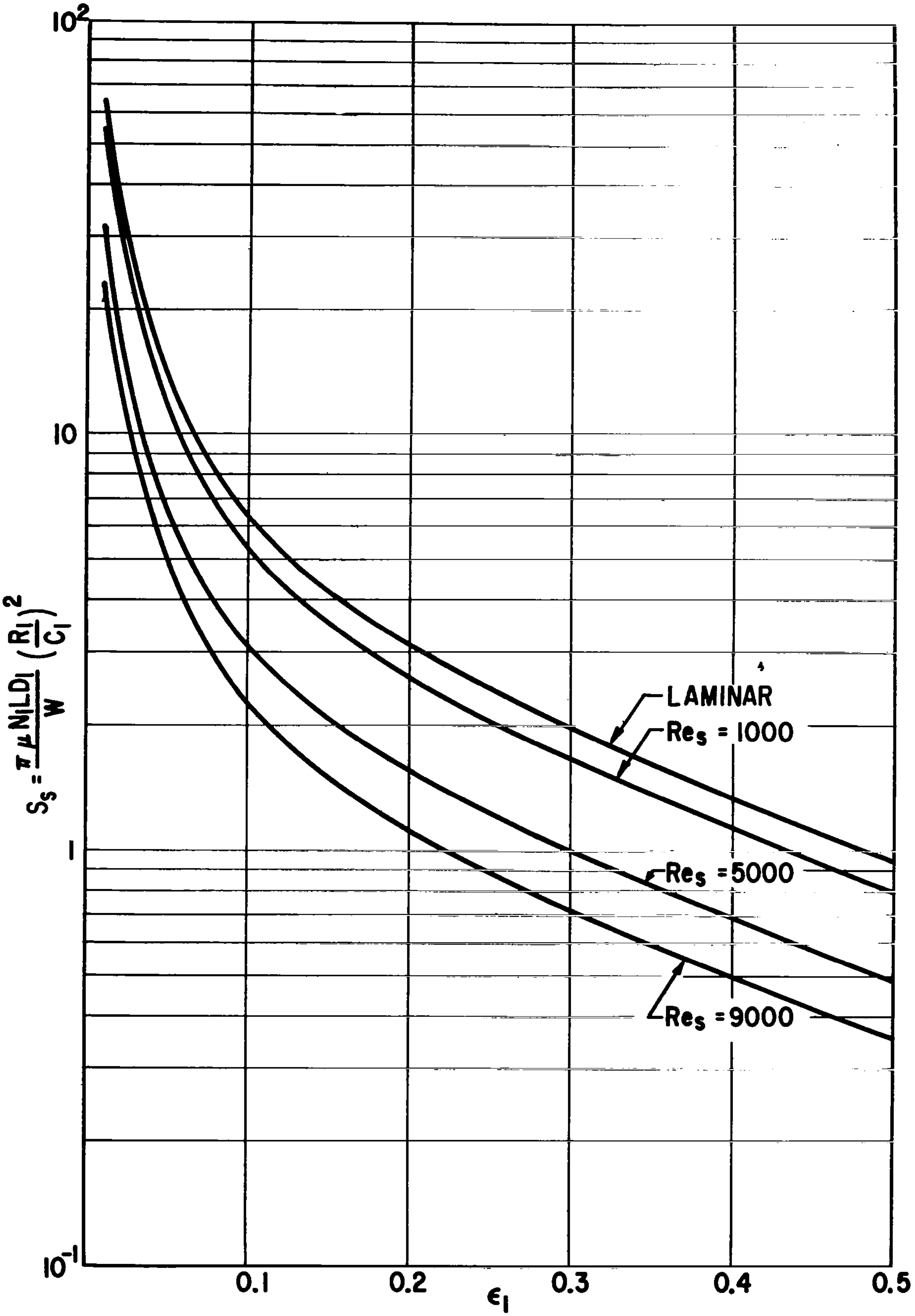

Figure 3. - Inner film static load capacity $C_2/C_1 = 0.7$, $P_s L D_1/W = 1.5$.

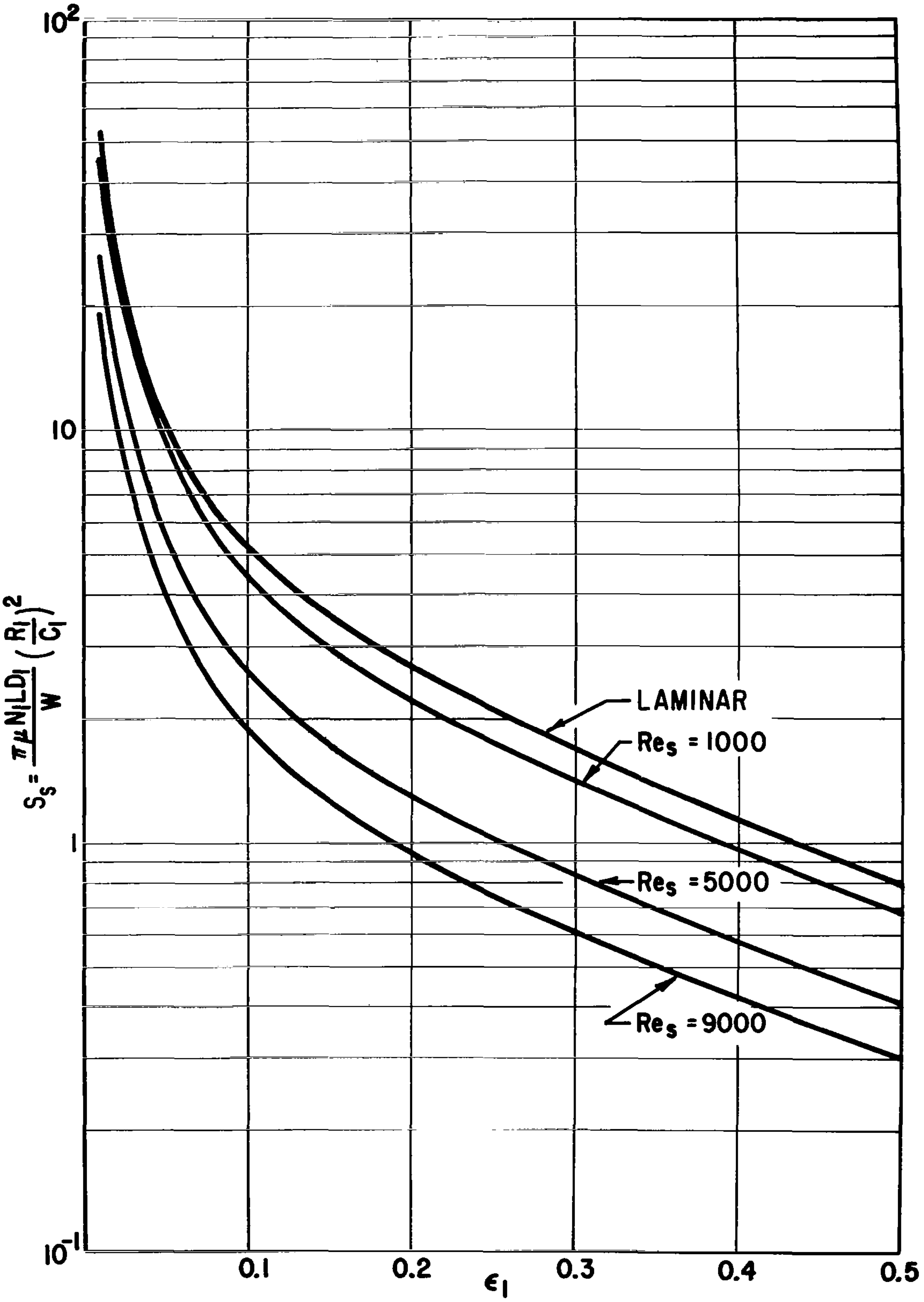

Figure 4. - Inner film static load capacity $C_2/C_1 = 0.7$, $P_s L D_1/W = 10$.

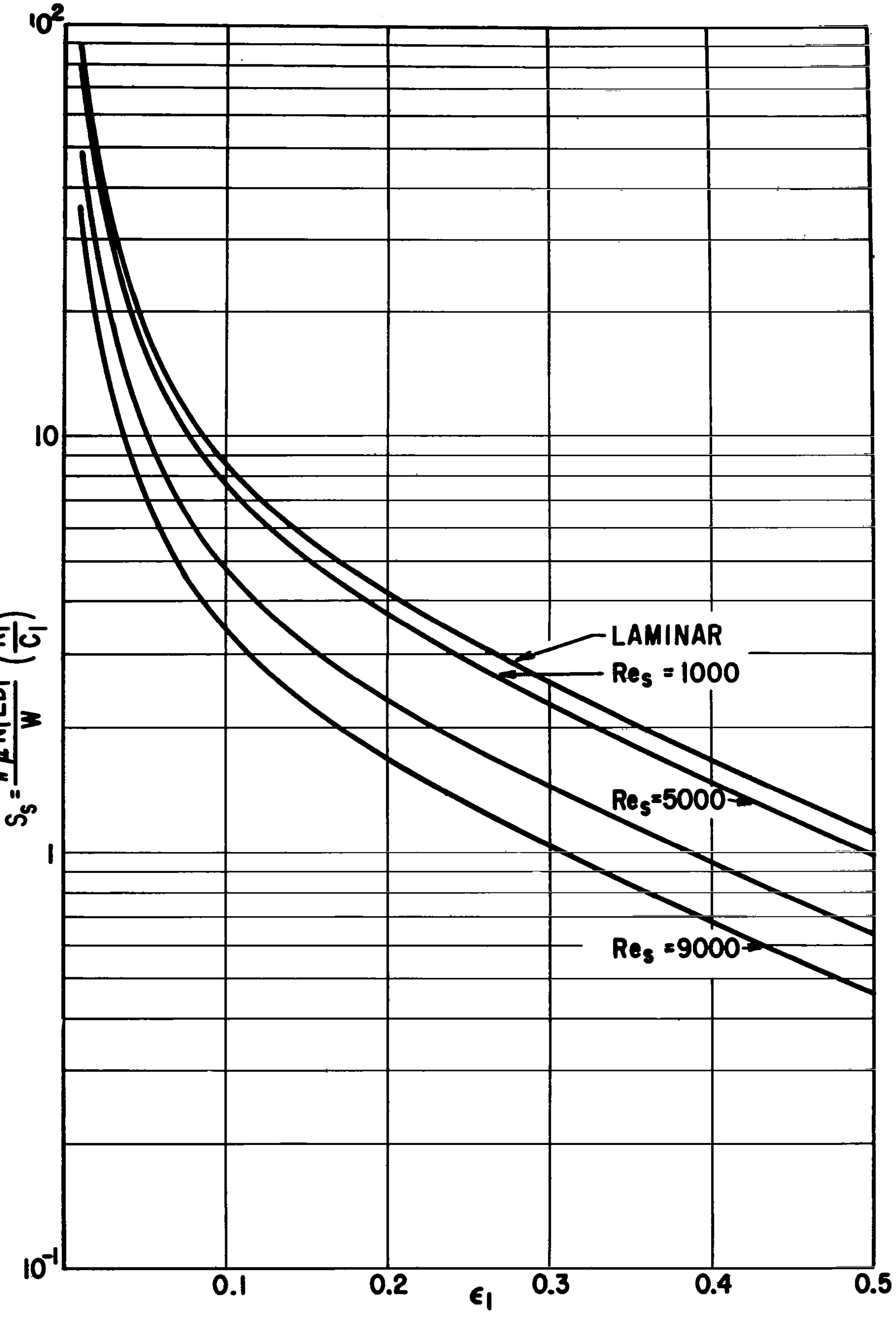

Figure 5. - Inner film static load capacity $C_2/C_1 = 1.3$, $P_sLD_1/W = 0.2$.

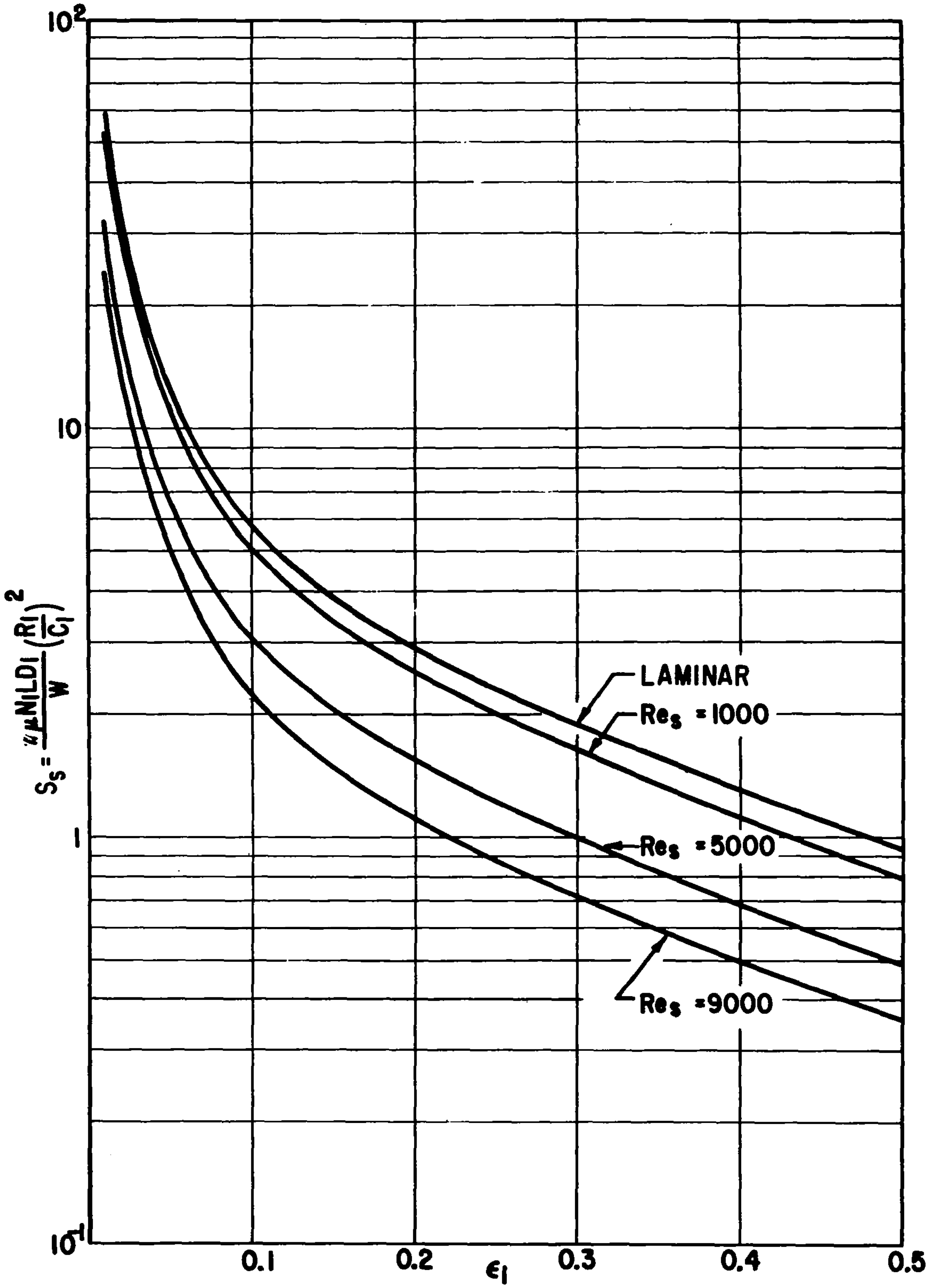

Figure 6. - Inner film static load capacity $C_2/C_1 = 1.3$, $P_s L D_1/W = 1.5$.

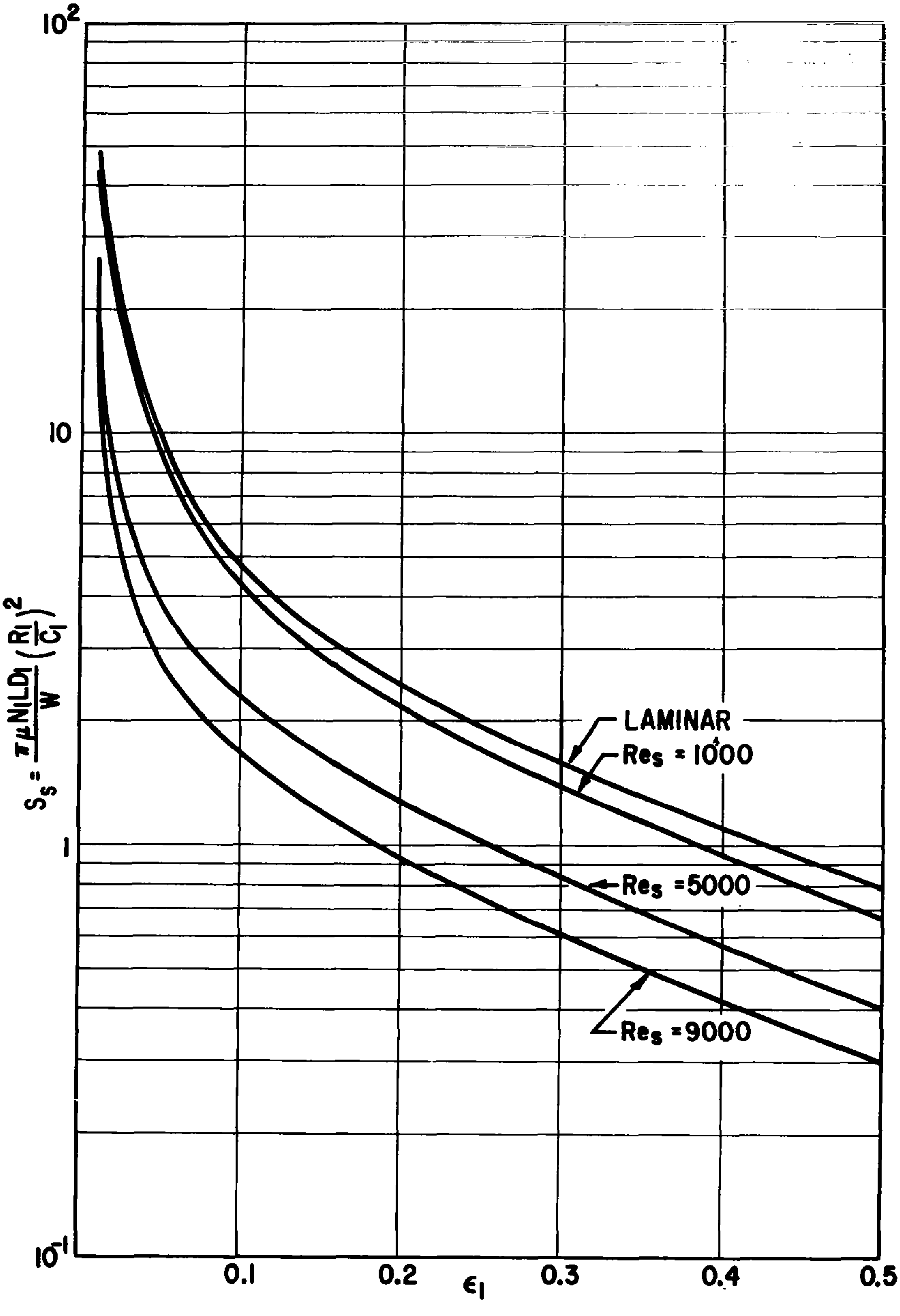

Figure 7. - Inner film static load capacity $C_2/C_1 = 1.3$, $P_sLD_1/W = 10$.

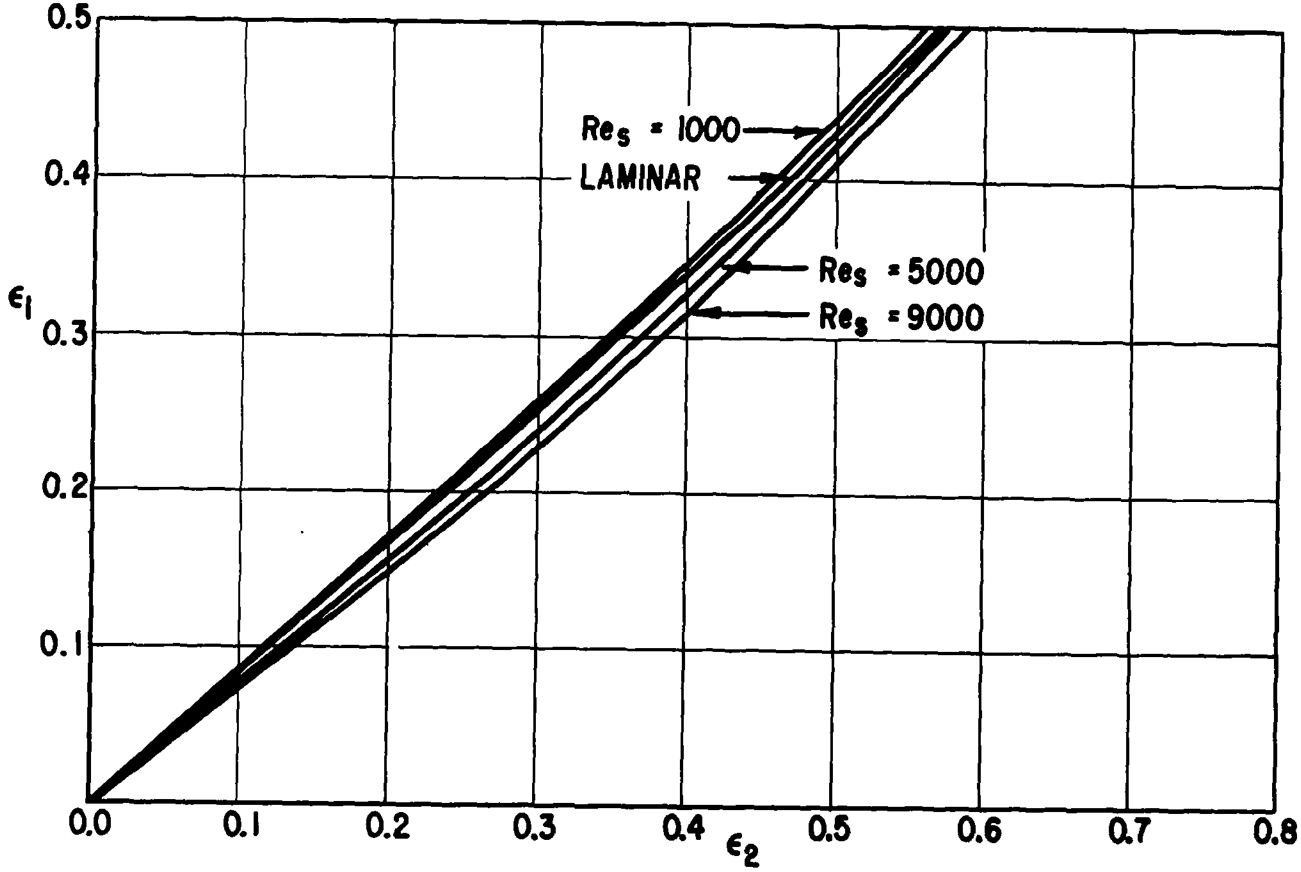

Figure 8. - Relationship between inner and outer film eccentricity ratios $C_2/C_1 = 0.7$, $P_sLD_1/W = 0.2$.

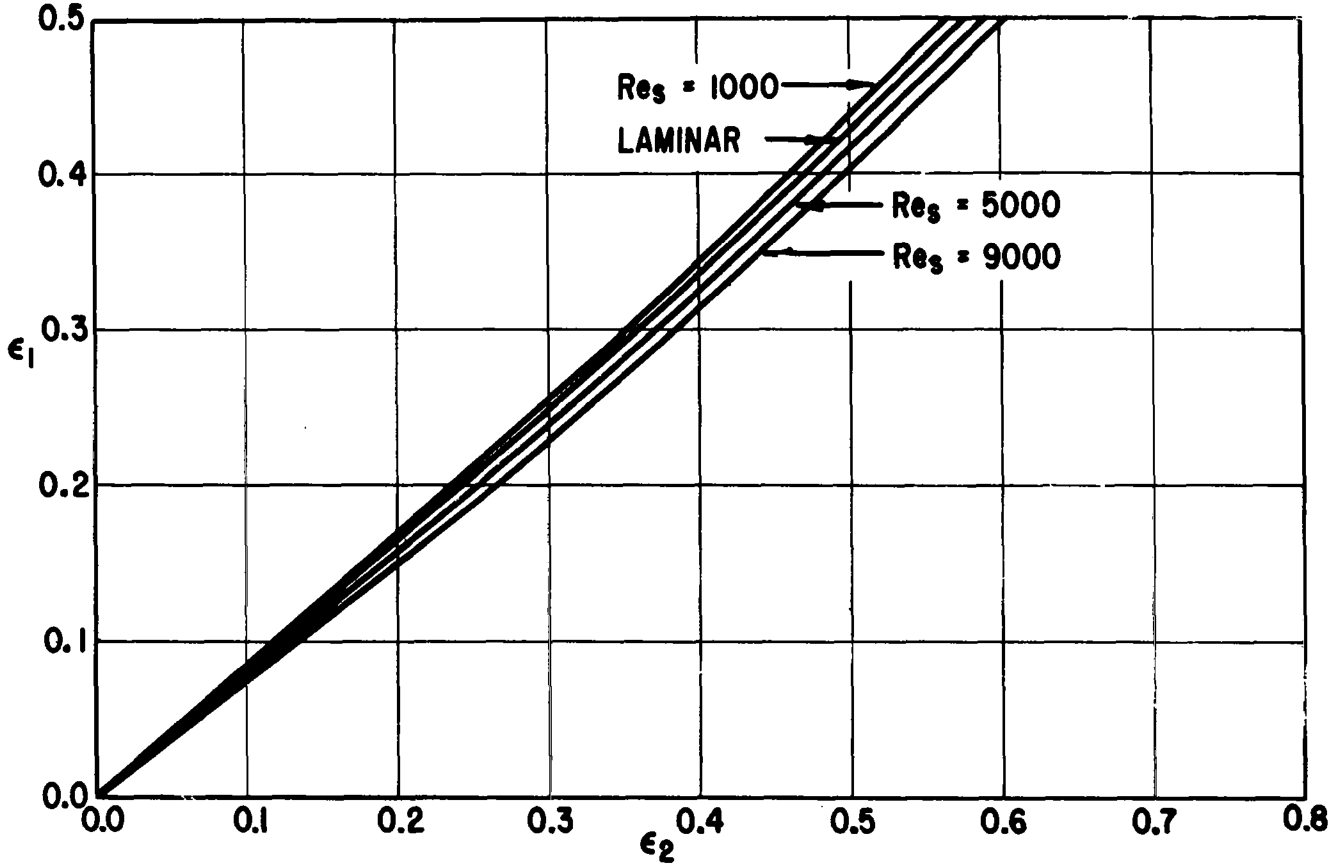

Figure 9. - Relationship between inner and outer film eccentricity ratios $C_2/C_1 = 0.7$, $P_sLD_1/W = 1.5$.

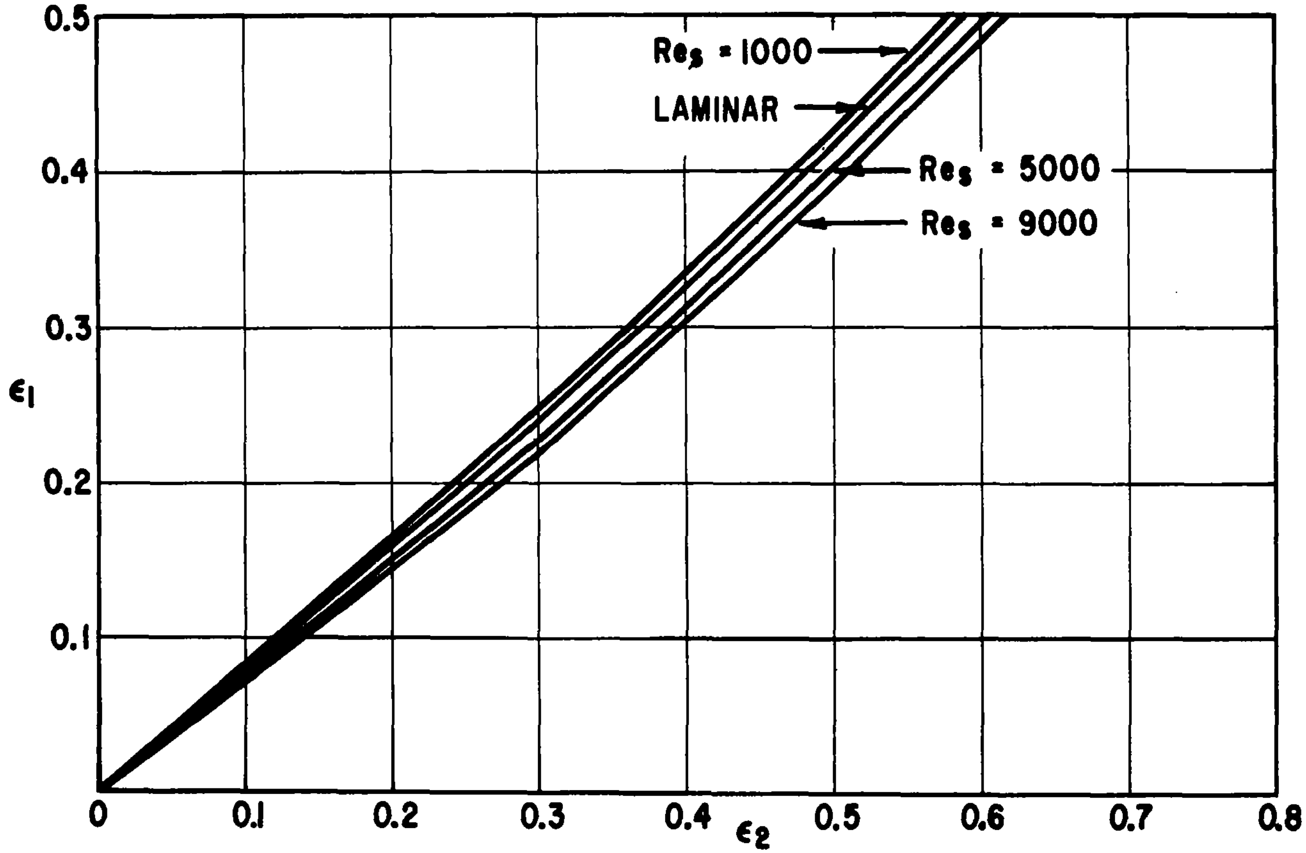

Figure 10. - Relationship between inner and outer film eccentricity ratios $C_2/C_1 = 0.7$, $P_sLD_1/W = 10$.

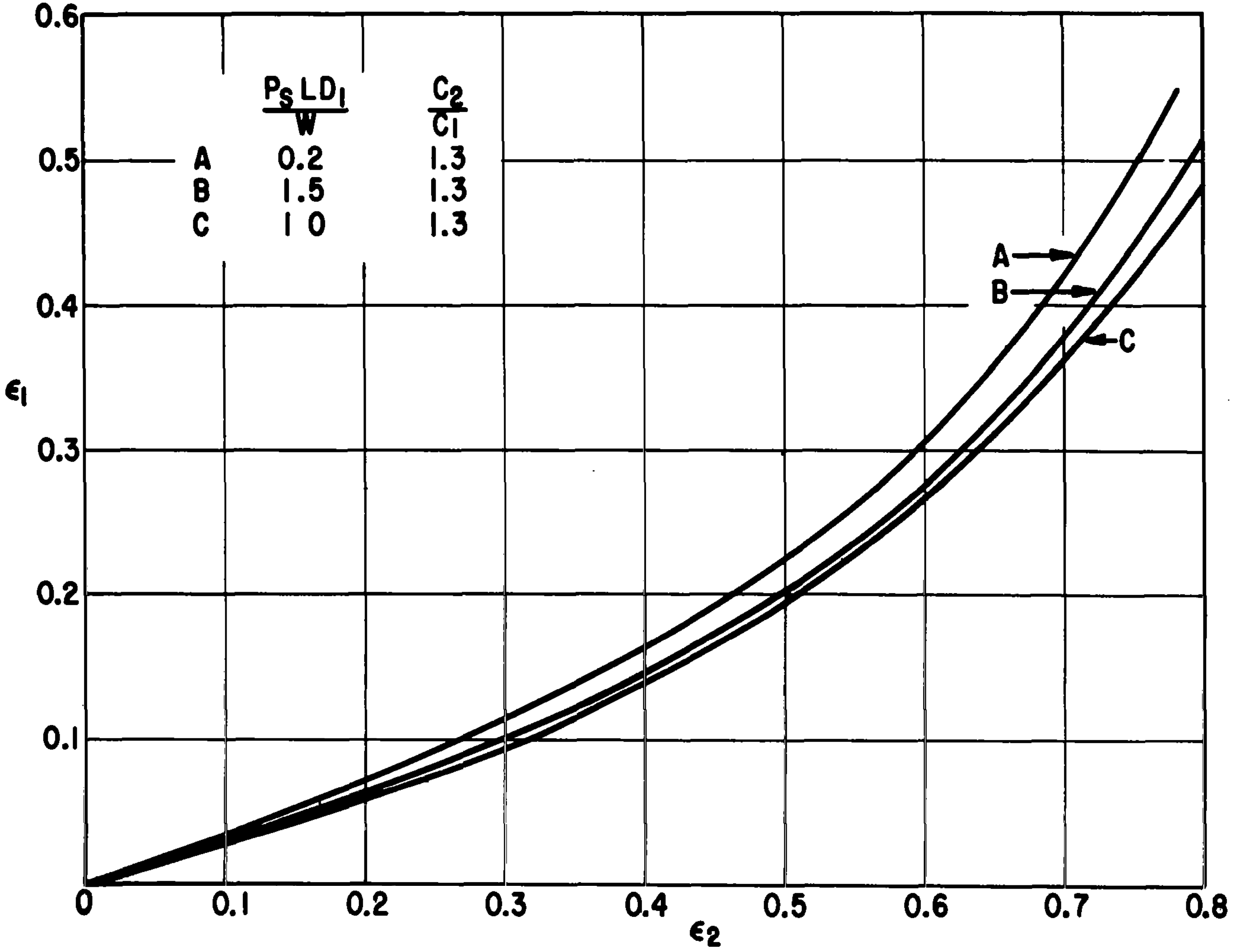

Figure 11. - Relationship between inner and outer film eccentricity ratios $C_2/C_1 = 1.3$. The effect of Reynolds' number is negligible.

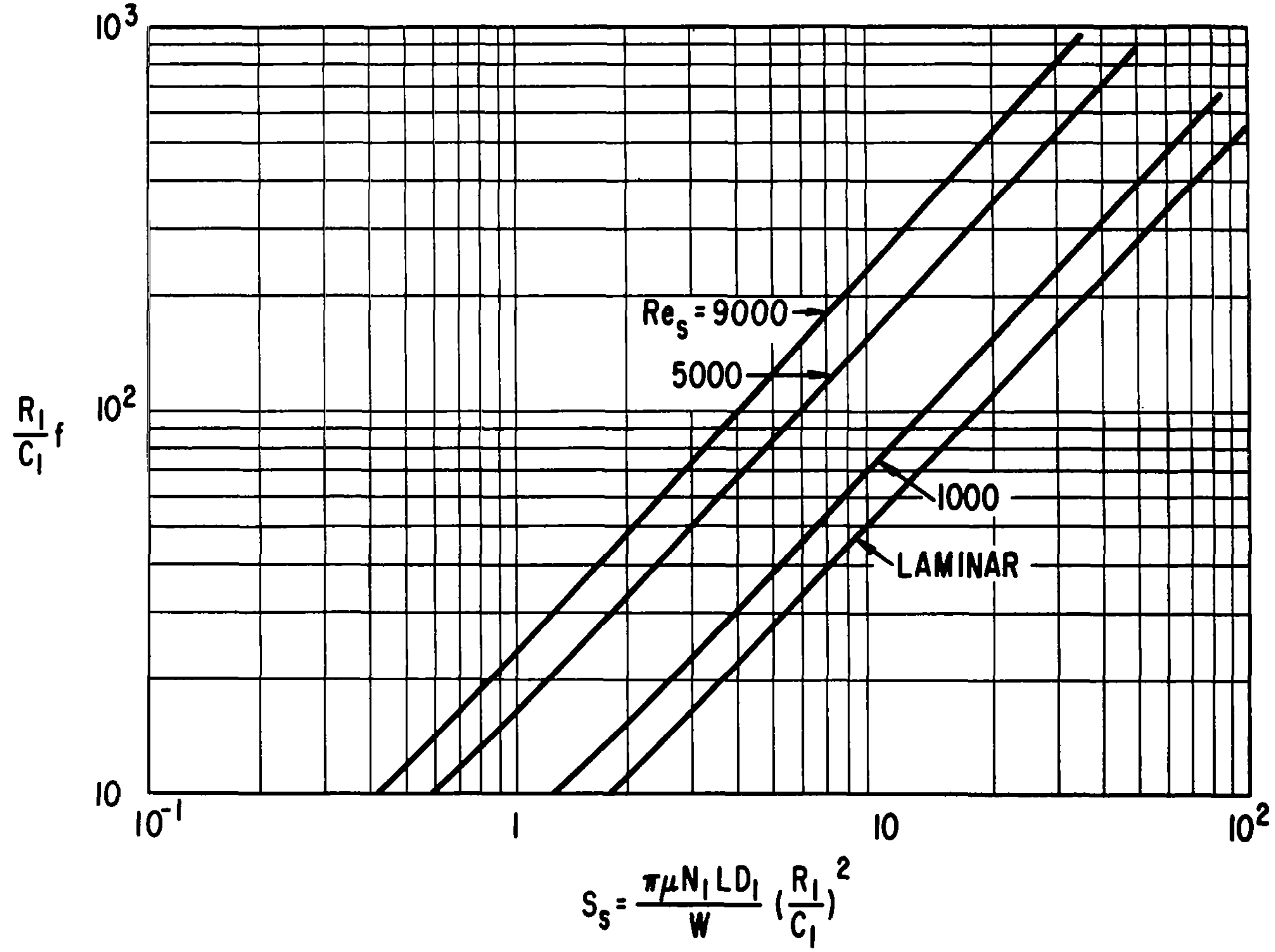

Figure 12. - Dimensionless bearing friction $C_2/C_1 = 0.7$, $P_s L D_1/W = 0.2$.

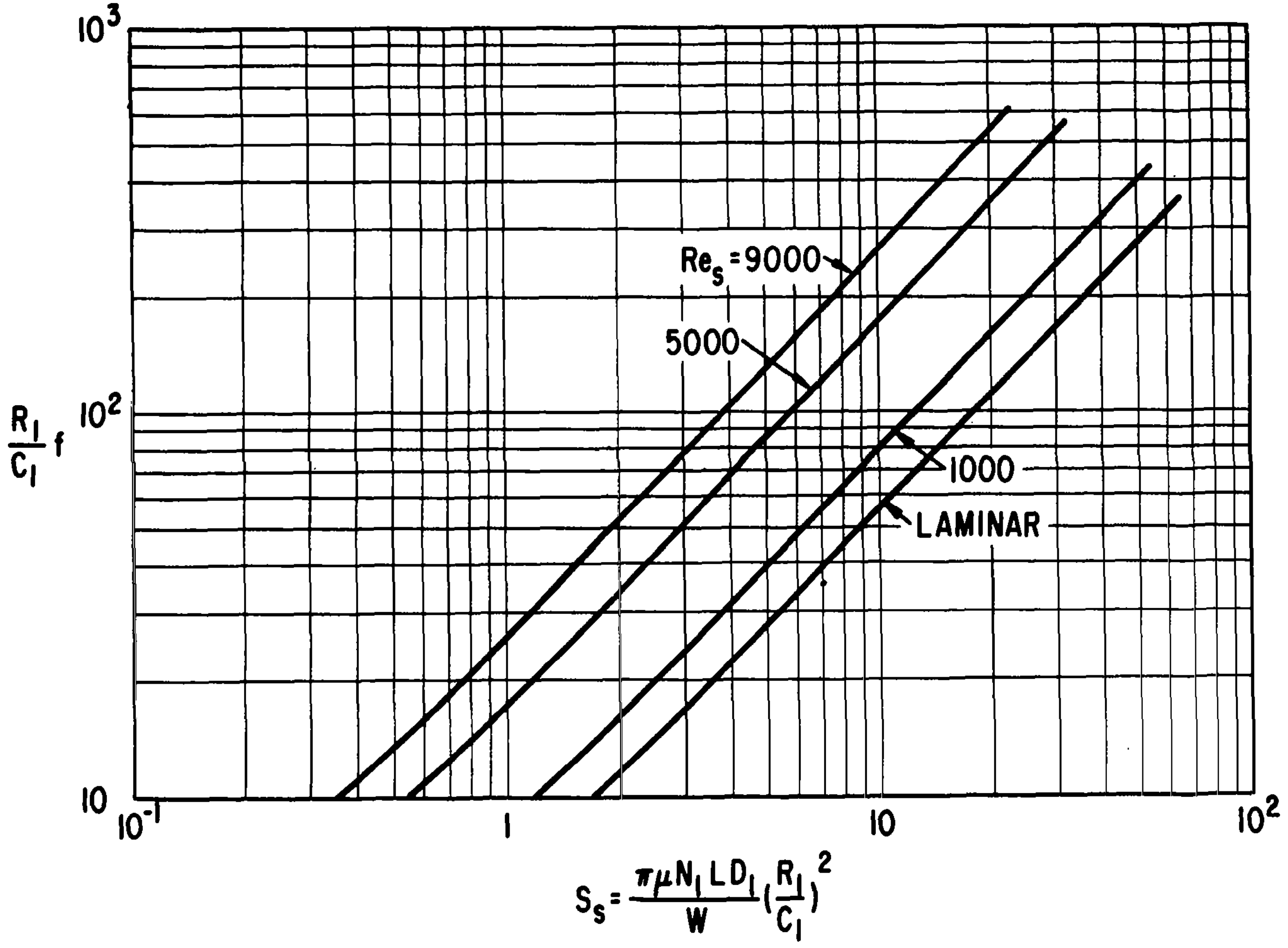

Figure 13. - Dimensionless bearing friction $C_2/C_1 = 0.7$, $P_sLD_1/W = 1.5$ and 10.

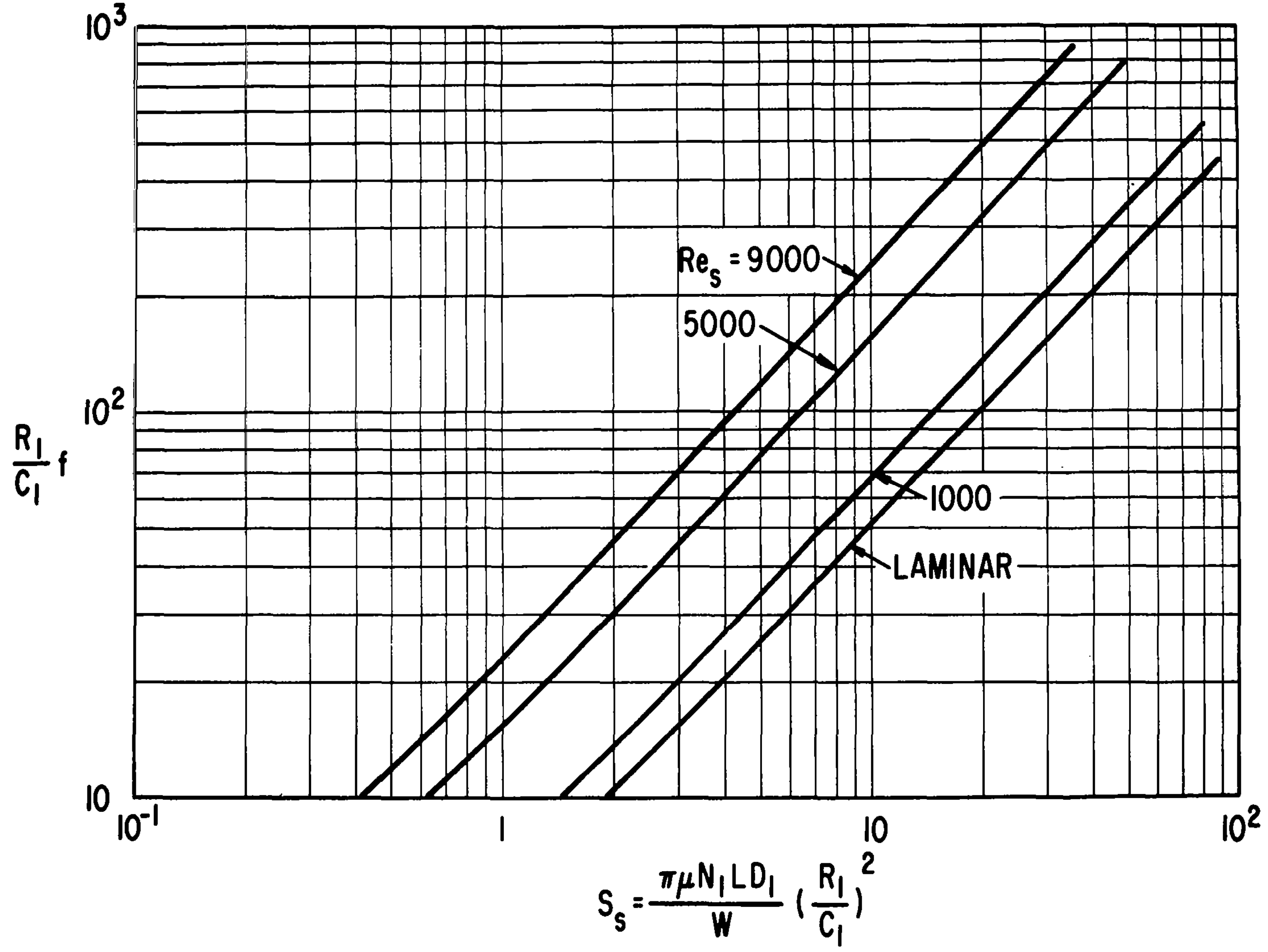

Figure 14. - Dimensionless bearing friction $C_2/C_1 = 1.3$, $P_s L D_1/W = 0.2$.

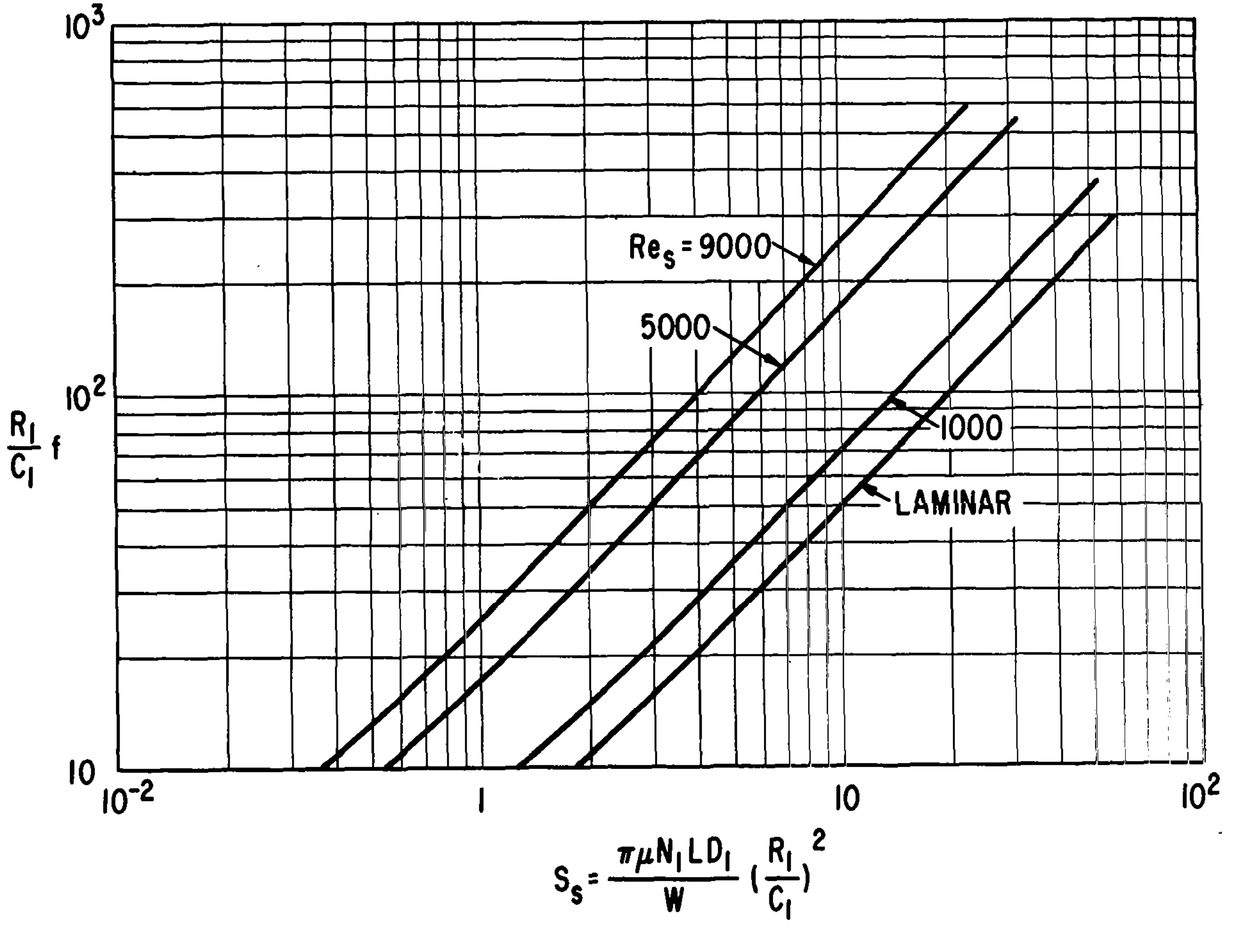

Figure 15. - Dimensionless bearing friction $C_2/C_1 = 1.3$, $P_s L D_1/W = 1.5$ and 10.

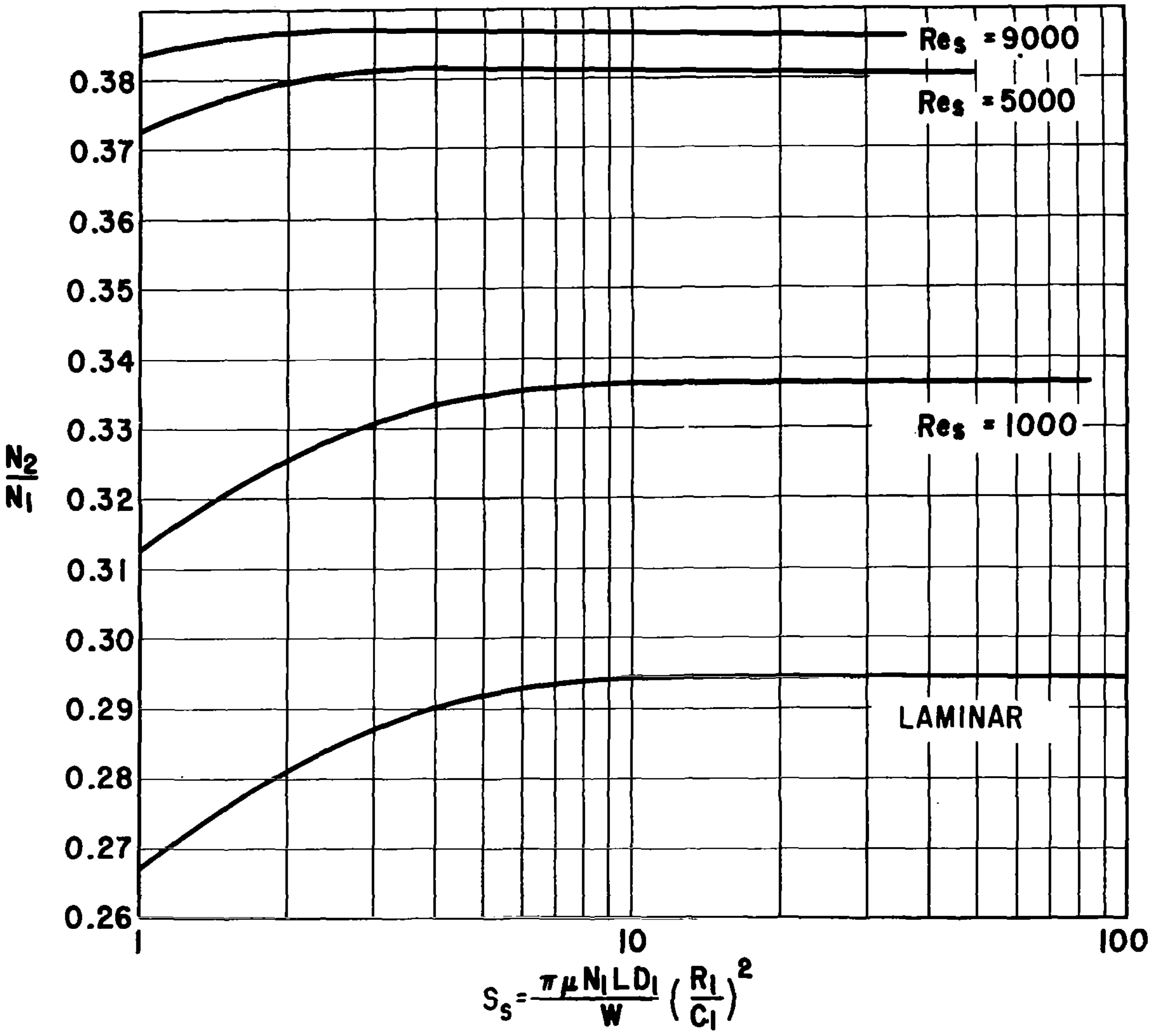

Res = 9000
Res = 5000
Res = 1000
LAMINAR
$\frac{N_2}{N_1}$
0.38
0.37
0.36
0.35
0.34
0.33
0.32
0.31
0.30
0.29
0.28
0.27
0.26
1
10
100
$S_s = \frac{\pi \mu N_1 L D_1}{W} \left(\frac{R_1}{C_1}\right)^2$

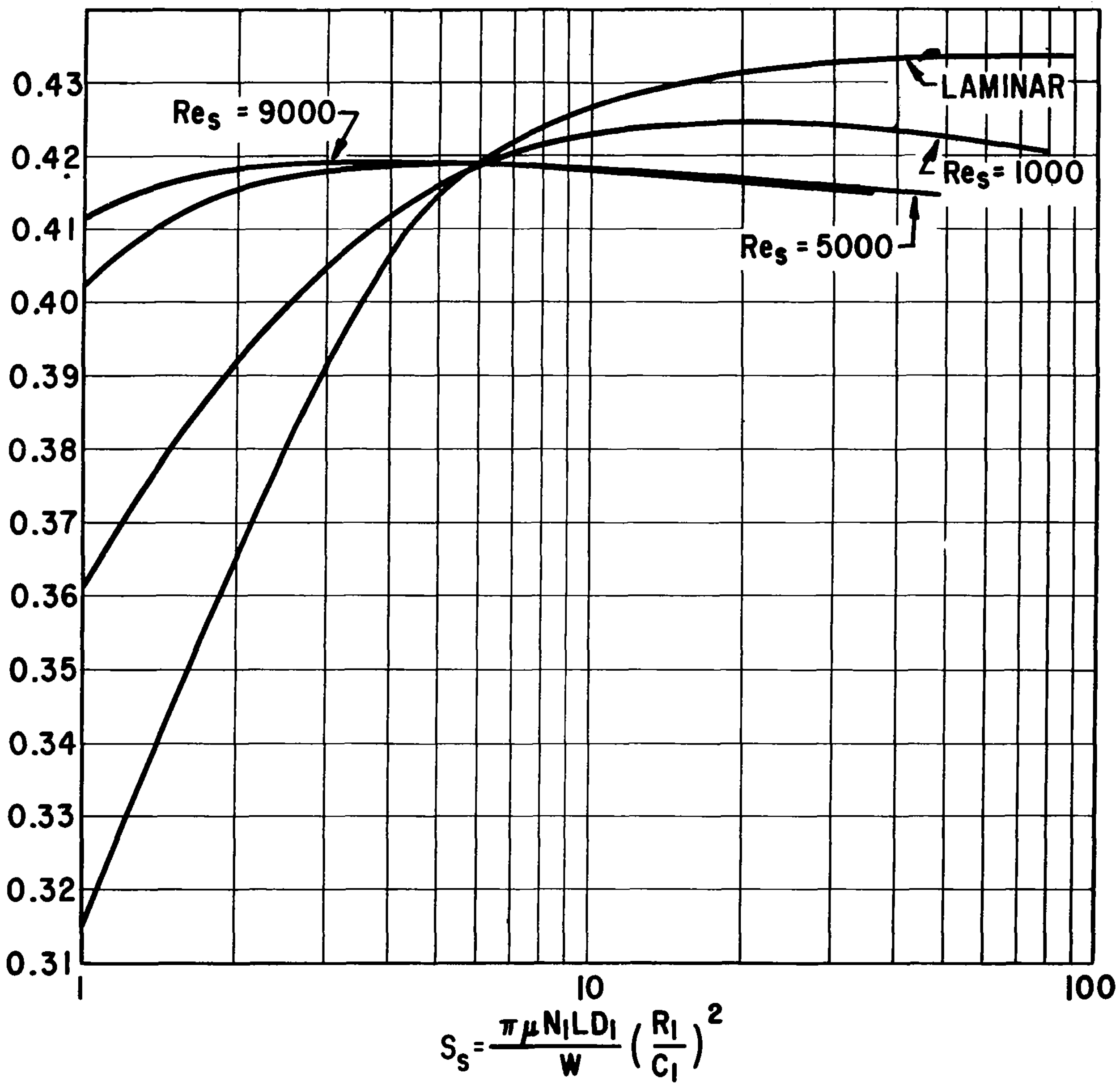

Figure 17. - Ring/shaft speed ratio $C_2/C_1 = 1.3$, $P_s L D_1/W = 0.2$.

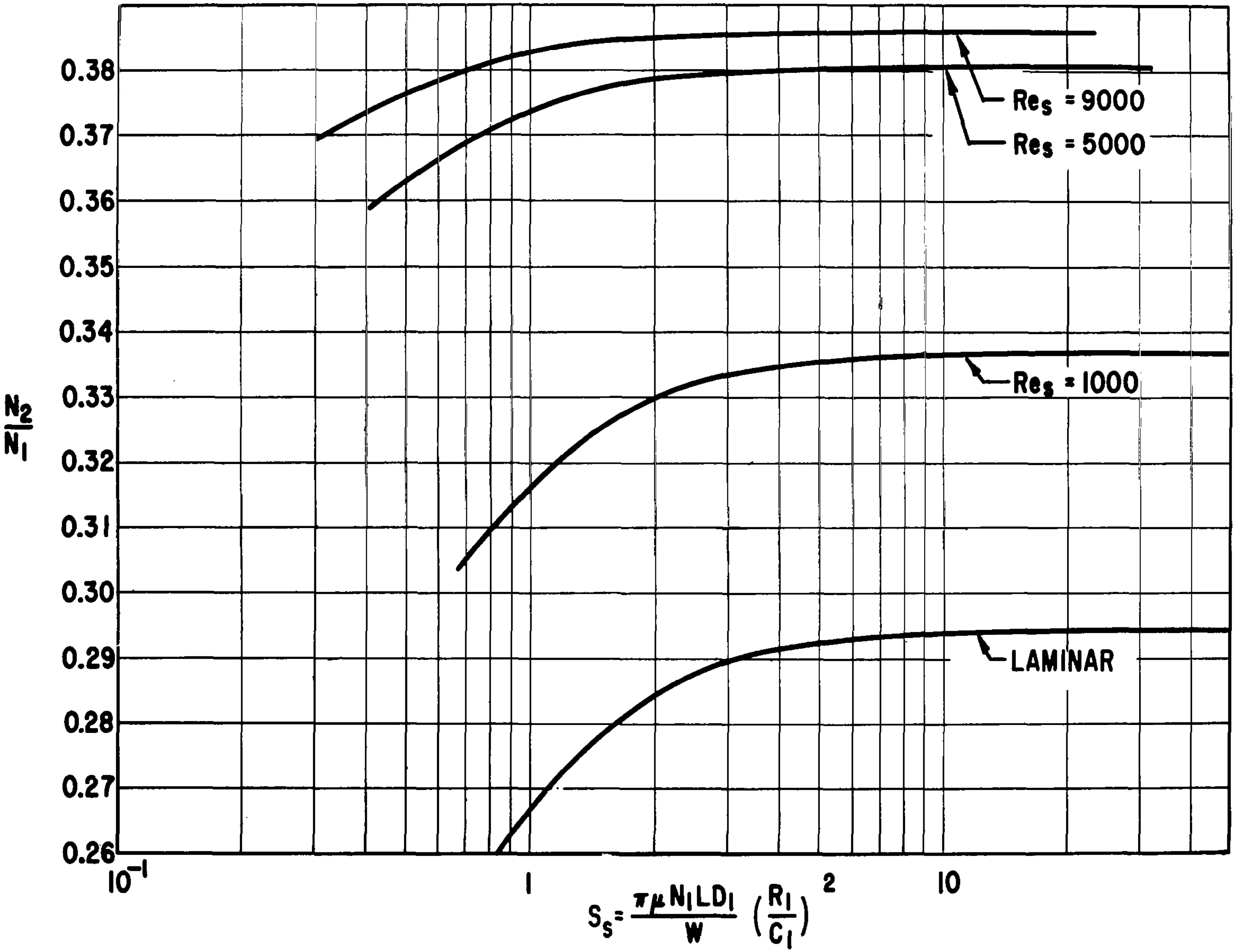

Figure 18. - Ring/shaft speed ratio $C_2/C_1 = 0.7$, $P_sLD_1/W = 1.5$.

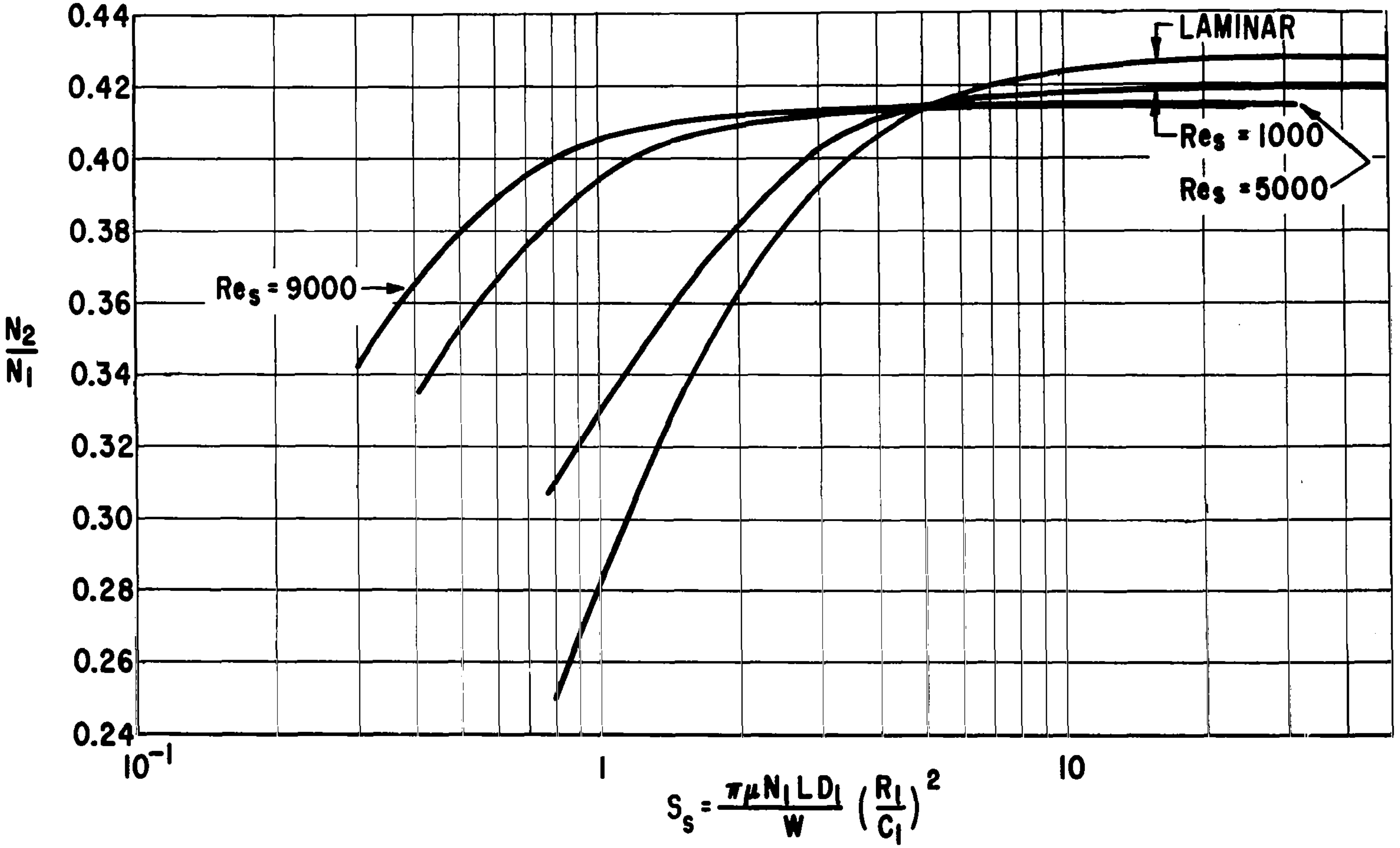

Figure 19. - Ring/shaft speed ratio $C_2/C_1 = 1.3$, $P_sLD_1/W = 1.5$.

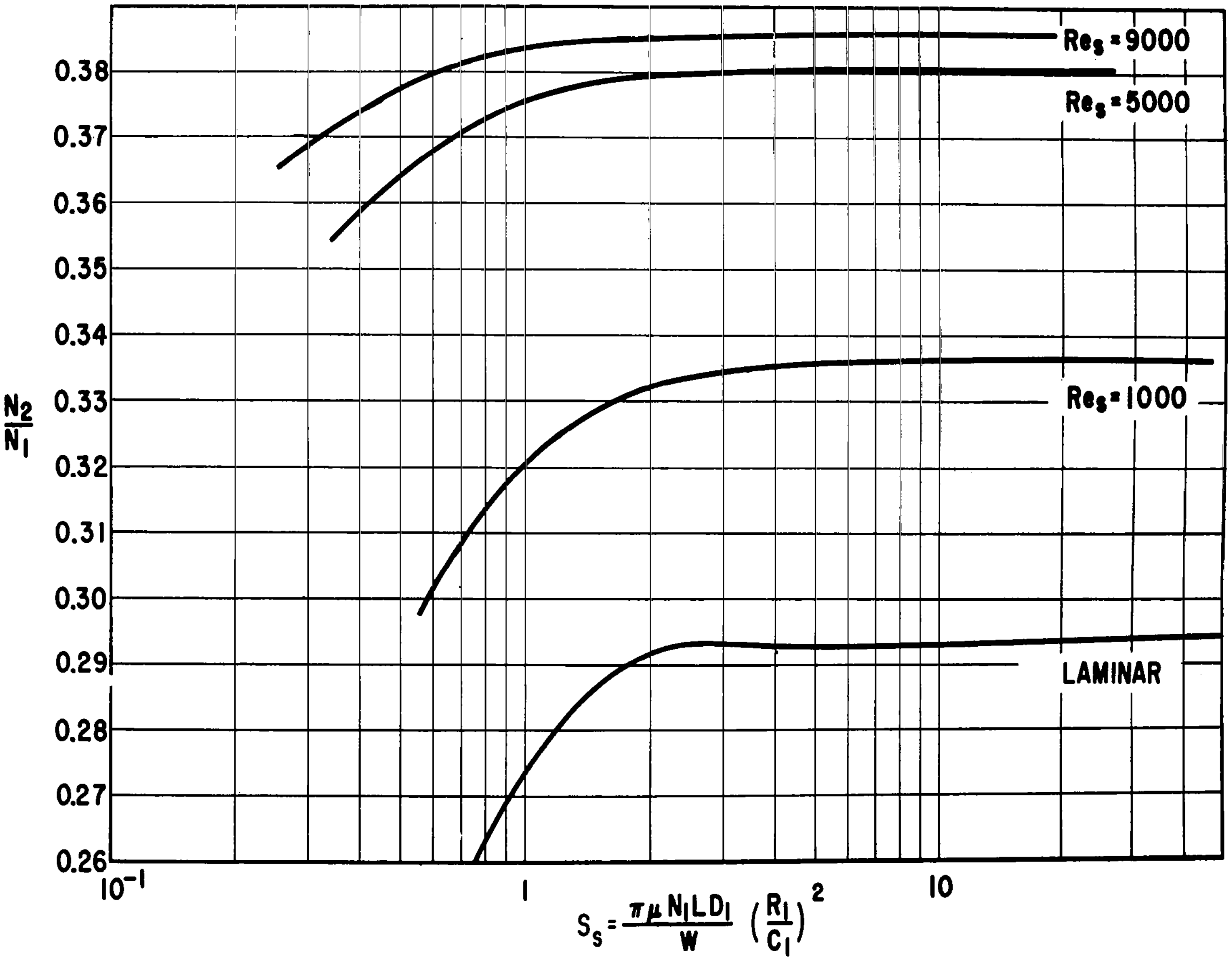

Figure 20. - Ring/shaft speed ratio $C_2/C_1 = 0.7$, $P_sLD_1/W = 10$.

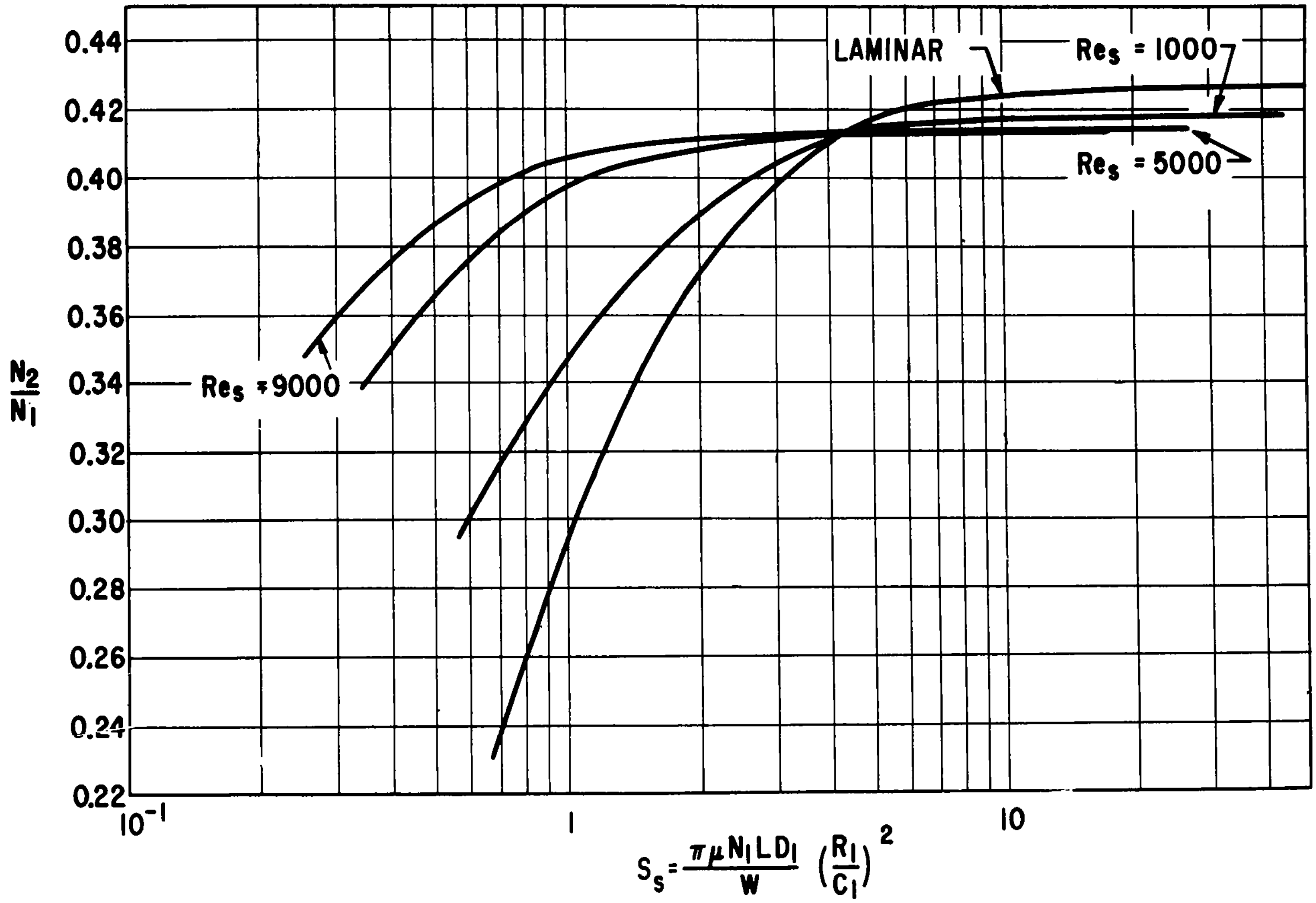

Figure 21. - Ring/shaft speed ratio $C_2/C_1 = 1.3$, $P_sLD_1/W = 10$.

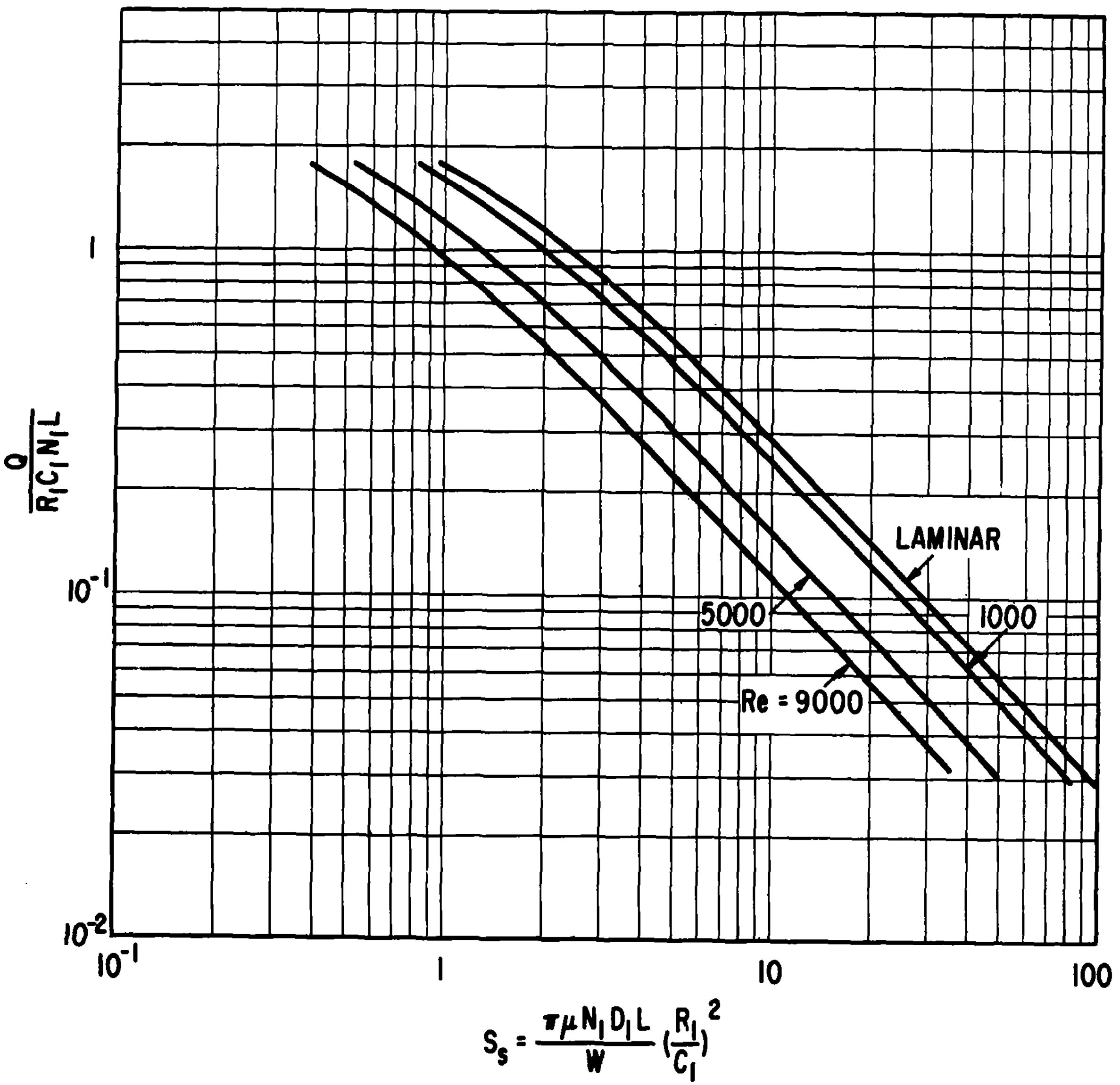

Figure 22. - Dimensionless flow $C_2/C_1 = 0.7$, $P_sLD_1/W = 0.2$.

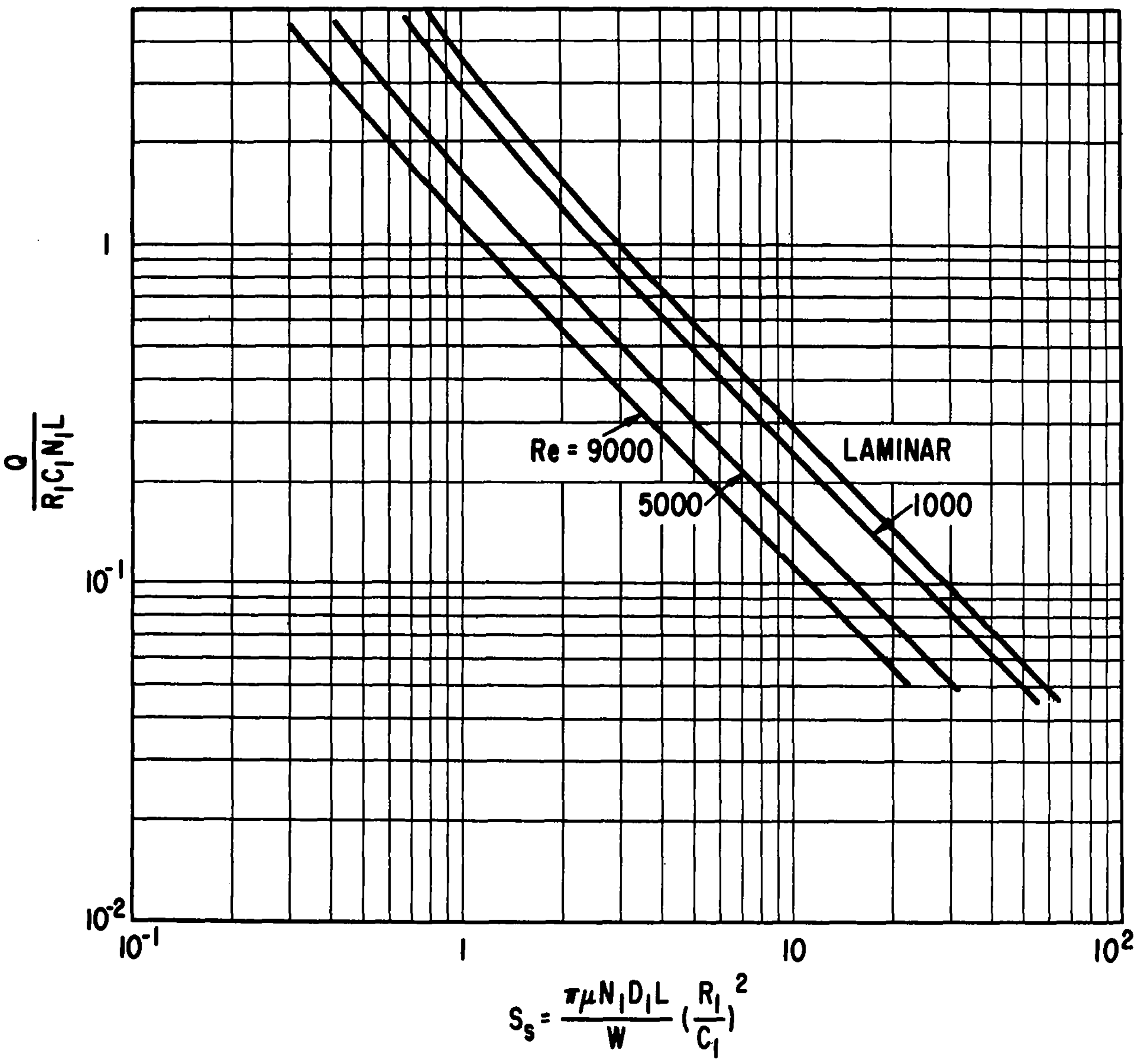

Figure 23. - Dimensionless flow $C_2/C_1 = 0.7$, $P_sLD_1/W = 1.5$.

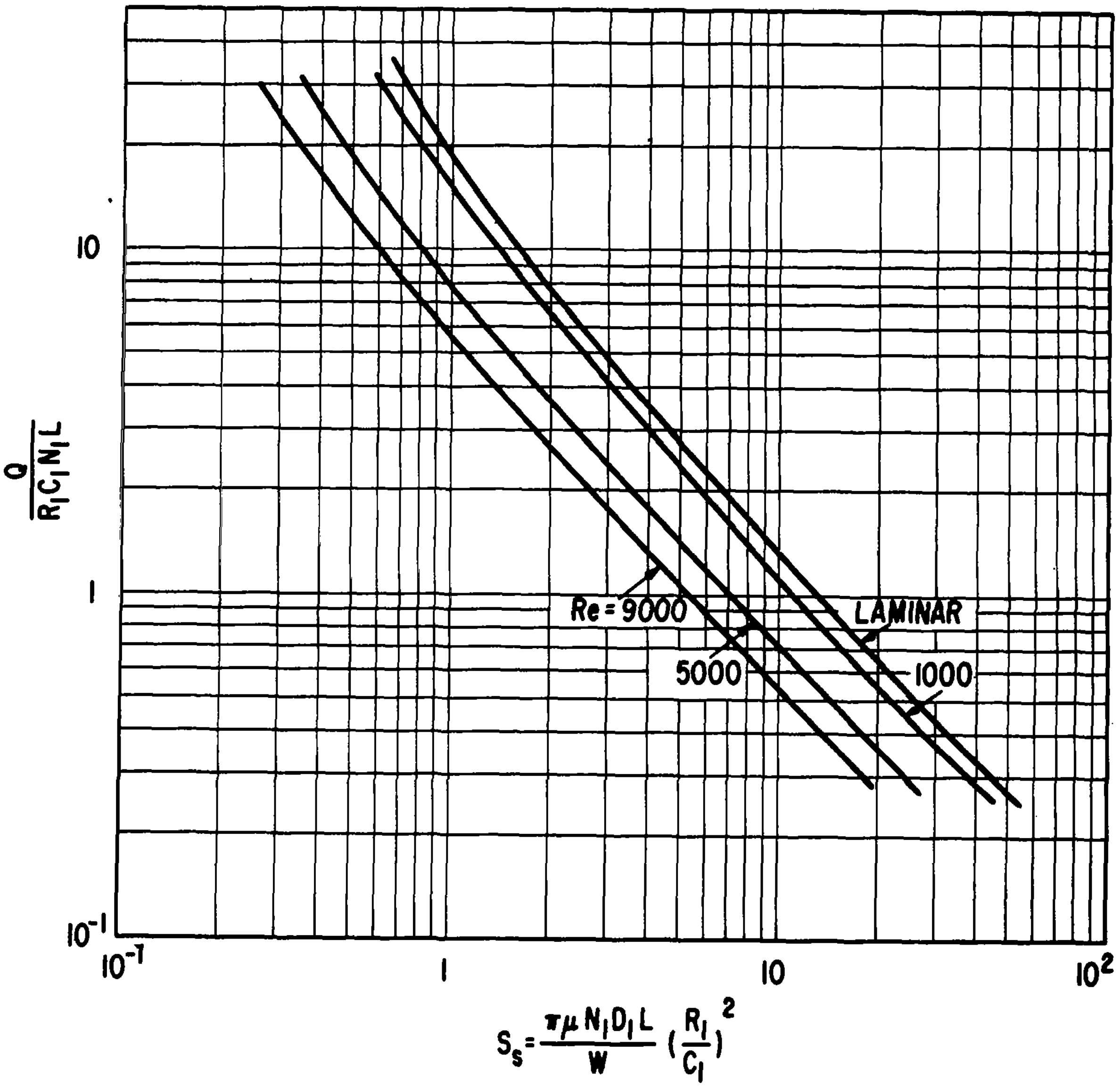

Figure 24. - Dimensionless flow $C_2/C_1 = 0.7$, $P_s L D_1/W = 10$.

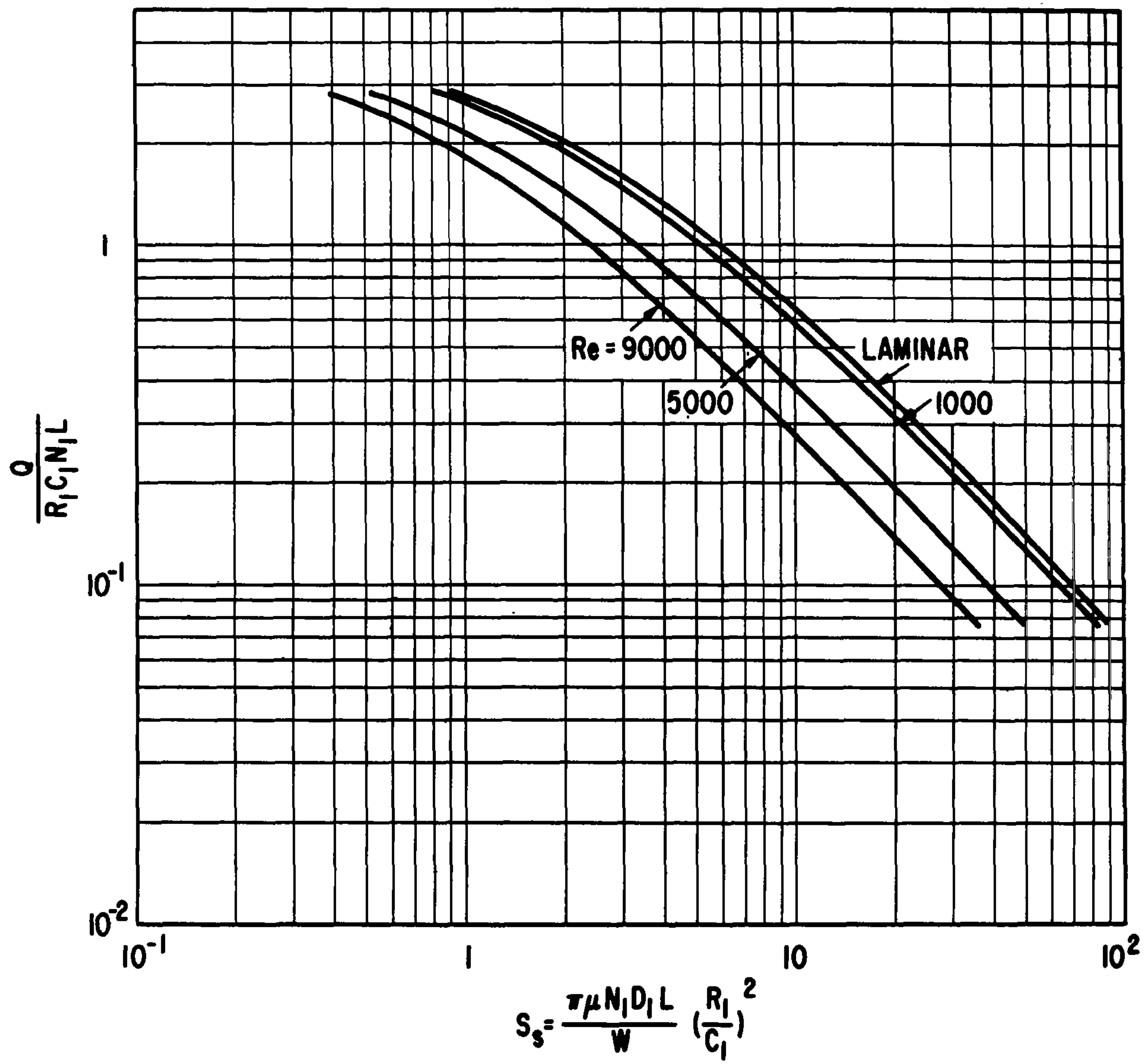

Figure 25. - Dimensionless flow $C_2/C_1 = 1.3$, $P_sLD_1/W = 0.2$.

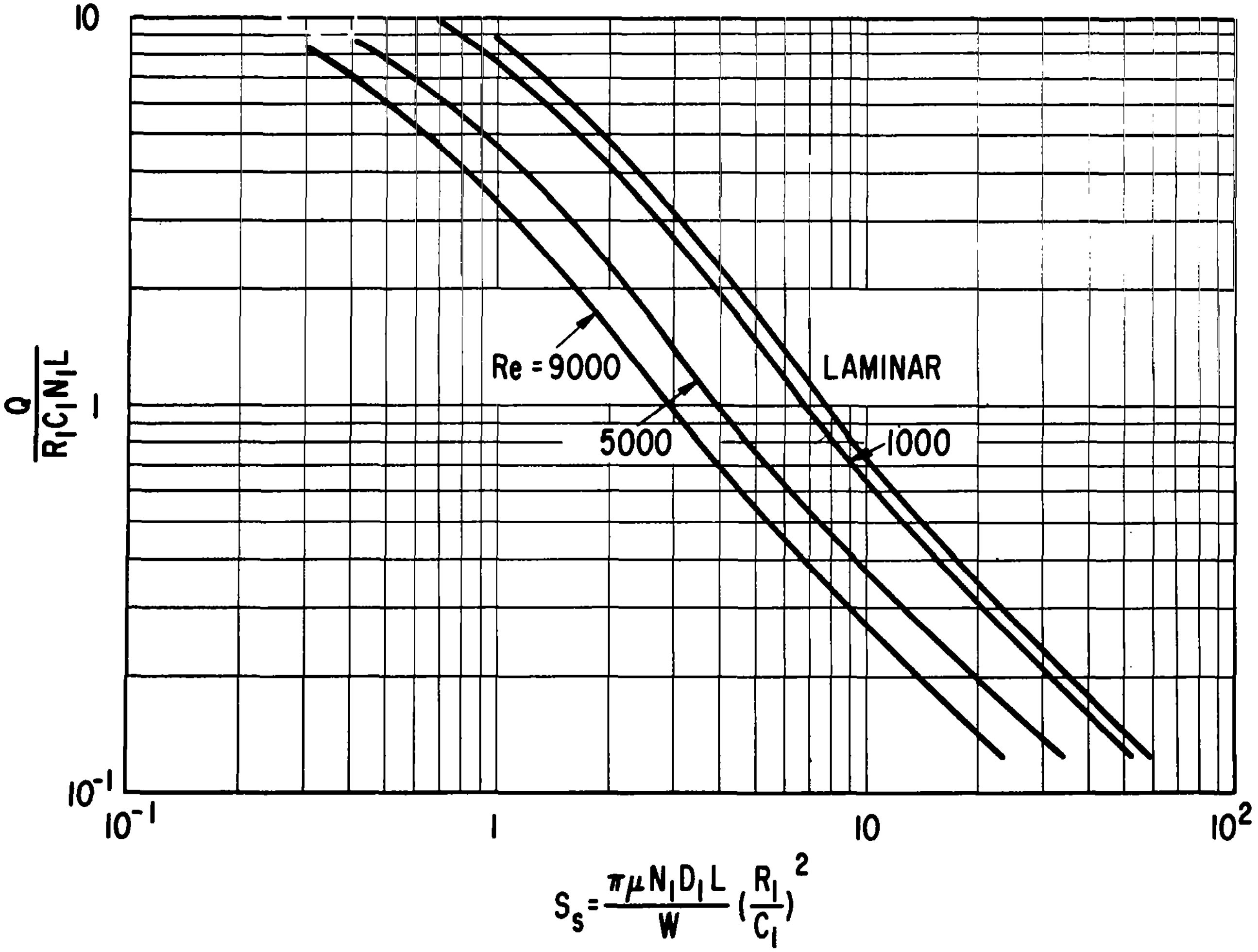

Figure 26. - Dimensionless flow $C_2/C_1 = 1.3$, $P_s L D_1/W = 1.5$.

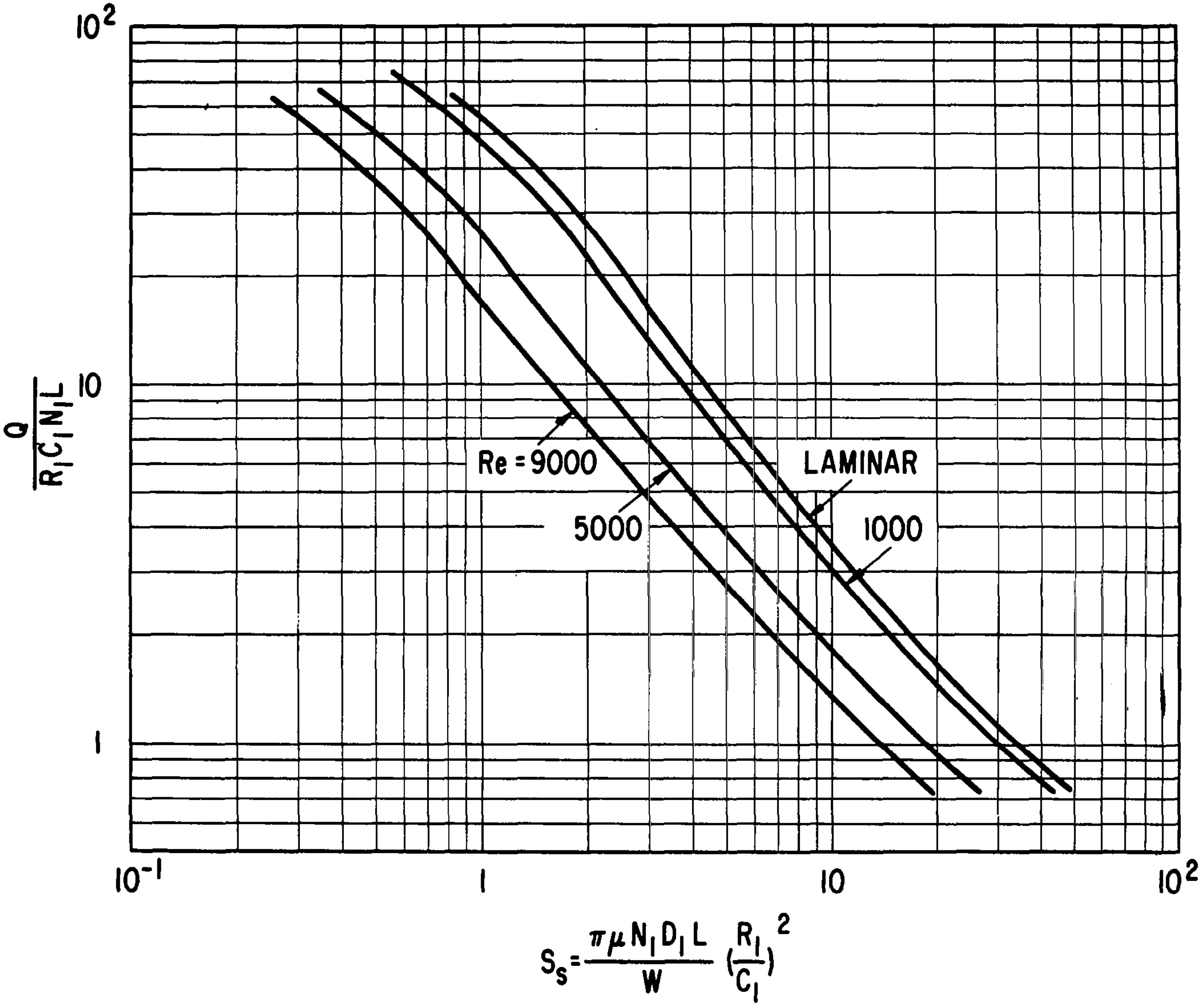

Figure 27. - Dimensionless flow $C_2/C_1 = 1.3$, $P_sLD_1/W = 10$.

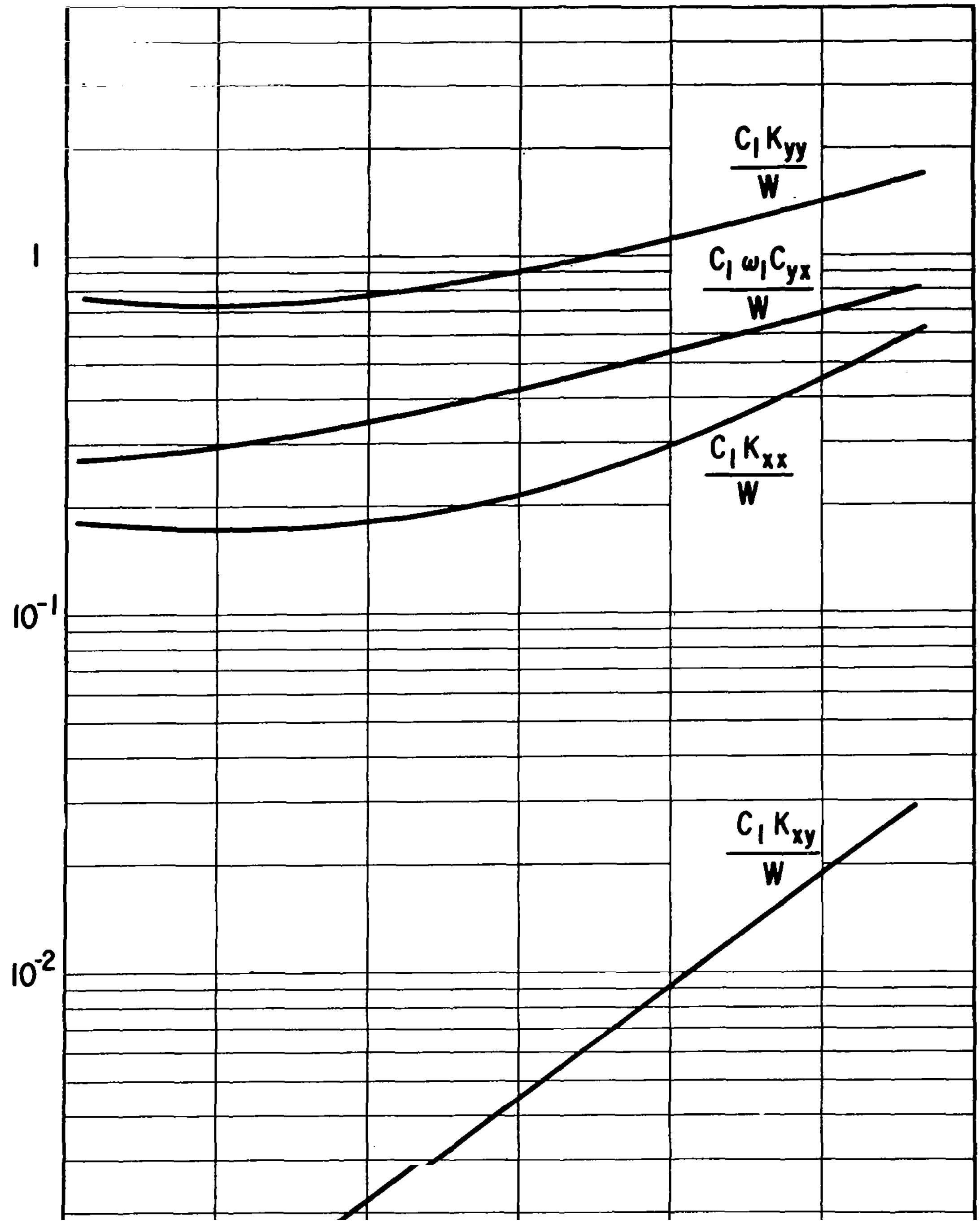
1
10^{-1}
10^{-2}
$\frac{C_1 K_{yy}}{W}$
$\frac{C_1 \omega_1 C_{yx}}{W}$
$\frac{C_1 K_{xx}}{W}$
$\frac{C_1 K_{xy}}{W}$

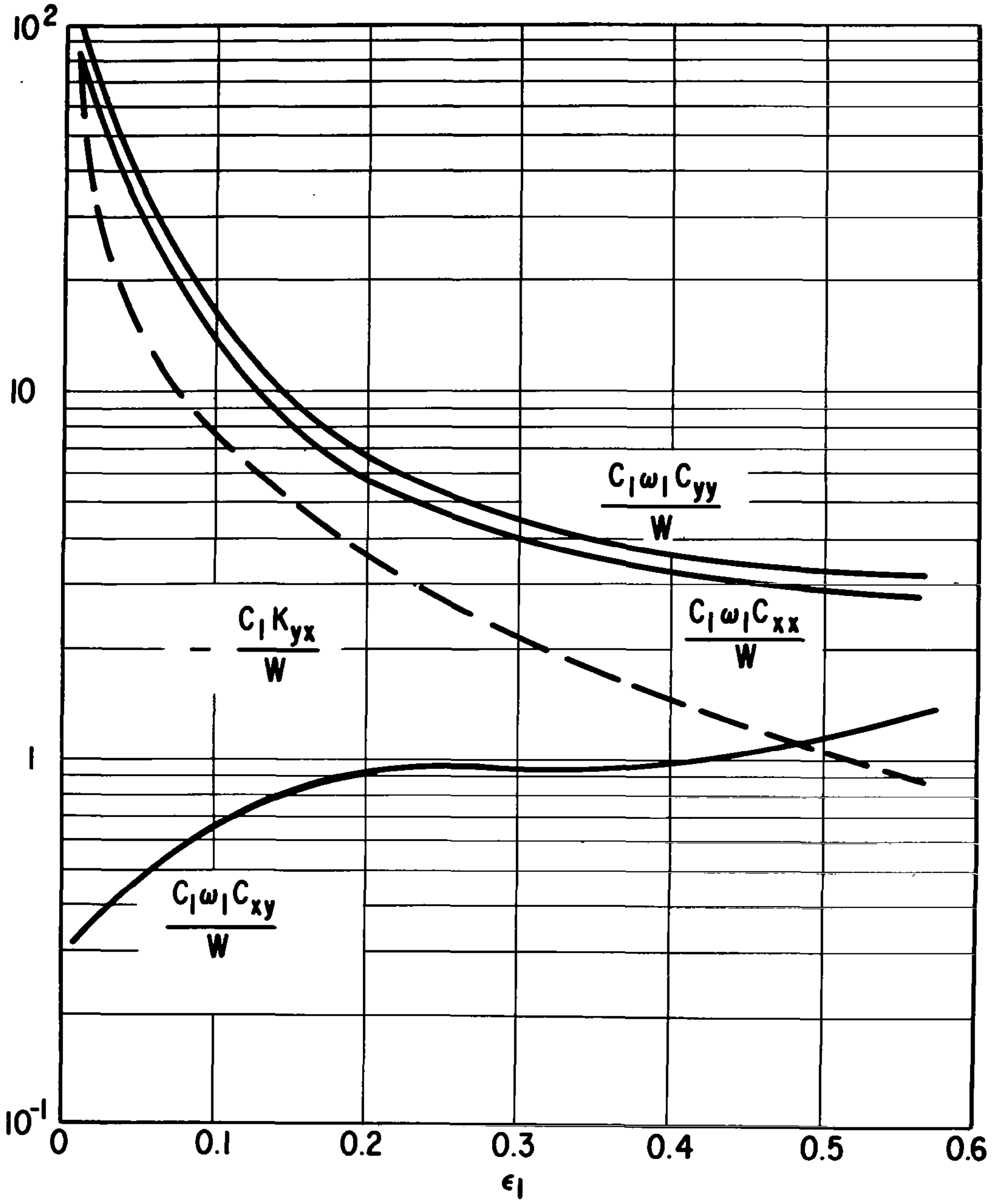

Figure 29. - Bearing dynamic coefficients $C_2/C_1 = 0.7$, $P_sLD_1/W = 1.5$.

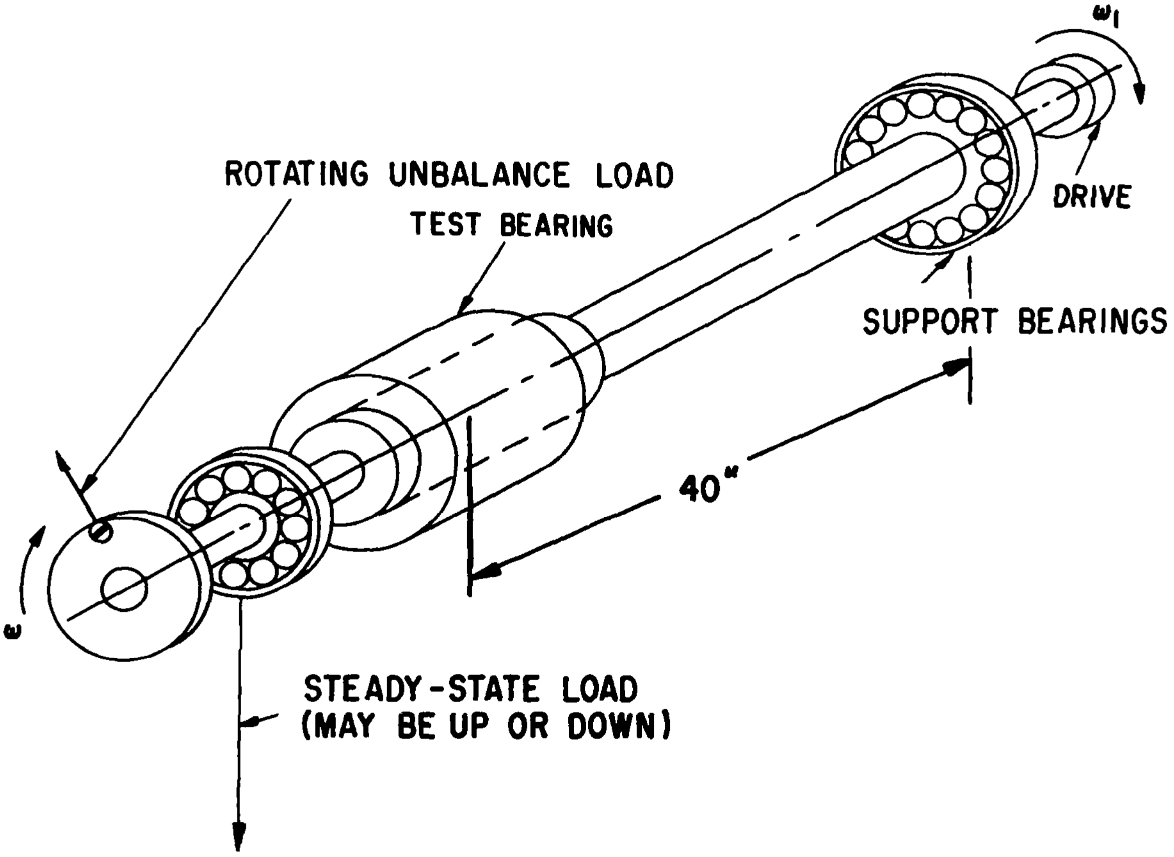

Figure 30. - Schematic of apparatus shaft and bearing assembly.

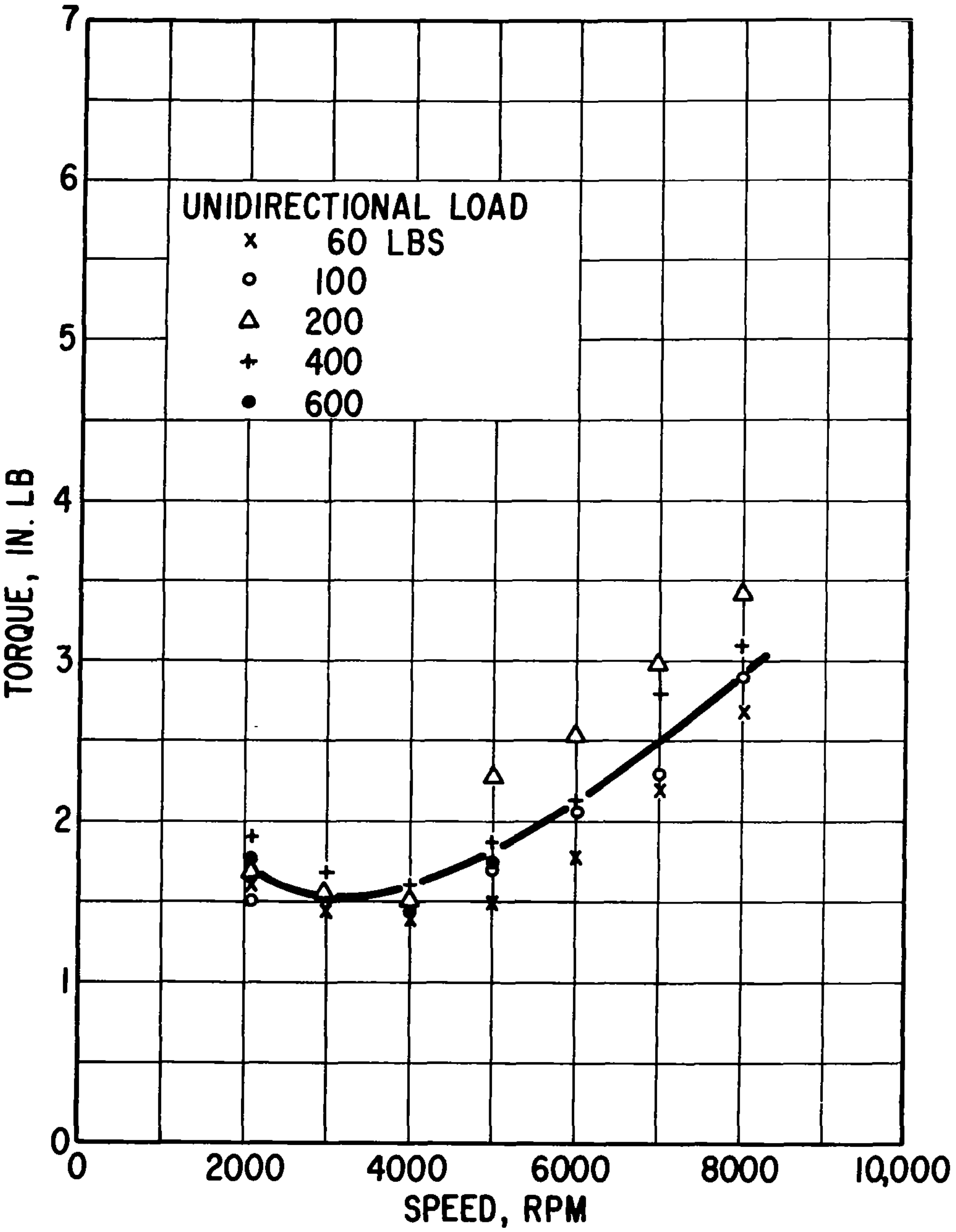

Figure 31. - Dynamic load bearing apparatus support and loader bearing friction torque.

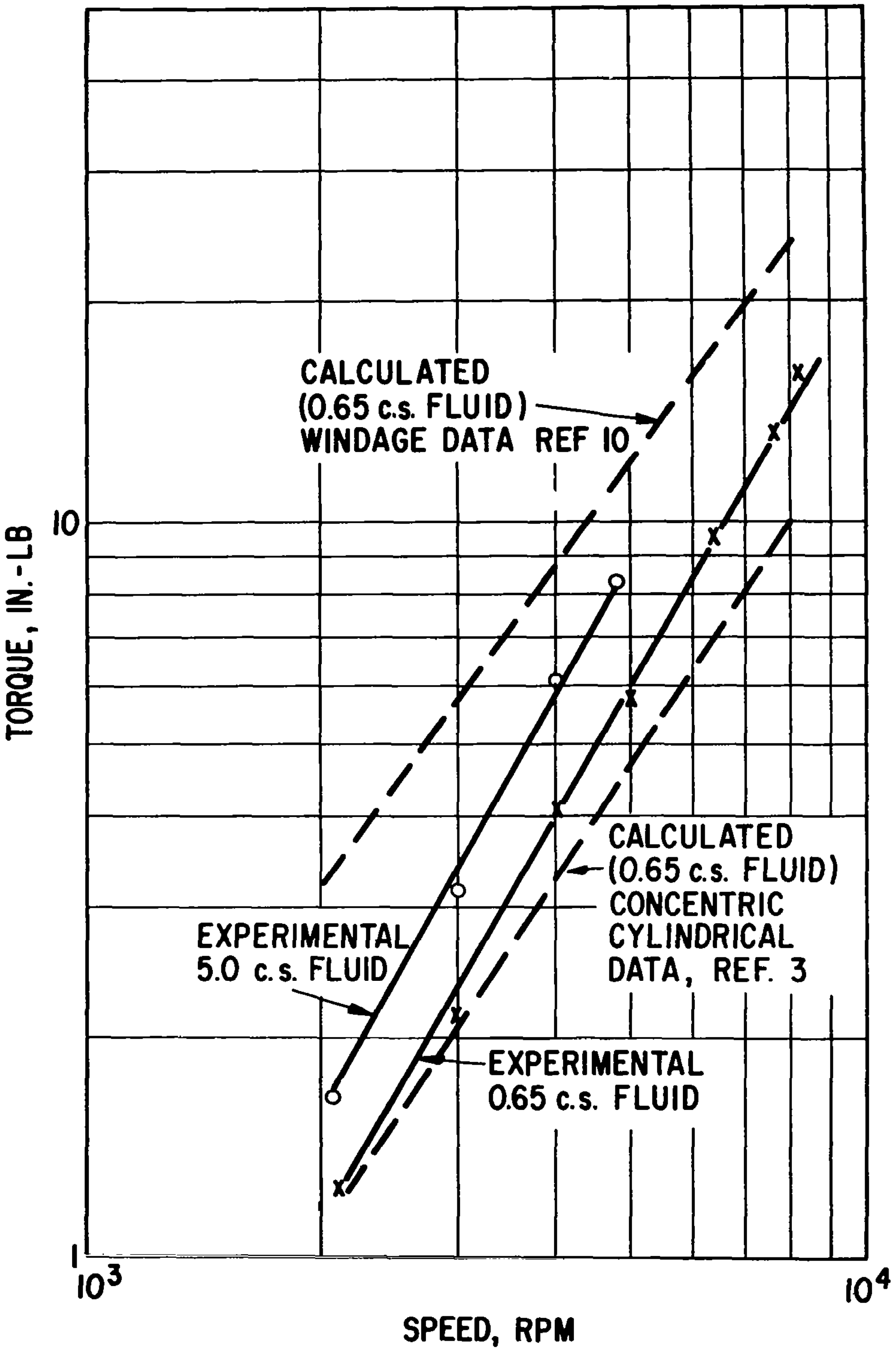

Figure 32. - Dynamic load bearing apparatus machined measured friction drag from test bearing and housing end seals.

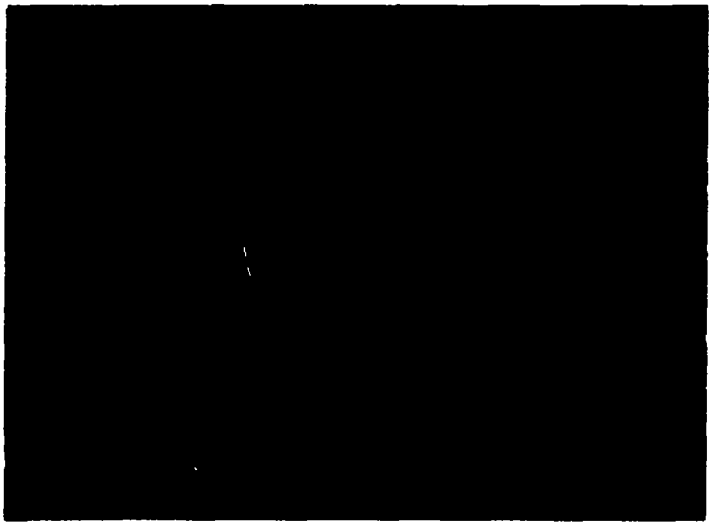

(a) 5000 rpm, 50 lb static load, 1 div. = 1.18 mils.

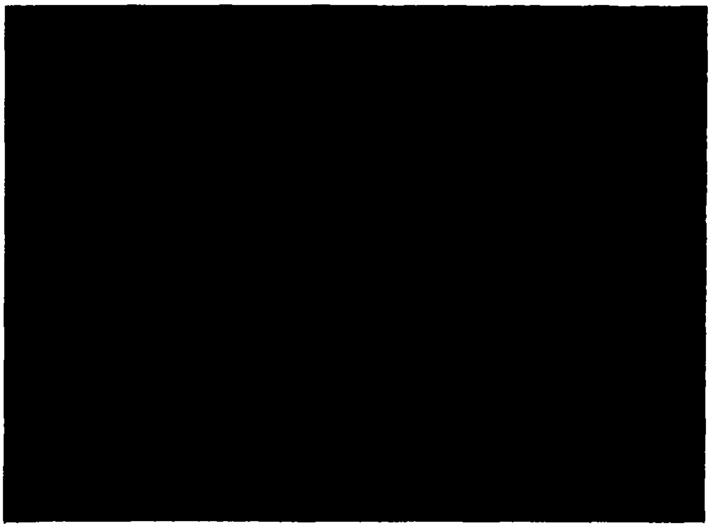

(b) 5000 rpm, 100 lb static load, 1 div. = 1.18 mils.

Figure 33. - Oscilloscope photographs of shaft motion with unstable inner film and stable outer film $C_2/C_1 = 0.7$, $P_sLD_1/W = 1.5$, 0.65 cs lubricant.

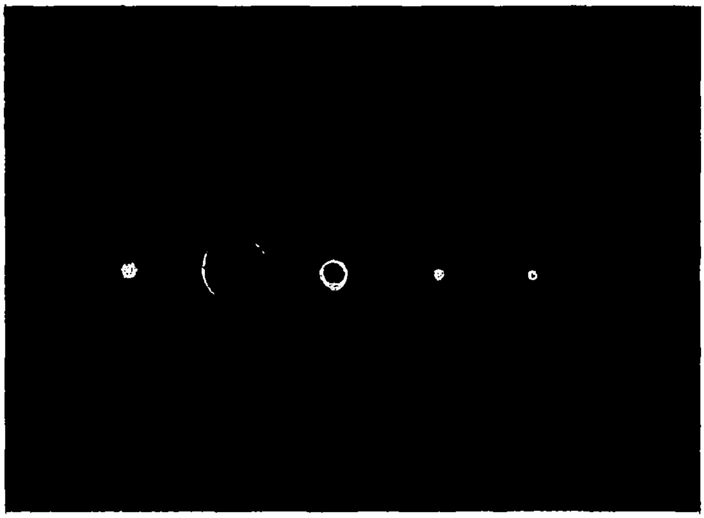

C_2/C_1 = 0.7, 5.0 cs fluid, 161 lbs static load,
1 div. = 0.59 mils

Figure 34. - Sequence of shaft motion measurements with increasing speed showing whirl onset and suppression. Sequence of orbits from left to right is: 4700, 5050, 6000, 7800 and 9000 rpm.

(a) 0.01 sec shutter speed.

(b) 0.02 sec shutter speed.

(c) 0.1 sec shutter speed.

Figure 35. - Oscilloscope photographs of shaft motion with both films unstable. 4000 rpm, 50 lb static load, 1 div. = 1.18 mils, $C_2/C_1 = 1.3$, 5.0 cs lubricant, $P_sLD_1/W = 1.5$.

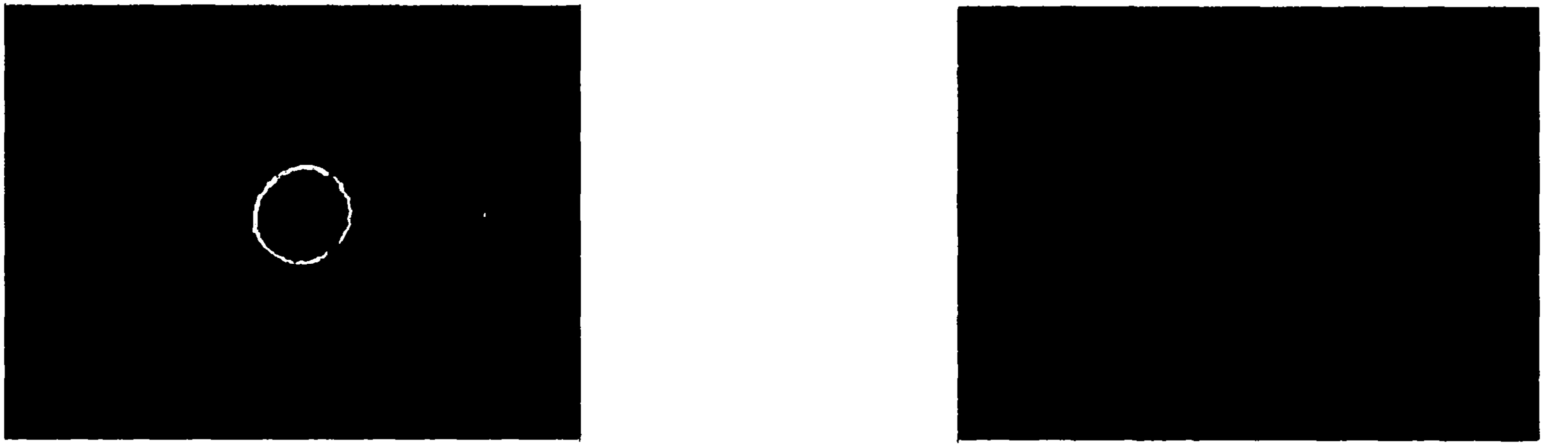

(a) Ring motion, 1 div. = 0.295 mils.

(b) Shaft motion, 1 div. = 0.59 mils.

7000 rpm, 100 lb static load, no rotating load, $C_2/C_1 = 1.3$, 5.0 cs, $P_sLD_1/W = 0.75$

(c) Ring motion, 1 div. = 0.295 mils.

(d) Shaft motion, 1 div. = 1.18 mils.

6000 rpm, 50 lb static load, with rotating load, $C_2/C_1 = 1.3$, 5.0 cs fluid, $P_sLD_1/W = 0.75$

Figure 36. - Oscilloscope photographs of ring and shaft motions with outer film unstable and inner film stable.

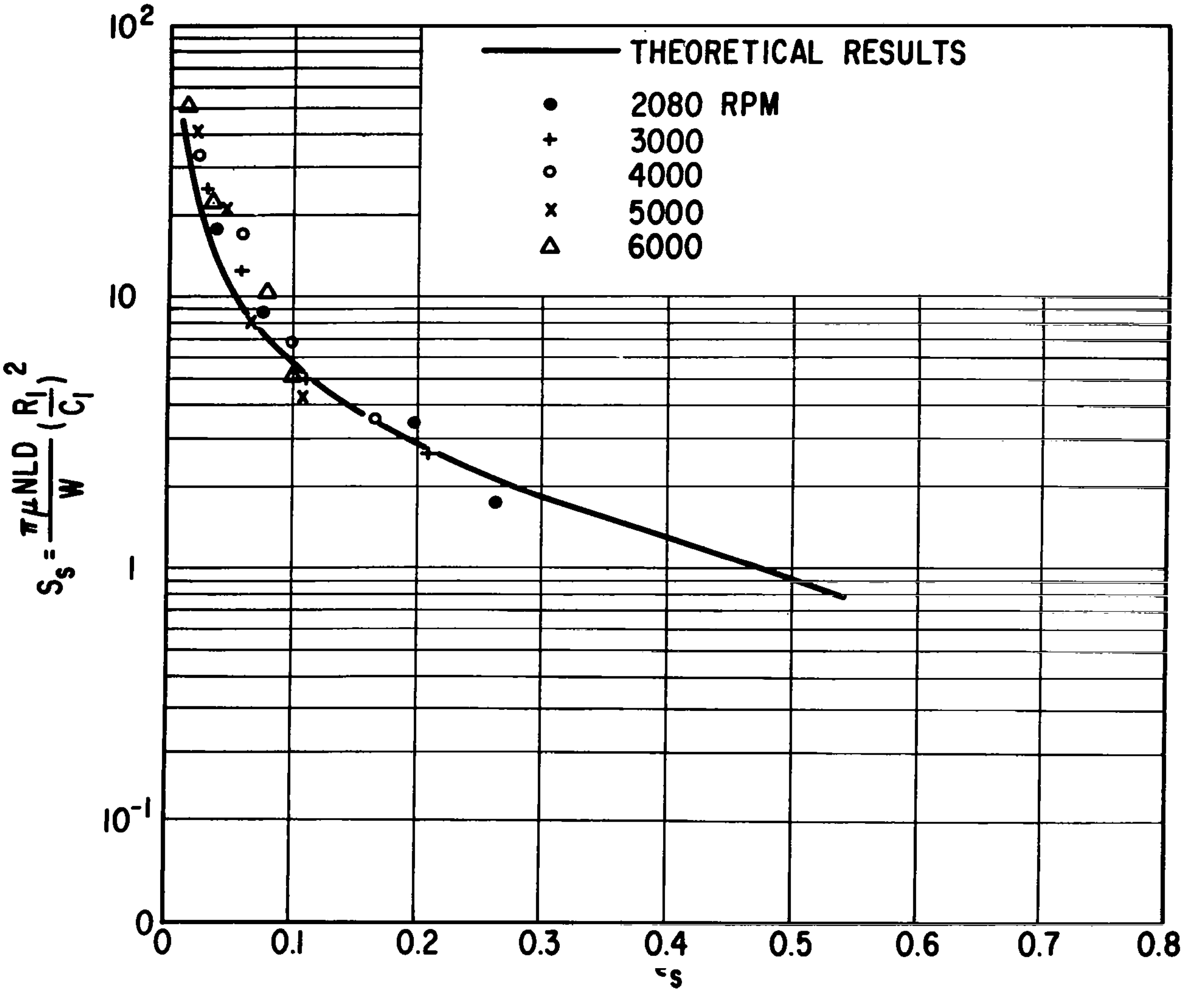
THEORETICAL RESULTS
● 2080 RPM
+ 3000
o 4000
x 5000
△ 6000
10^2
10
1
10^{-1}
0
0
0.1
0.2
0.3
0.4
0.5
0.6
0.7
0.8
ϵ_s
$S_s = \frac{\pi \mu N L D}{W} \left(\frac{R_1}{C_1}\right)^2$

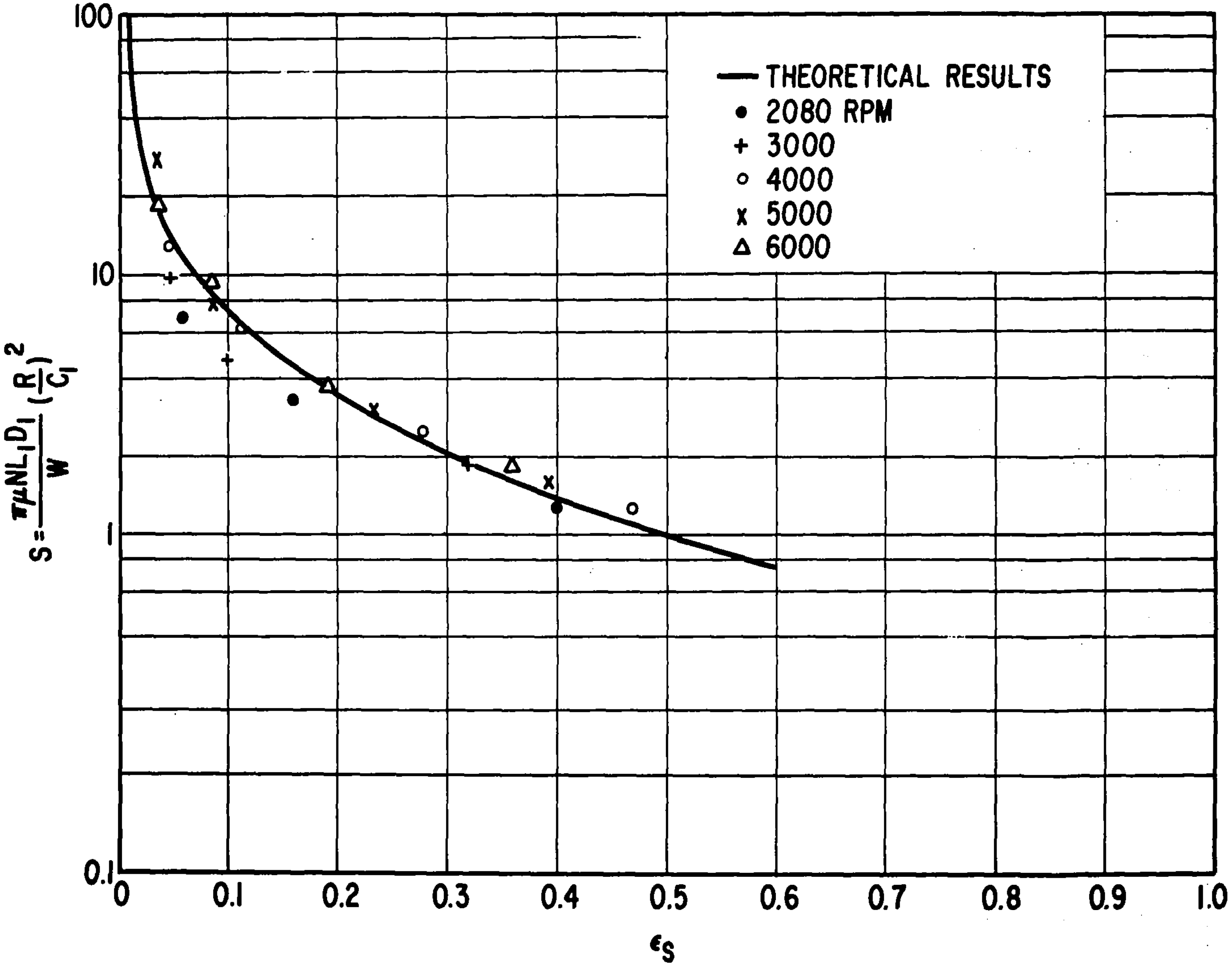

Figure 38. - Floating-ring bearing static load capacity measurements - laminar flow, $C_2/C_1 = 0.7$, $P_sLD_1/W = 1.5$.

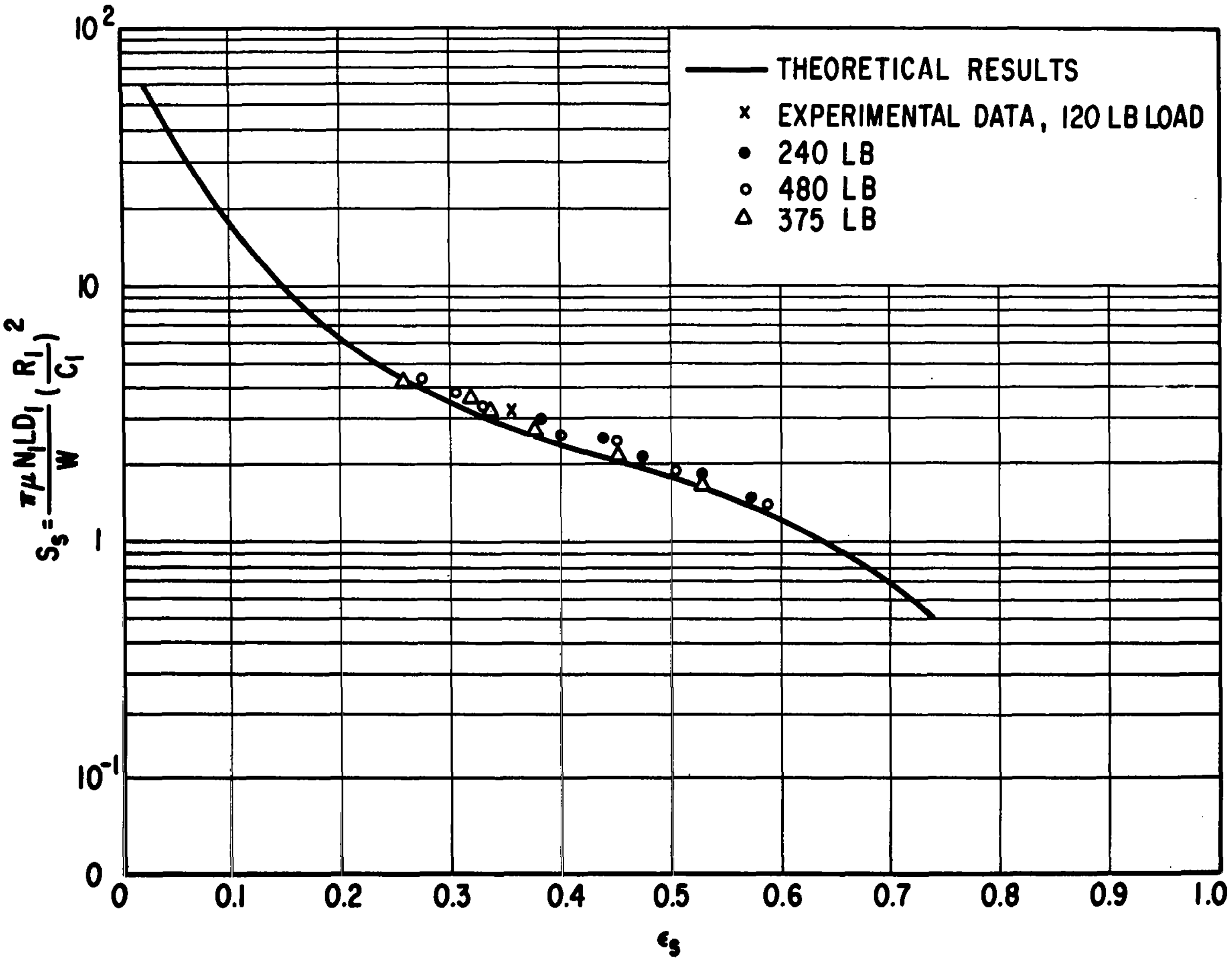

Figure 39. - Floating-ring bearing static load capacity measurements - laminar flow, $C_2/C_1 = 1.3$, $P_sLD_1/W = 1.5$.

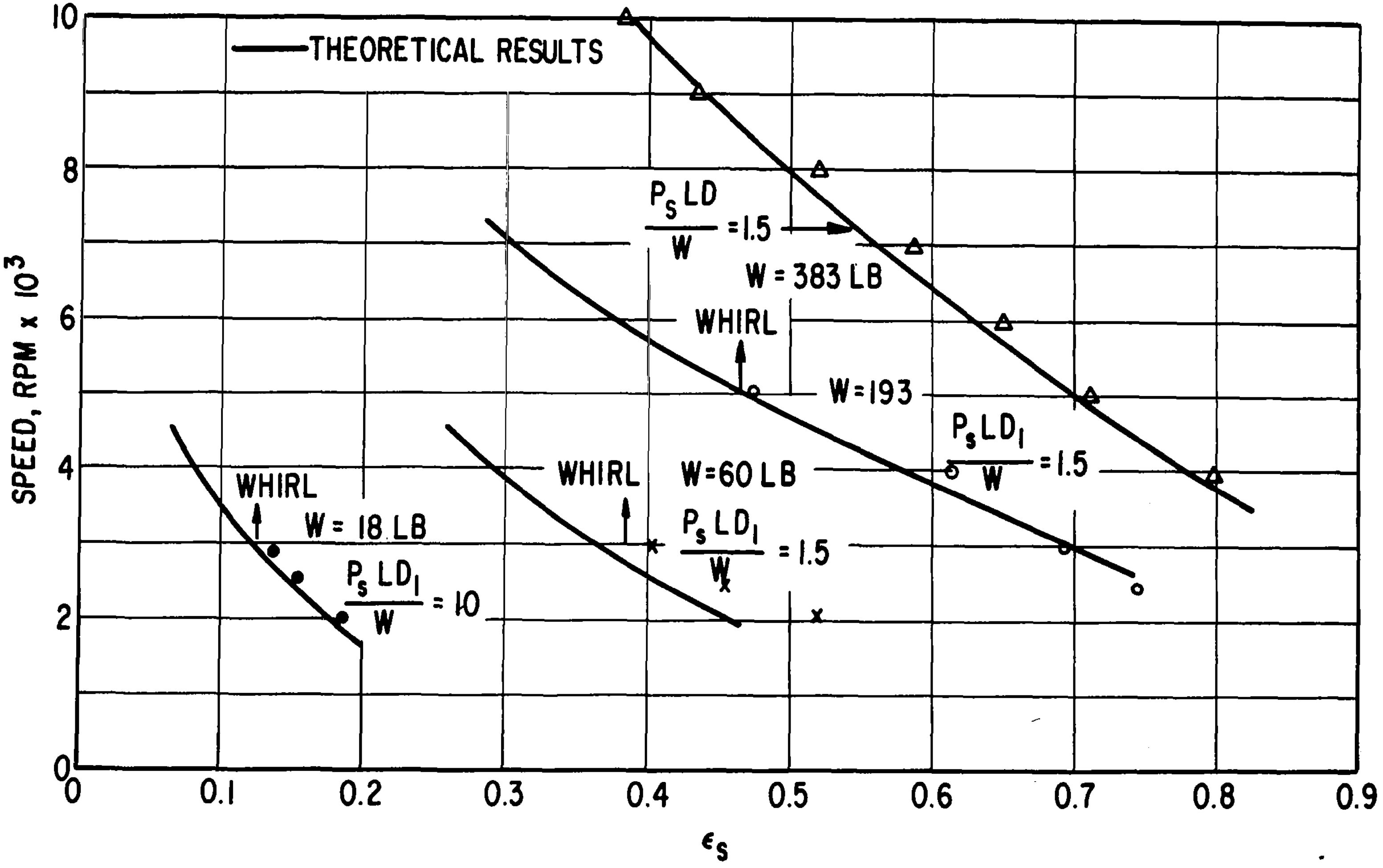

Figure 40. - Floating-ring bearing static load capacity measurements - turbulent flow, C_2/C_1 = 0.7.

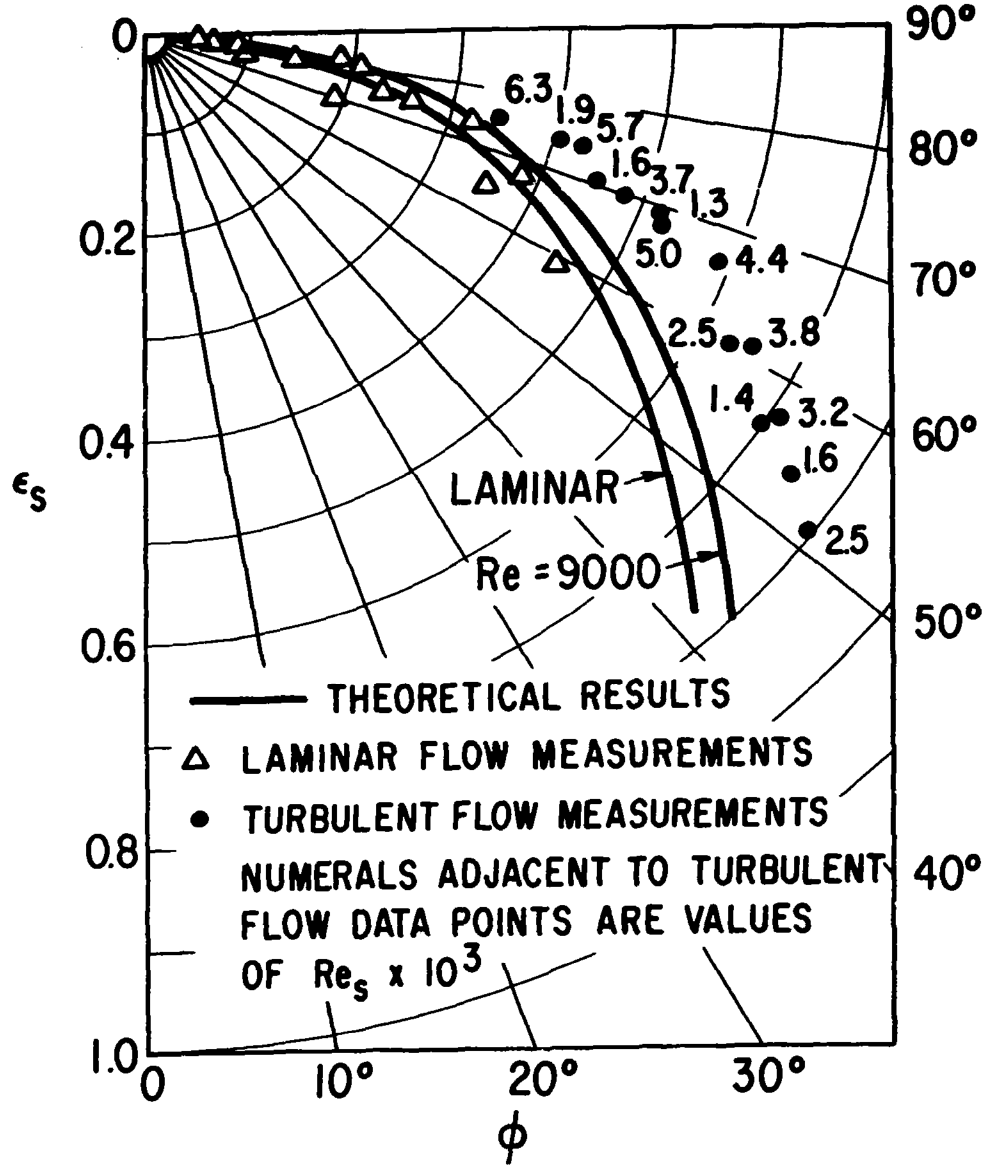

Figure 41. - Floating-ring bearing attitude angle - eccentricity measurements - $C_2/C_1 = 0.7$, $P_sLD_1/W = 1.5$.

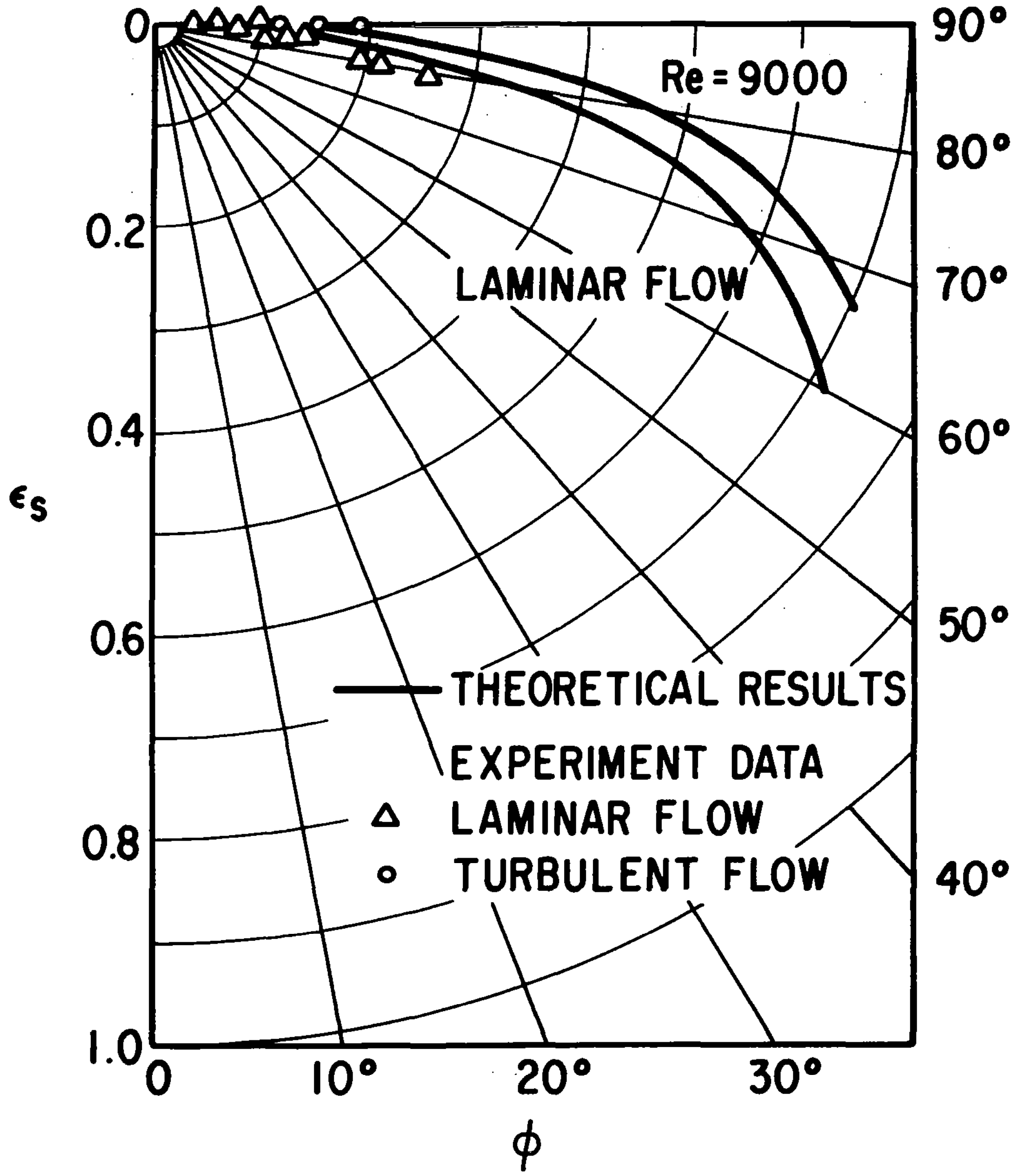

Figure 42. - Floating-ring bearing attitude angle - eccentricity measurements - $C_2/C_1 = 0.7$, $P_sLD_1/W = 10$.

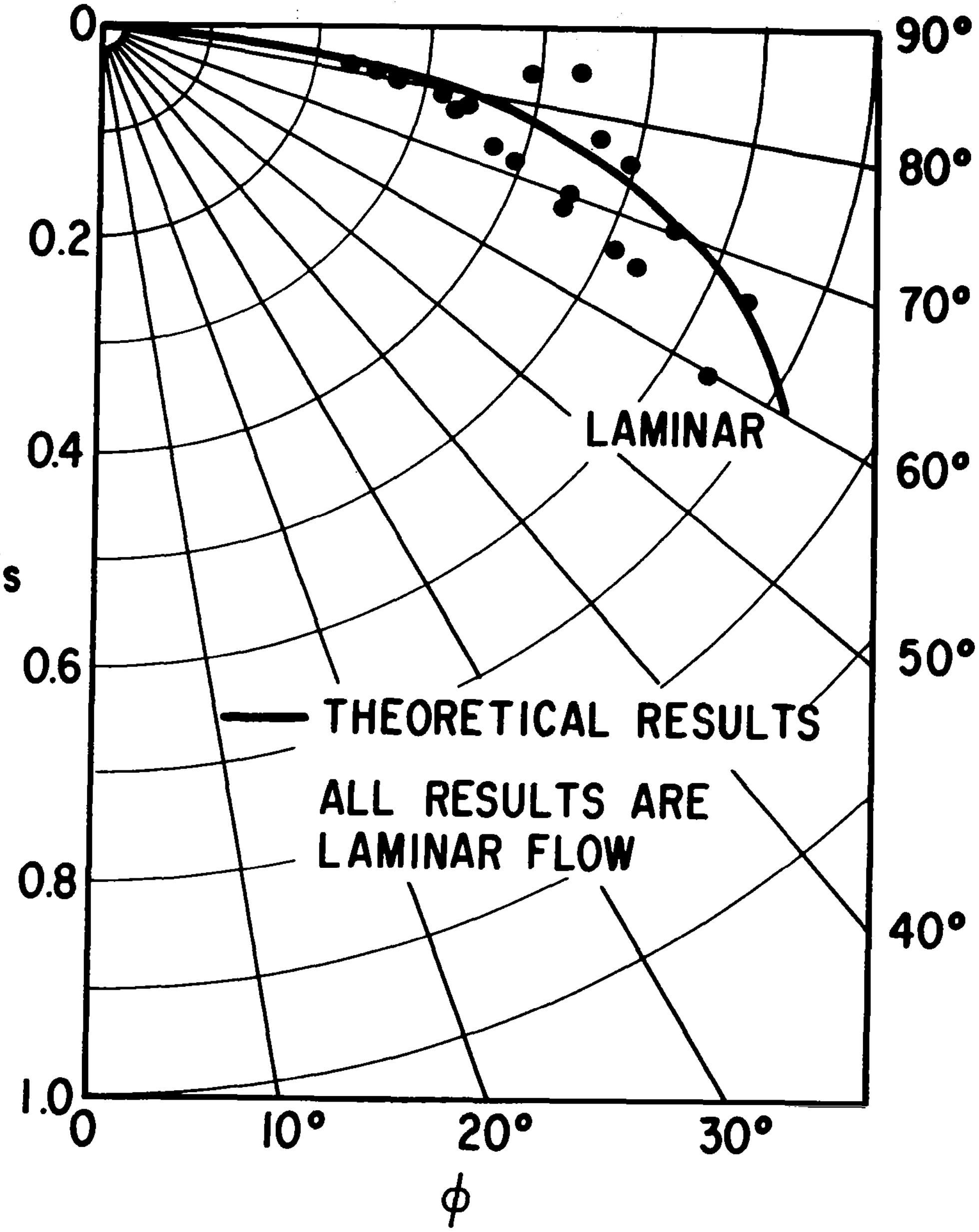

Figure 43. - Floating-ring bearing attitude angle - eccentricity measurements - $C_2/C_1 = 1.3$, $P_sLD_1/W = 1.5$.

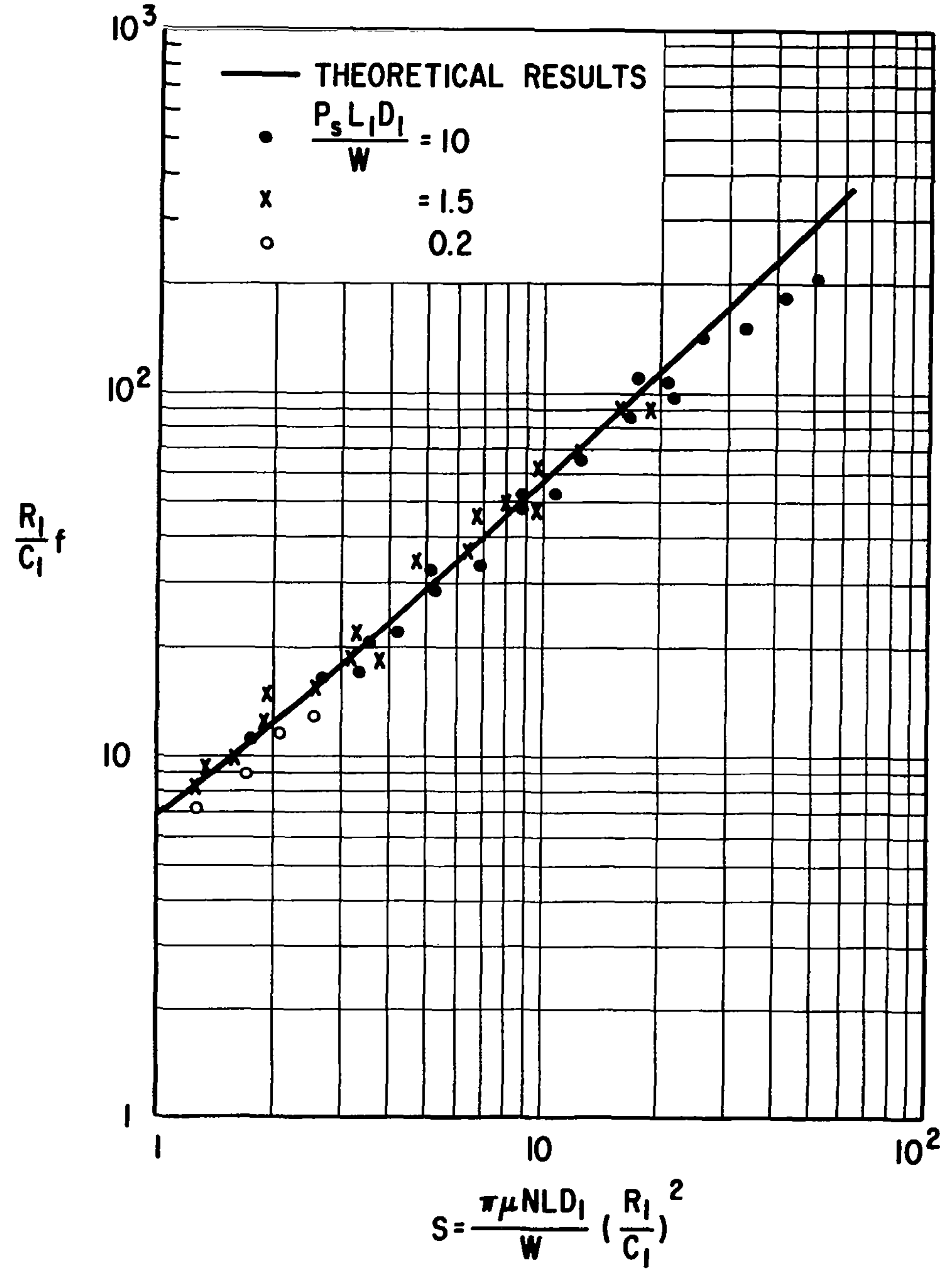

Figure 44. - Floating-ring bearing friction torque measurements - laminar flow $C_2/C_1 = 0.7$.

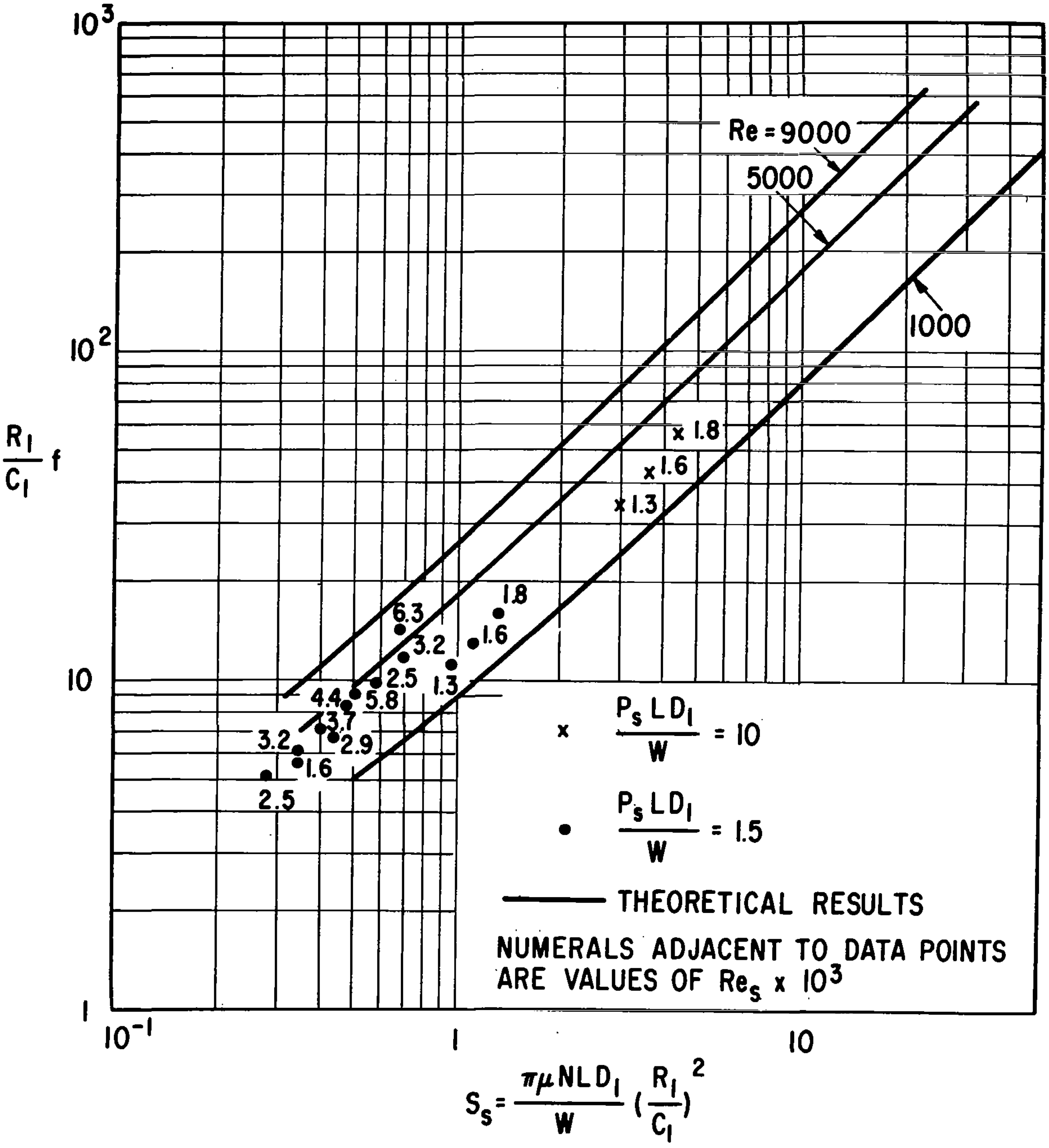

Figure 45. - Floating-ring bearing friction torque measurements - turbulent flow $C_2/C_1 = 0.7$.

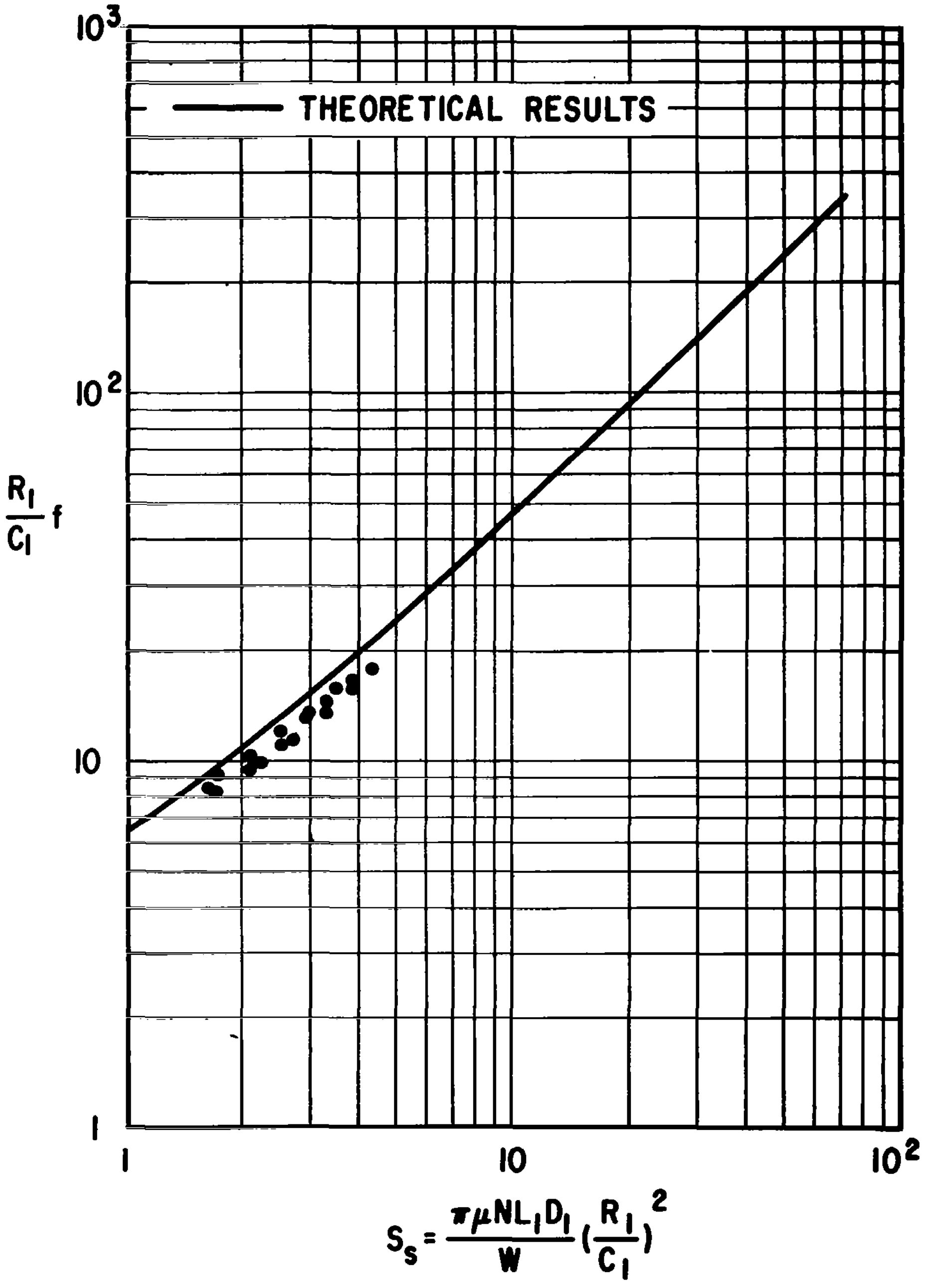

Figure 46. - Floating-ring bearing friction torque measurements - laminar flow $C_2/C_1 = 1.3$.

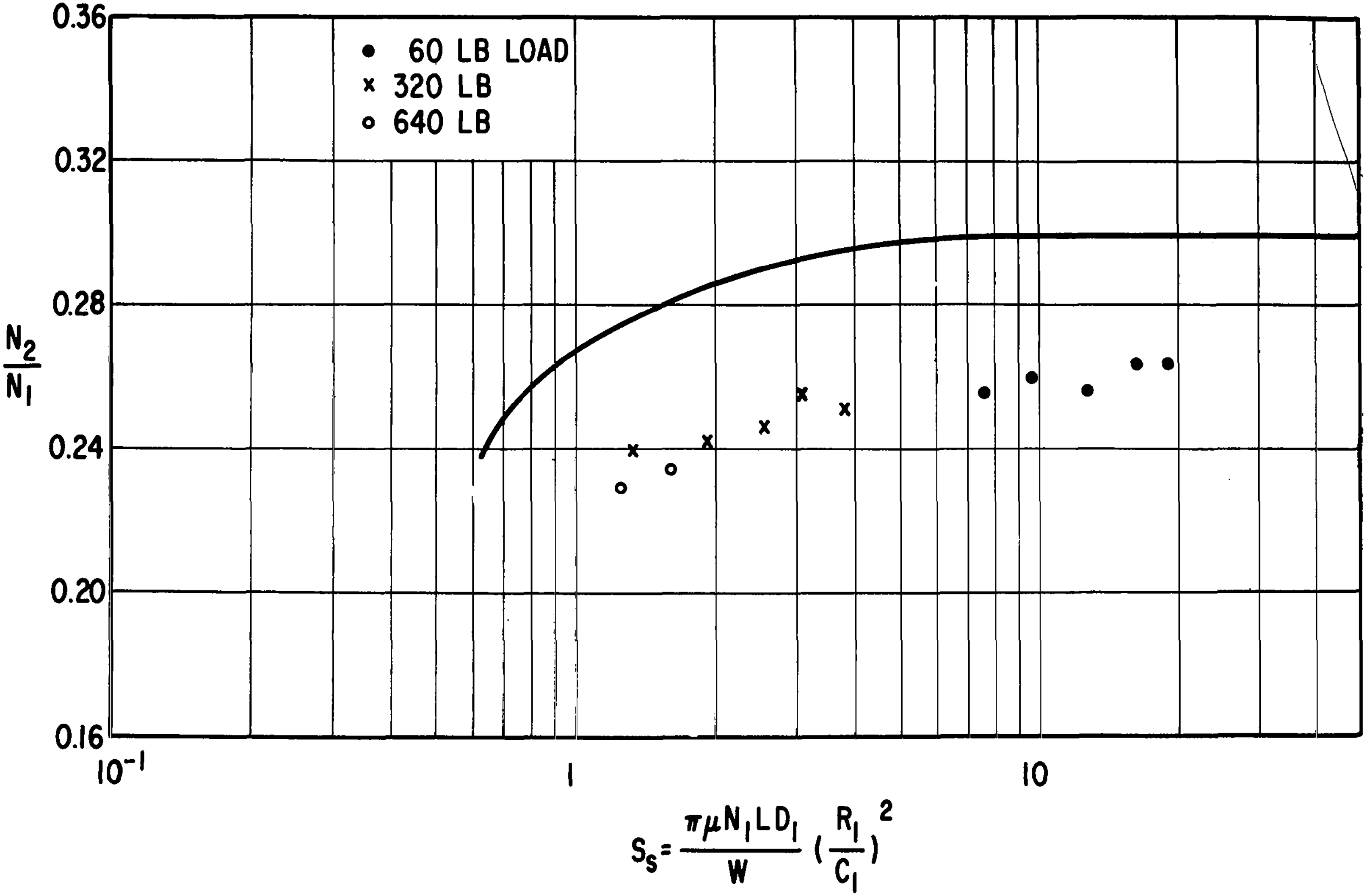

Figure 47. - Floating-ring bearing ring speed measurements - laminar flow $C_2/C_1 = 0.7$, $P_s L D_1/W = 1.5$.

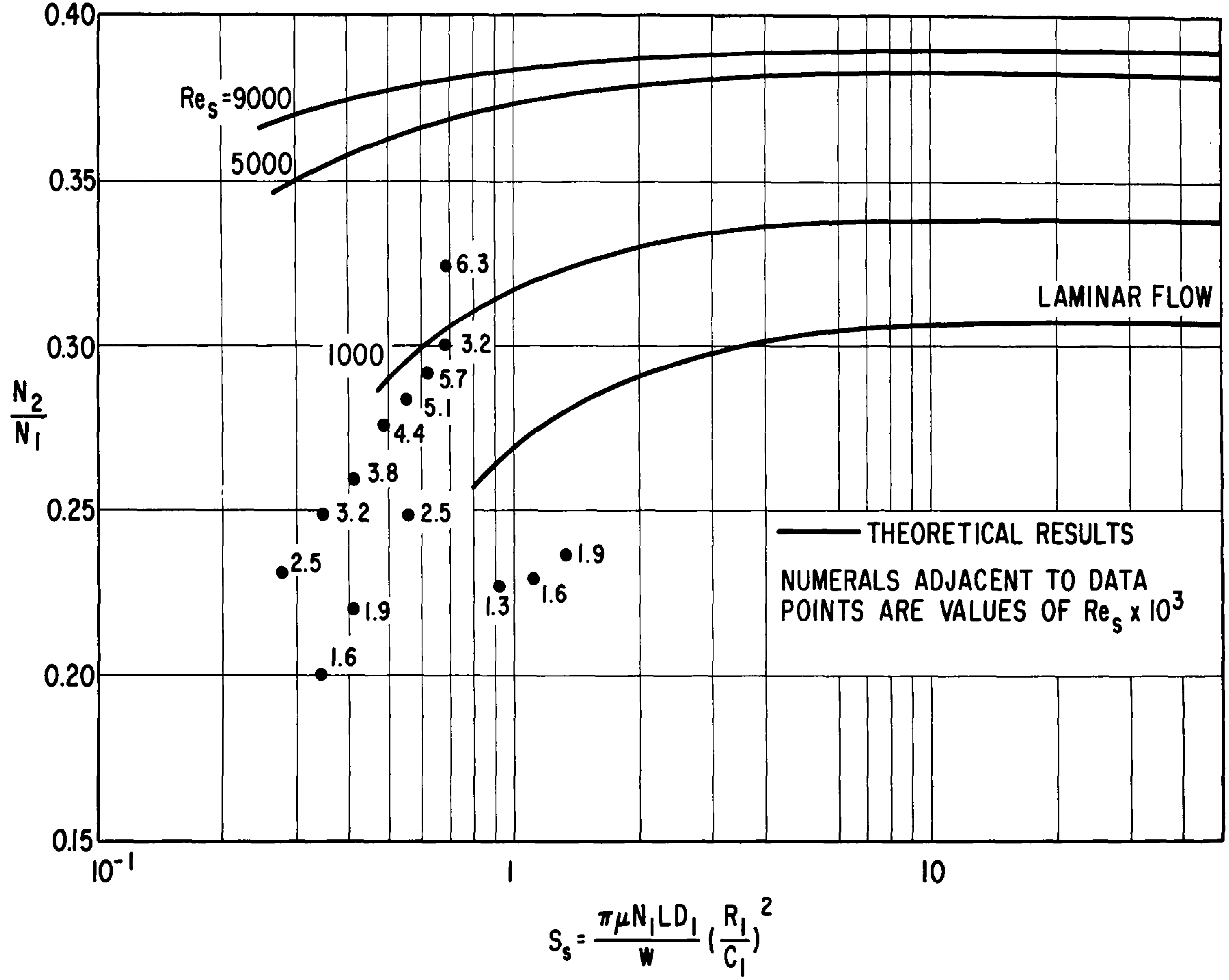

Figure 48. - Floating-ring bearing ring speed measurements - turbulent flow $C_2/C_1 = 0.7$, $P_s L D_1/W = 1.5$.

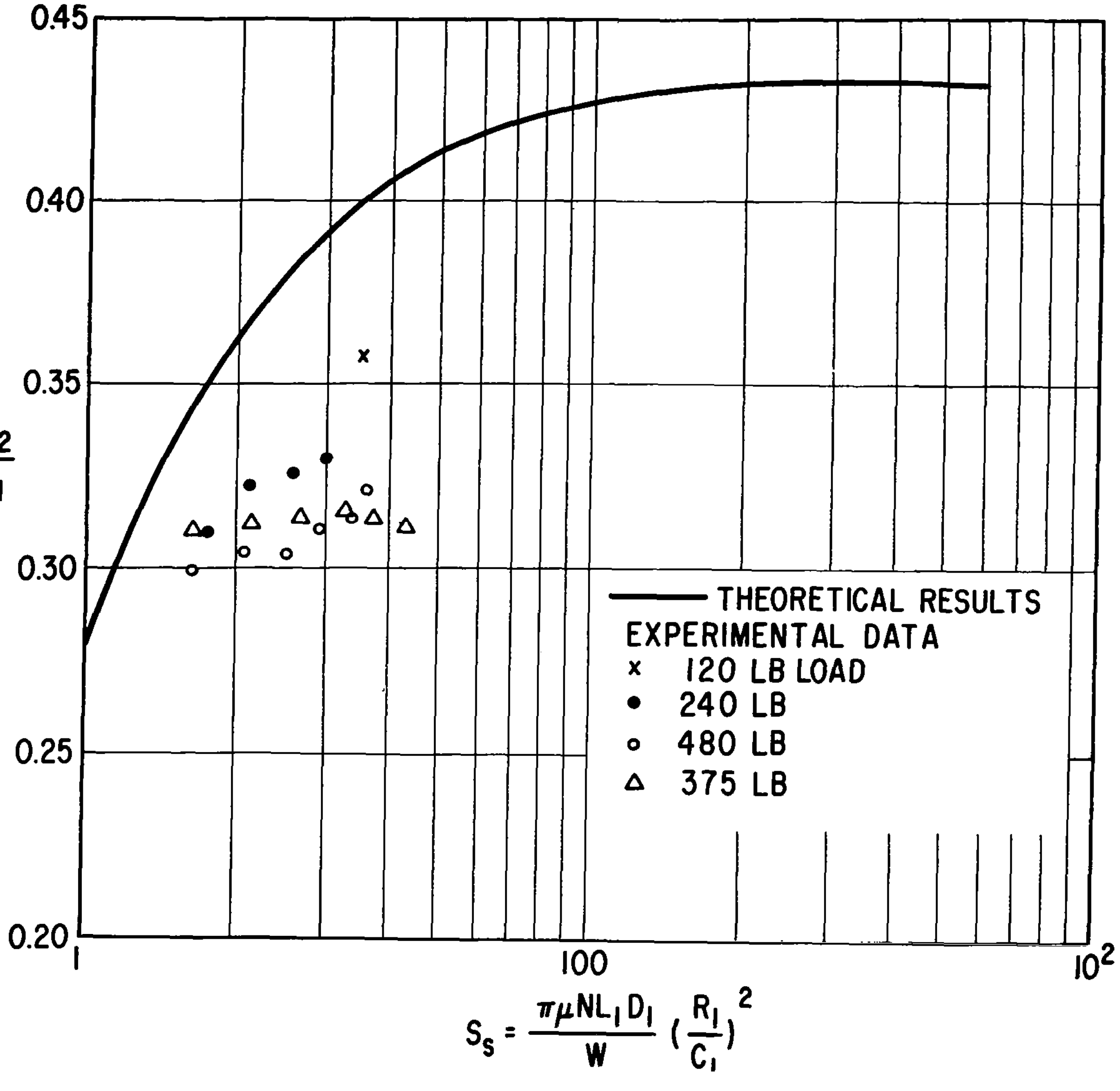
0.45
0.40
0.35
0.30
0.25
0.20
$\frac{N_2}{N_1}$
1
100
10^2
$S_s = \frac{\pi \mu N L_1 D_1}{W} \left(\frac{R_1}{C_1}\right)^2$
THEORETICAL RESULTS
EXPERIMENTAL DATA
× 120 LB LOAD
● 240 LB
○ 480 LB
△ 375 LB

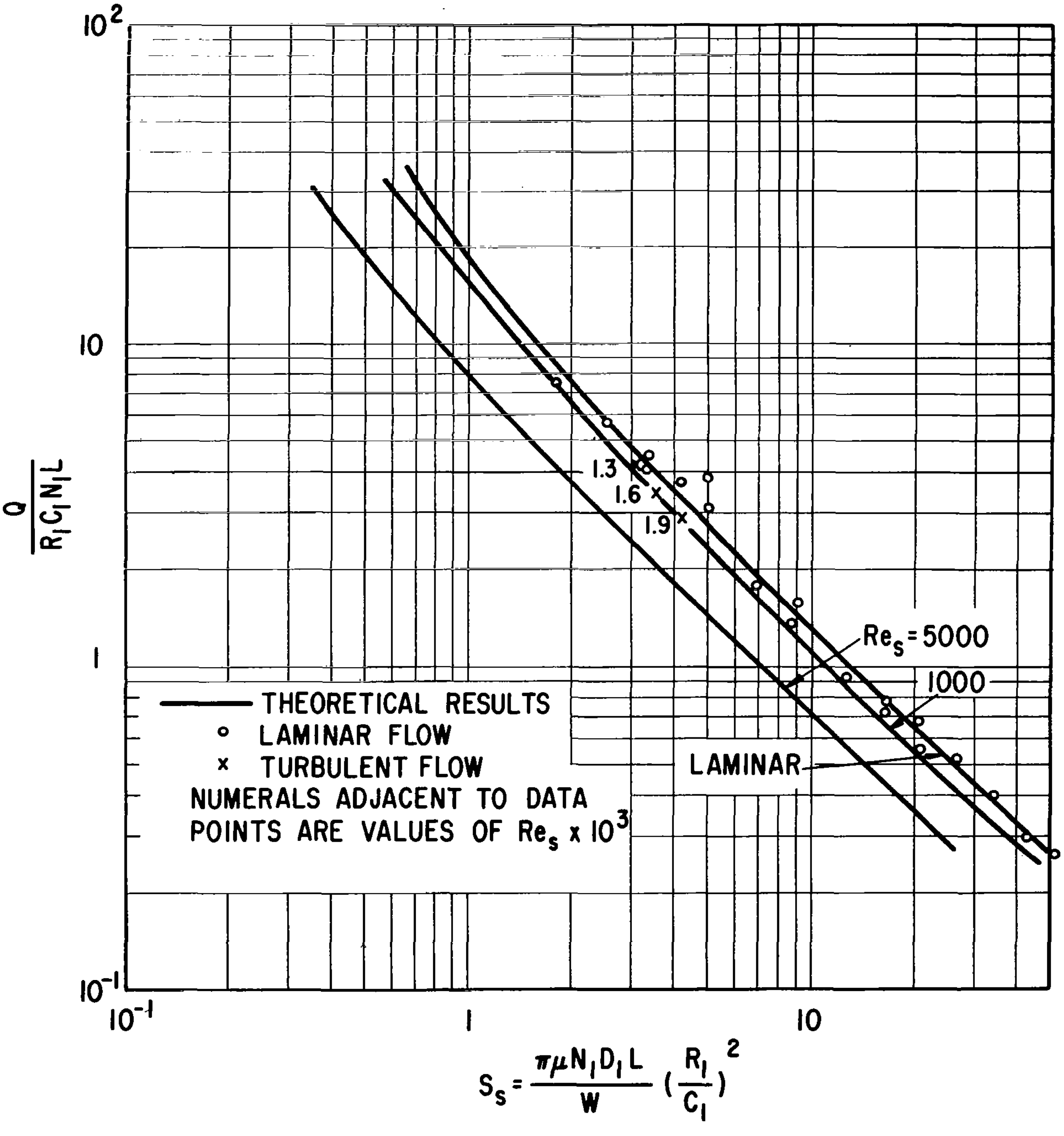

Figure 50. - Floating-ring bearing flow rate measurements - $C_2/C_1 = 0.7$, $P_s L D_1/W = 10$.

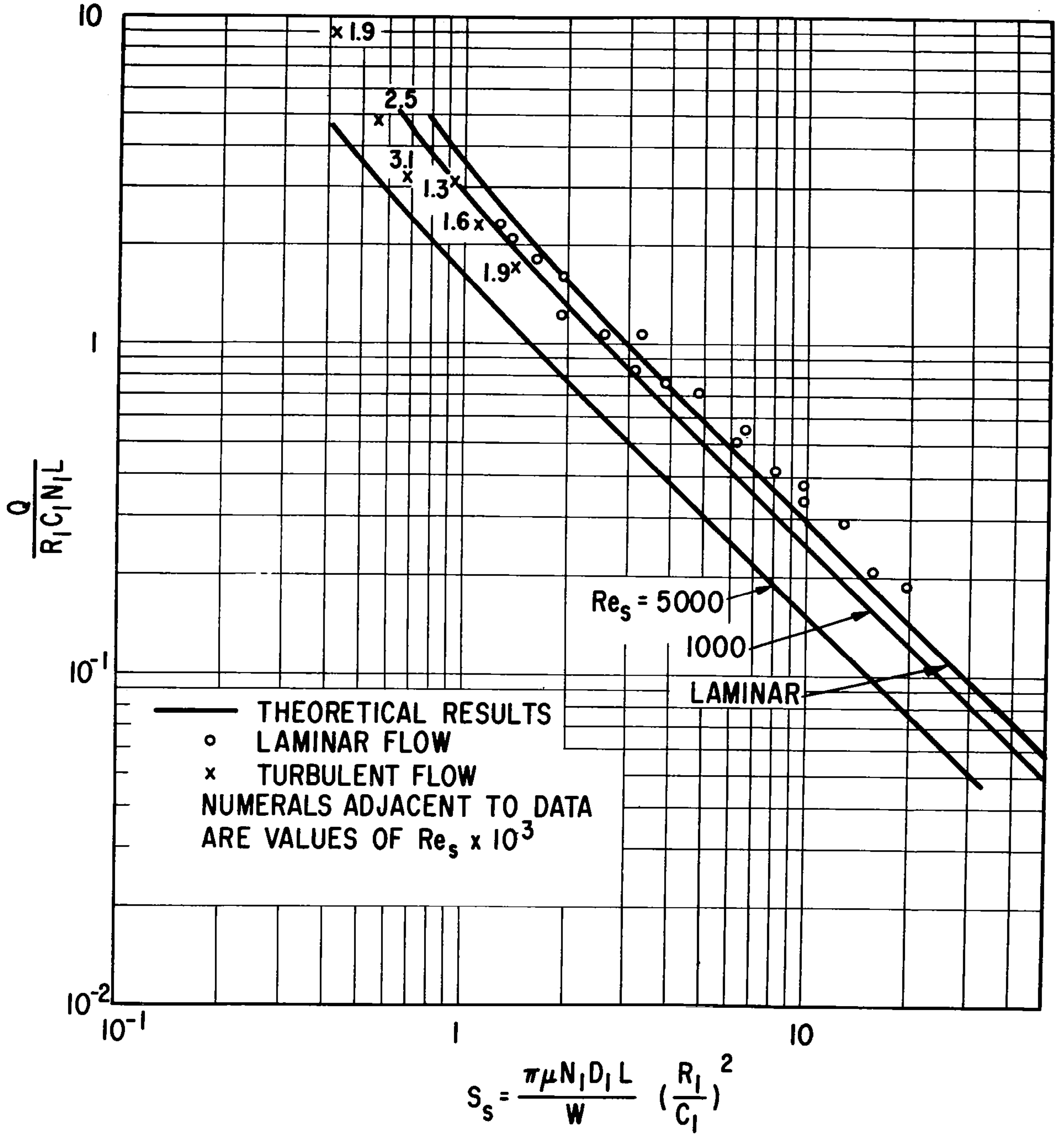

Figure 51. - Floating-ring bearing flow rate measurements - $C_2/C_1 = 0.7$, $P_sLD_1/W = 1.5$.

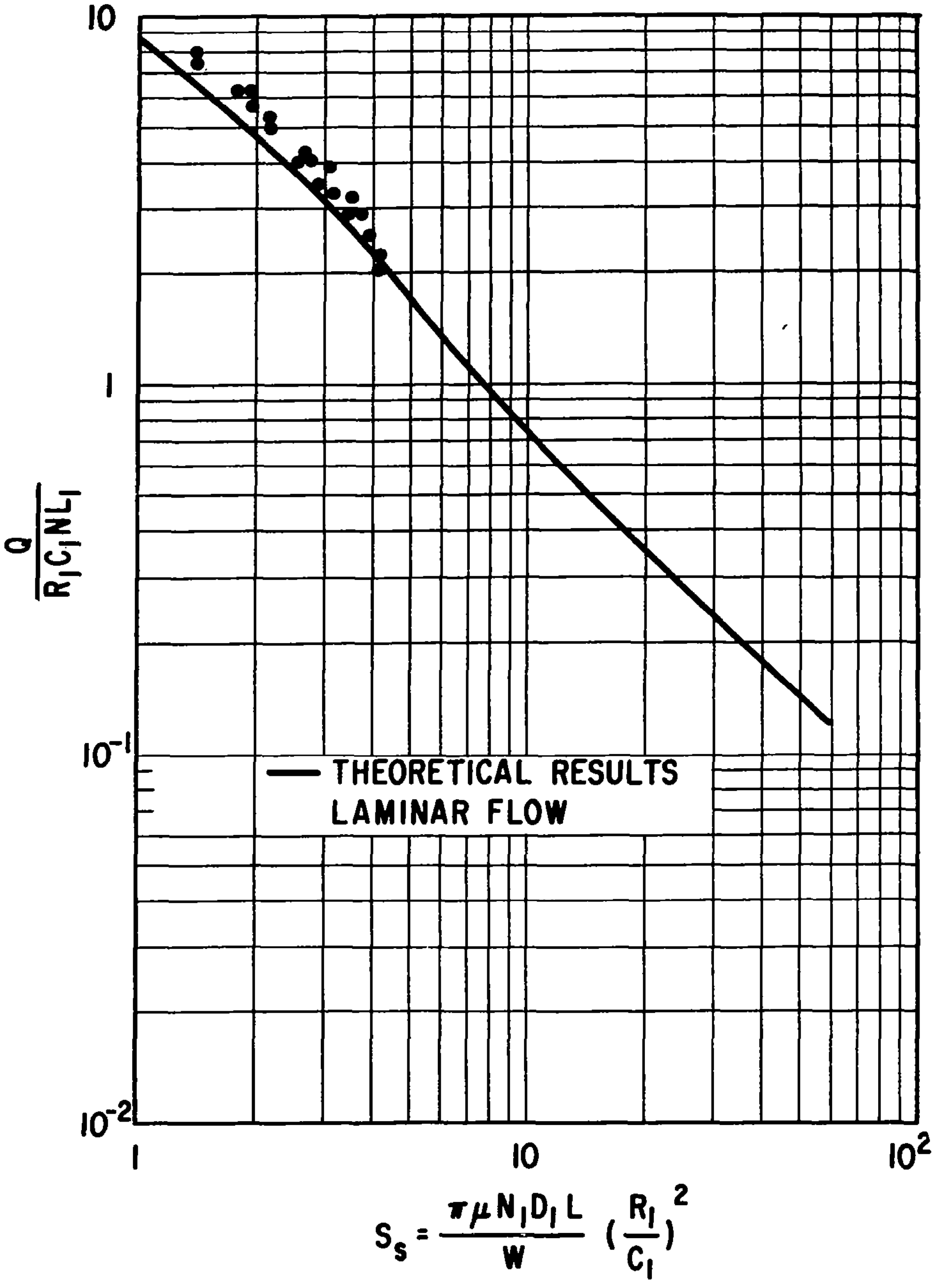

Figure 52. - Floating-ring bearing flow rate measurements - $C_2/C_1 = 1.3$, $P_sLD_1/W = 1.5$.

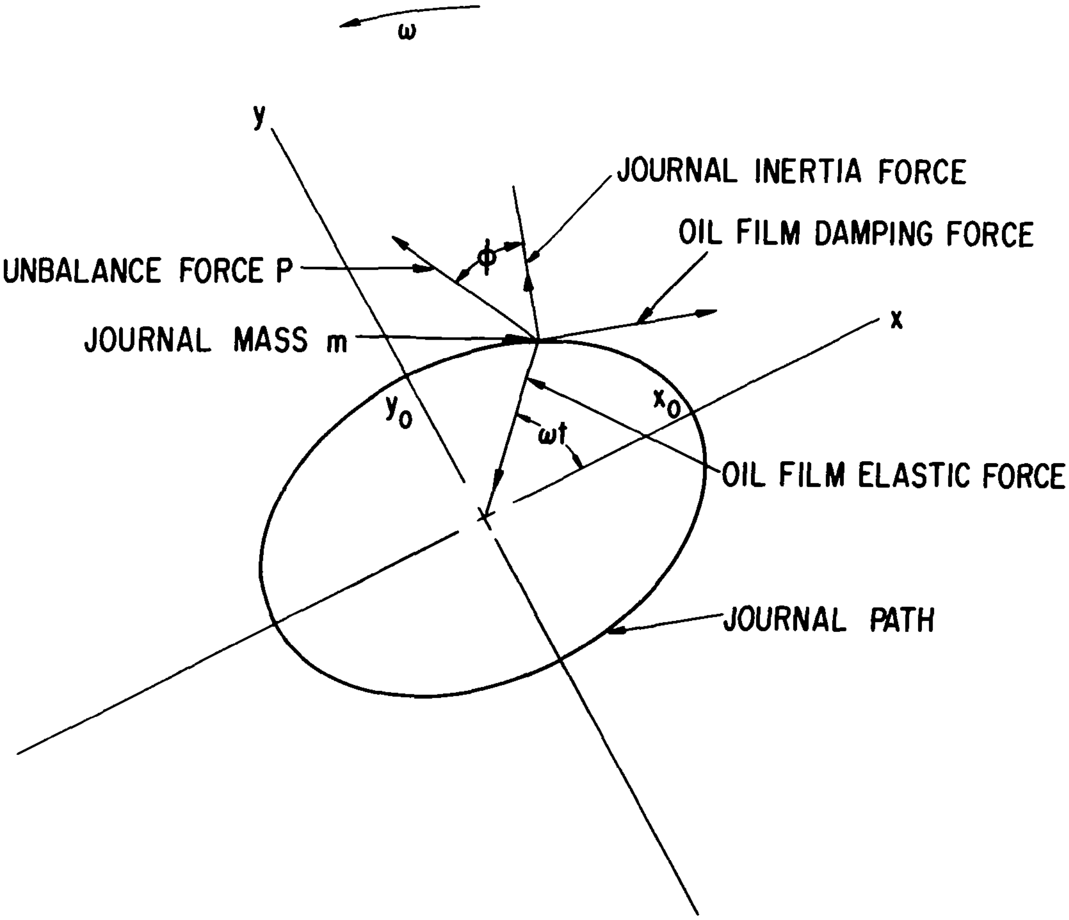

Figure 53. - Typical shaft locus path showing force equilibrium.

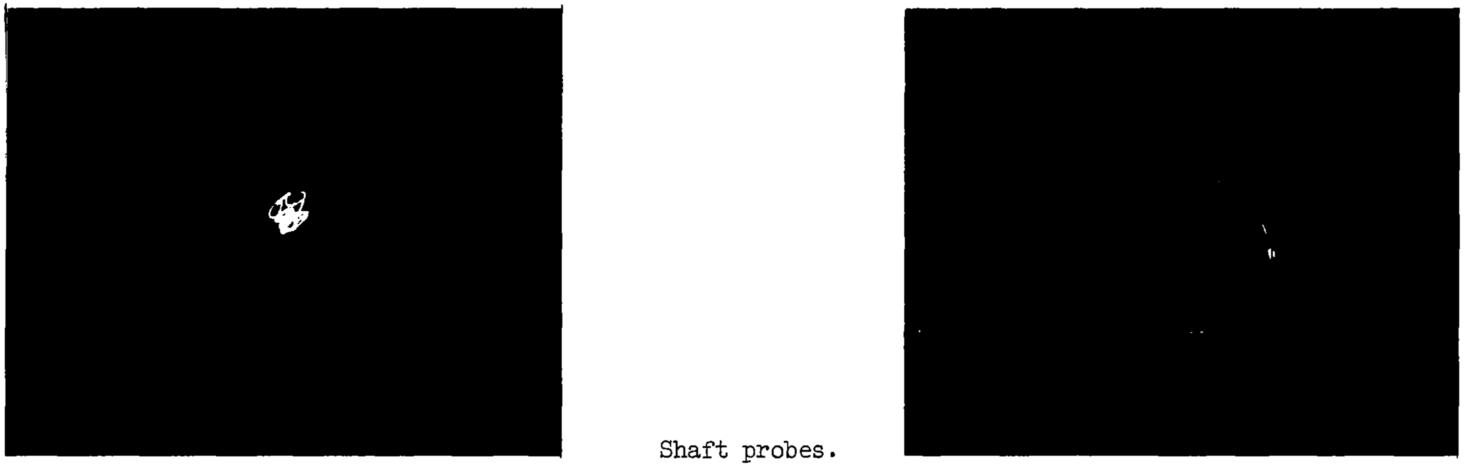

Shaft probes.

(a) No unbalance, 1 div. = 0.295 mils.

(b) 3.4 in.-oz unbalance,
1 div. = 0.295 mils.

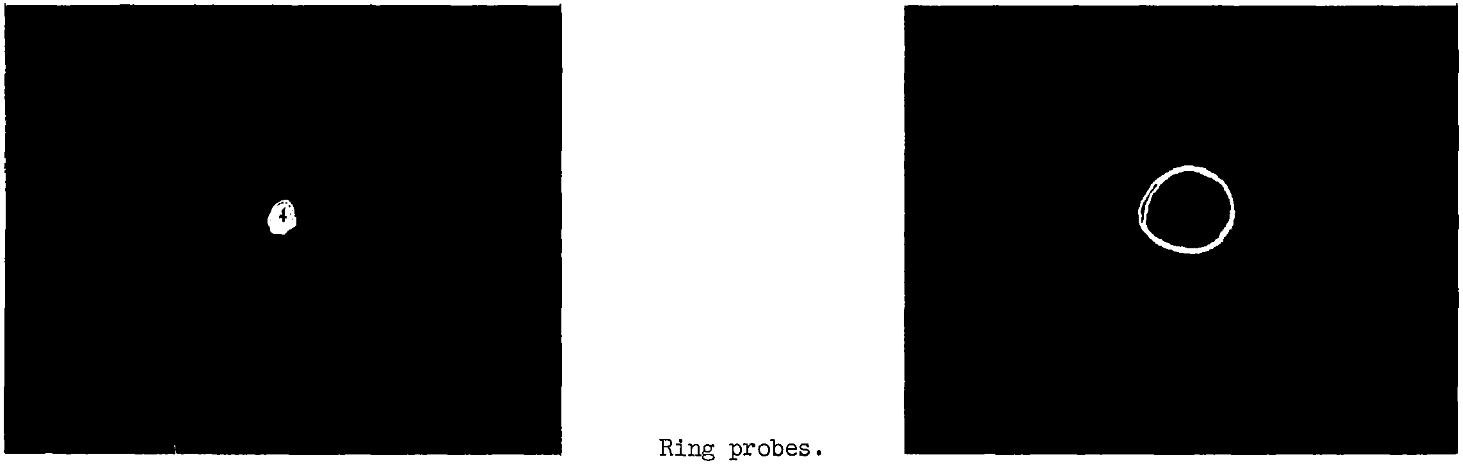

Ring probes.

(c) No unbalance, 1 div. = 0.118 mils.

(d) 3.4 in.-oz unbalance,
1 div. = 0.118 mils.

Figure 54. - Shaft and ring motions with and without synchronous unbalance load. 4000 rpm, 60 lb load, signals passed through band pass filters set for synchronous frequency.

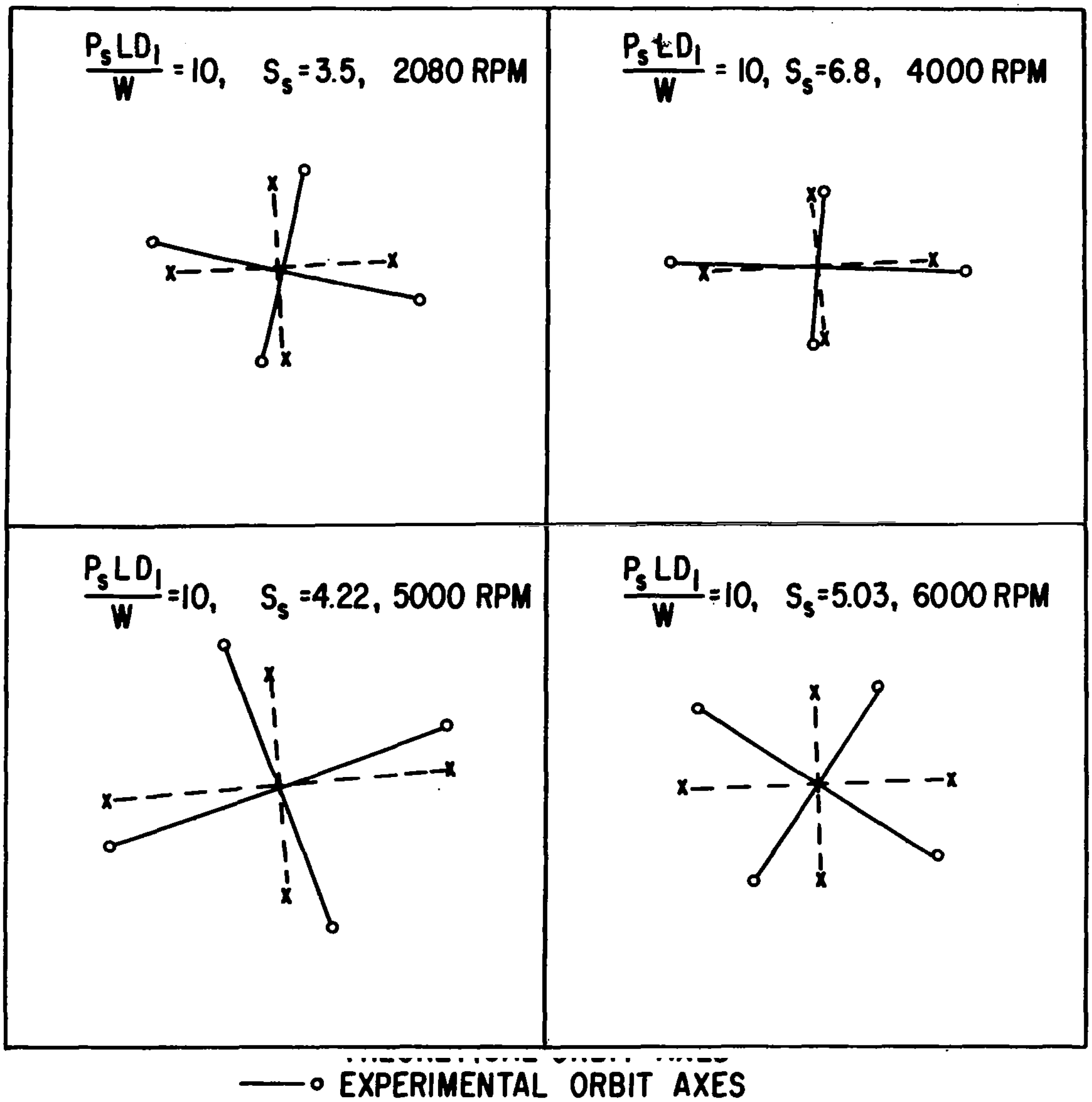
$\frac{P_s L D_1}{W} = 10$, $S_s = 3.5$, 2080 RPM
$\frac{P_s L D_1}{W} = 10$, $S_s = 6.8$, 4000 RPM
$\frac{P_s L D_1}{W} = 10$, $S_s = 4.22$, 5000 RPM
$\frac{P_s L D_1}{W} = 10$, $S_s = 5.03$, 6000 RPM
——○ EXPERIMENTAL ORBIT AXES

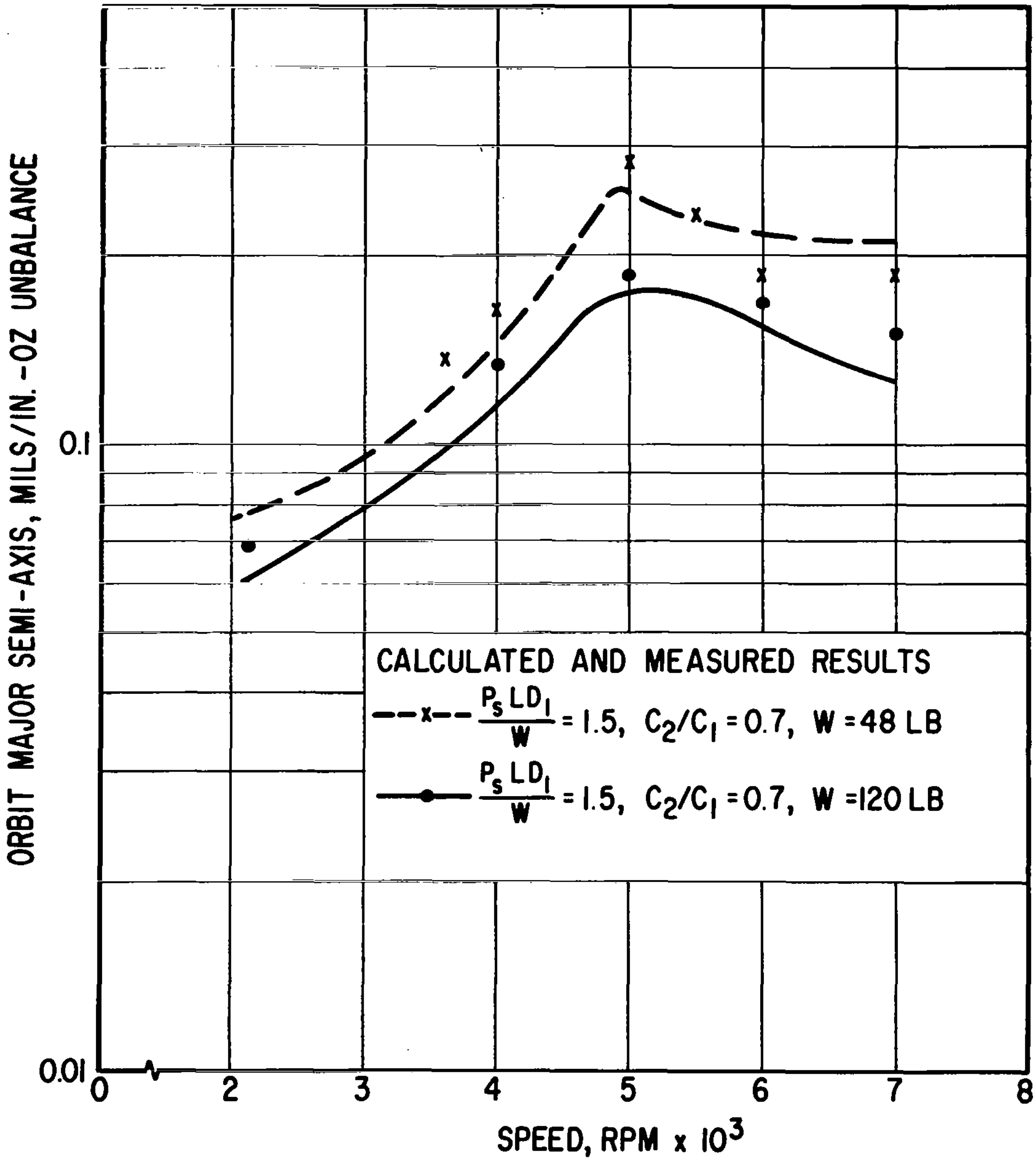

Figure 56. - Floating-ring bearing - dynamic load response amplitude, laminar flow, $C_2/C_1 = 0.7$, $P_sLD_1/W = 10$.

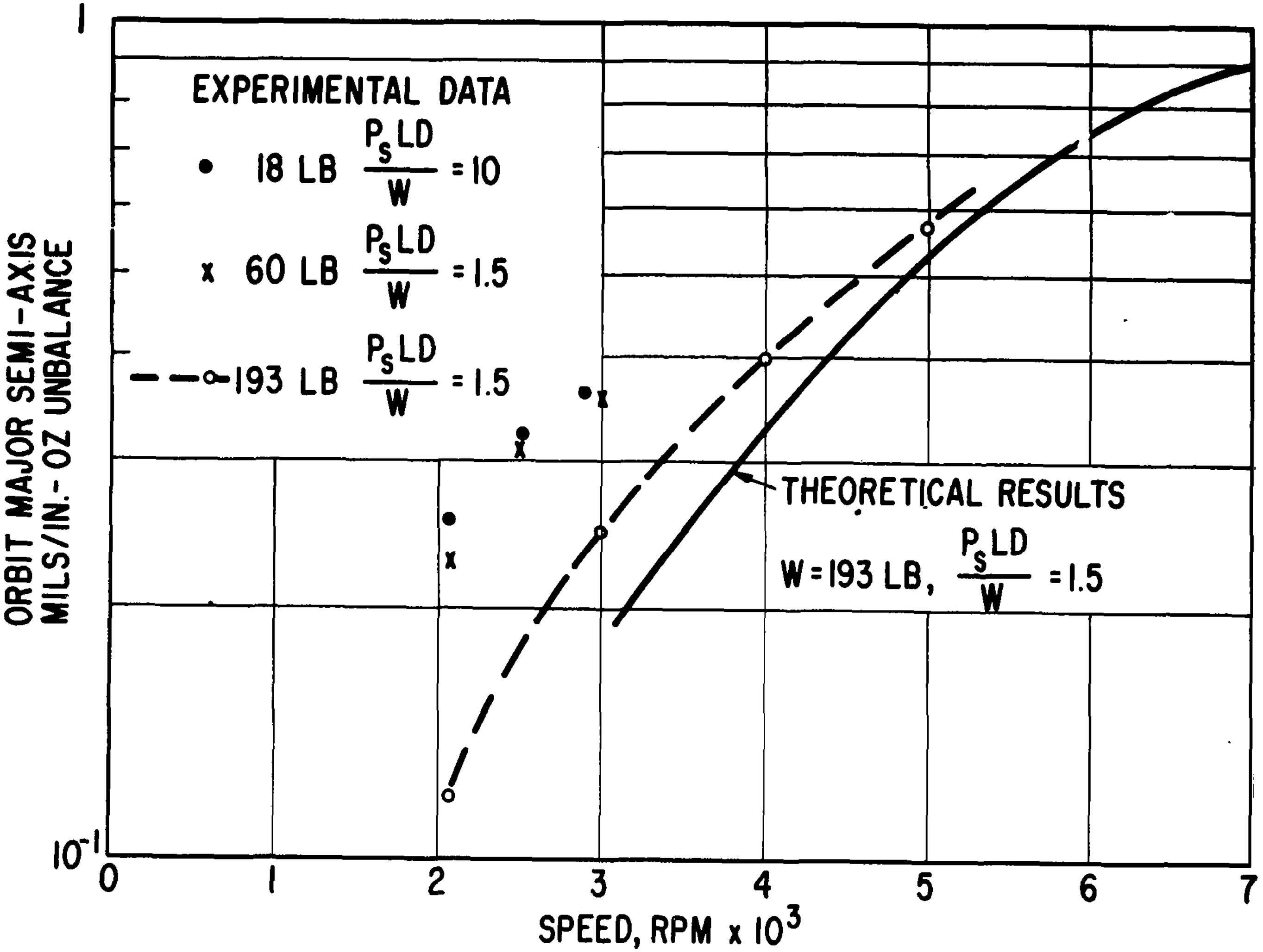

Figure 57. - Floating-ring bearing - dynamic load response amplitude, turbulent flow, $C_2/C_1 = 0.7$.

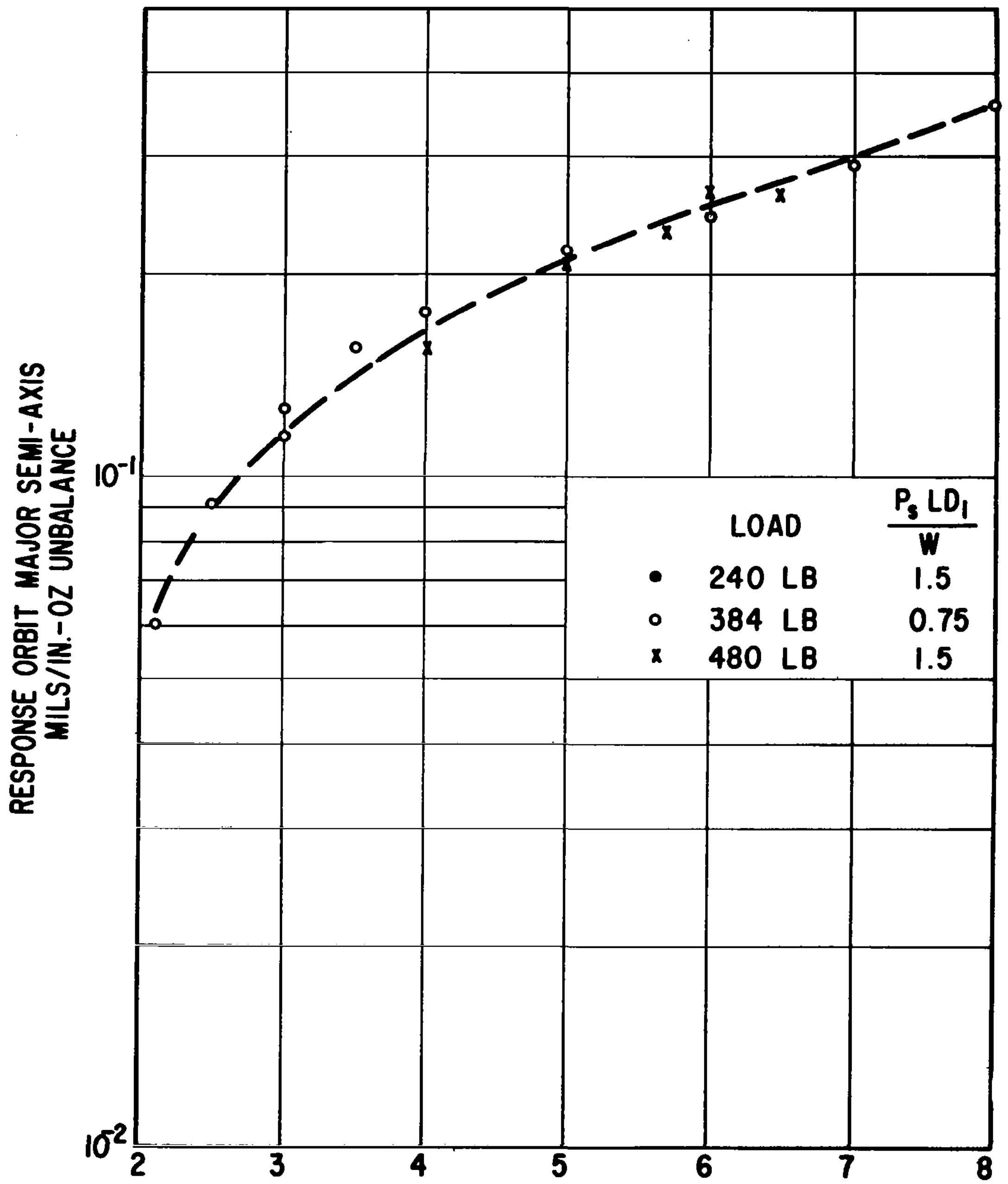RESPONSE ORBIT MAJOR SEMI-AXIS
MILS/IN.-OZ UNBALANCE
10^{-1}
10^{-2}
2
3
4
5
6
7
8
LOAD
$\frac{P_s L D_1}{W}$
● 240 LB 1.5
○ 384 LB 0.75
x 480 LB 1.5

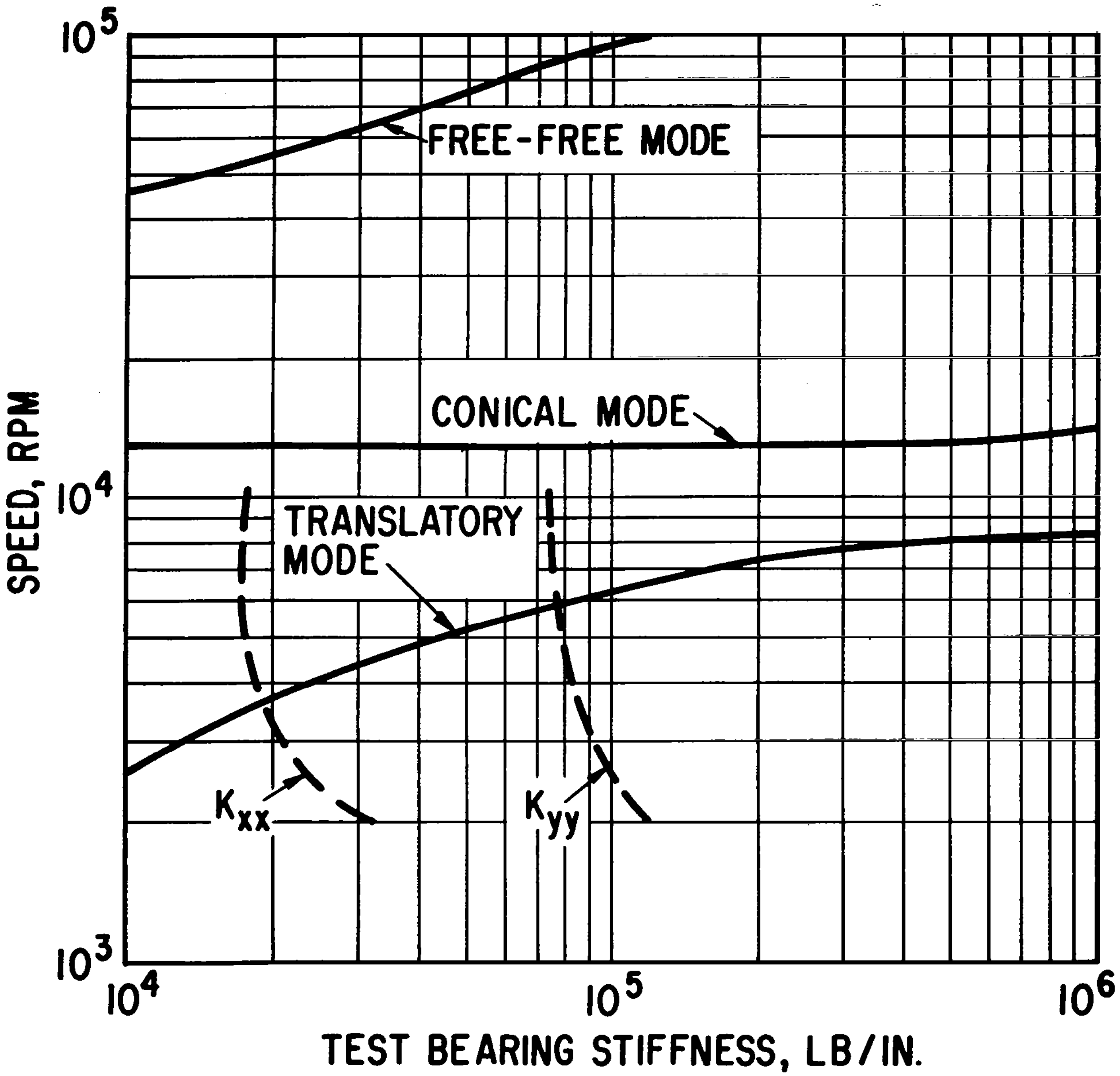

Figure 59. - Critical speed map for the dynamic load bearing apparatus.
(1) The broken lines are the theoretical direct stiffnesses of the floating-ring bearing for $P_sLD_1/W = 1.5$, $C_2/C_1 = 0.7$, 5.0 cs lubricant, W = 300 lb.
(2) Support bearing stiffness is assumed constant at 1.3×10^6 lb/in.

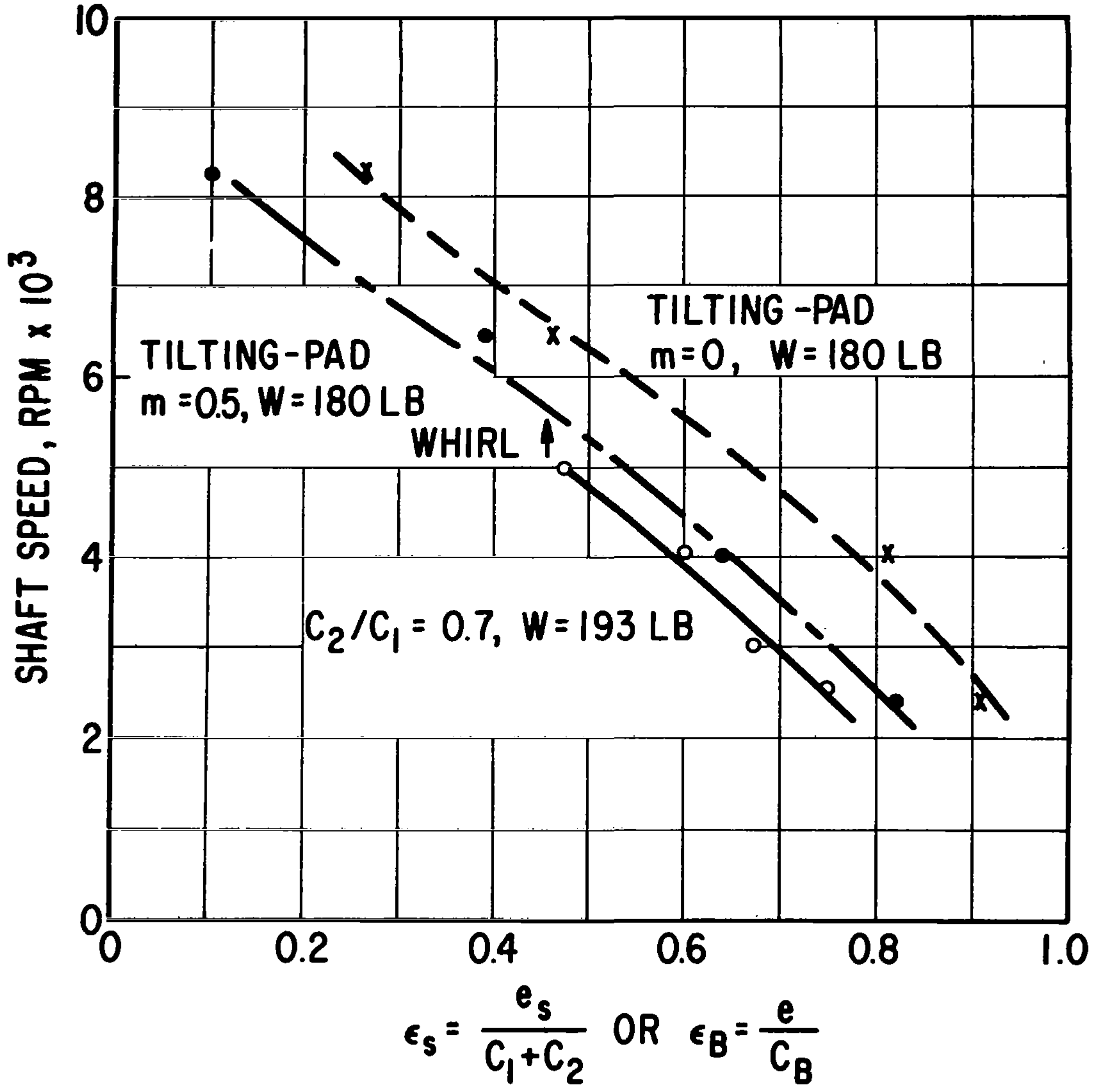

Figure 60. - Comparison of measured static load eccentricity ratios - tilting-pad and floating-ring bearings.

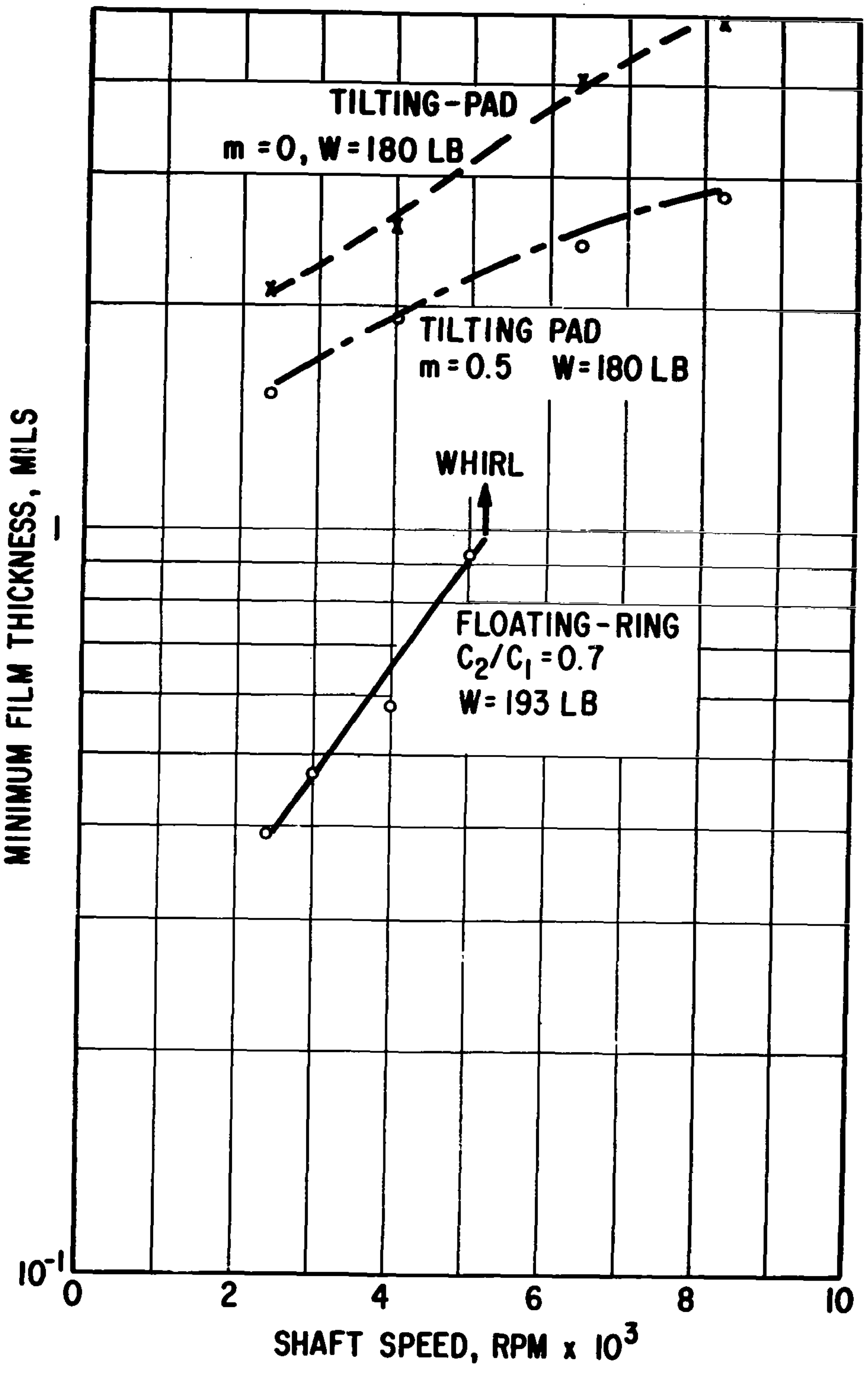

Figure 61. - Comparison of measured static load minimum film thicknesses, tilting-pad and floating-ring bearings. (1) Floating-ring bearing film thicknesses are for outer film C_2 = 2.1 mils, $C_1 + C_2$ = 5.1 mils. (2) Film thickness at the pivots is used for the tilting-pad bearing - C_p = 6.0 mils.

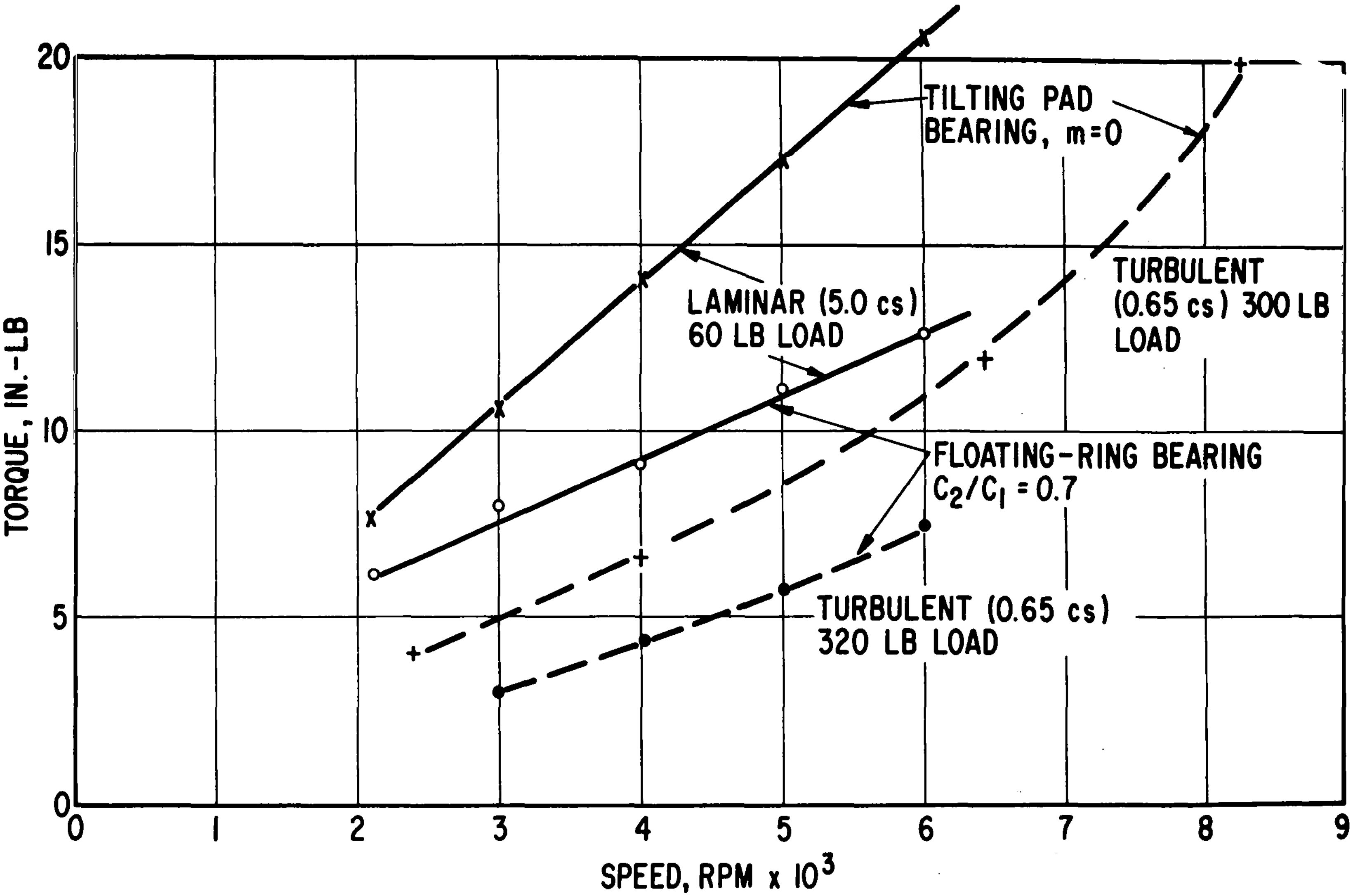

Figure 62. - Comparison of torque - tilting-pad and floating-ring bearings.

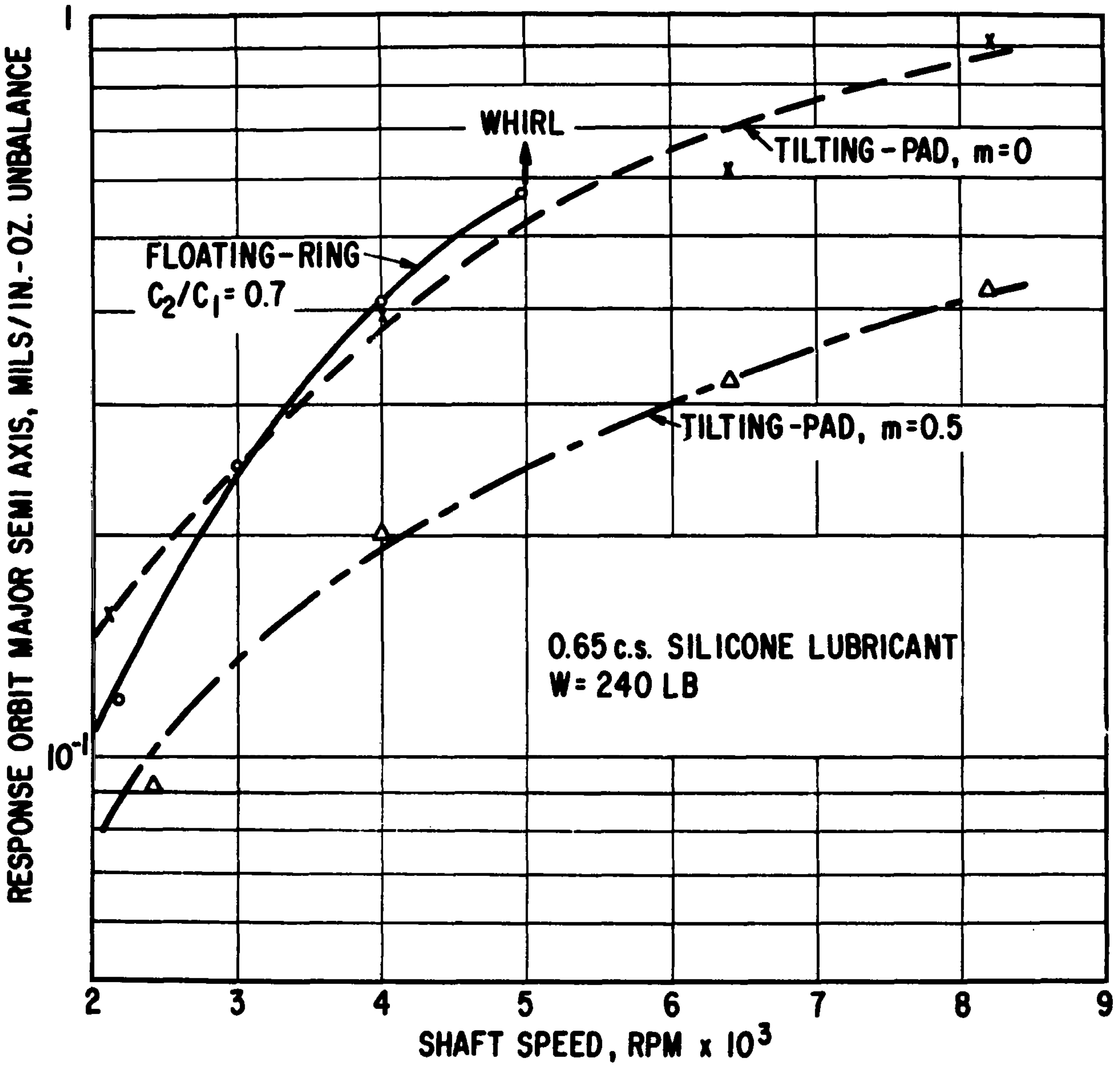

Figure 63. - Comparison of dynamic load response - tilting-pad and floating-ring bearings.

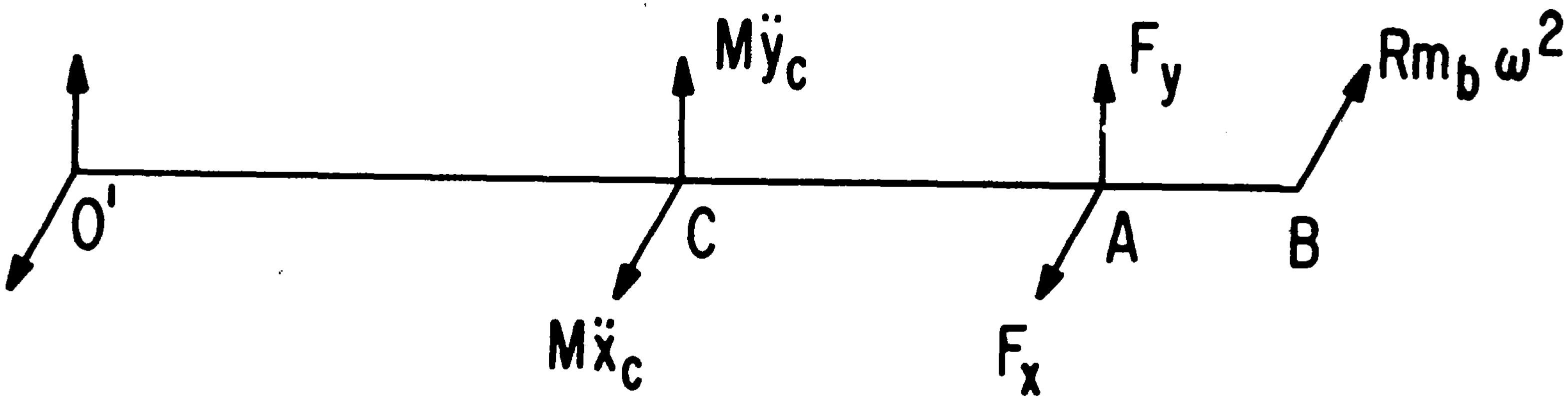

Figure 64. - Forces acting on experimental rotor.

NASA-Langley, 1967 —— 15 E-3717